

Dissertation for the Degree of Doctor of Philosophy

A Wearable and Context-Aware Brain
Machine Interface System with Integrated
Neuromodulation for Closed-Loop Driver
Drowsiness Detection

by

Gang Li

Department of Electronic Engineering
The Graduate School,
Pukyong National University

February 2016

A Wearable and Context-Aware Brain Machine Interface System with Integrated Neuromodulation for Closed-Loop Driver Drowsiness Detection

**페루프 온전자 줄음 감지를 위한 웨어러블 및
상황인지 복합신경조절 뇌□기계 인터페이스**

Advisor: Prof. Wan-Young Chung

by
Gang Li

A dissertation submitted in partial fulfillment of the requirements for the
degree of

Doctor of Philosophy

in Department of Electronic Engineering, The Graduate School,
Pukyong National University

February 2016

A Wearable and Context-Aware Brain Machine Interface System
with Integrated Neuromodulation for Closed-Loop Driver
Drowsiness Detection

A dissertation

by

Gang Li

Approved by:

Professor Hyek-Hwan Choi,
(Chairman)

Professor Jung-Jin Kim,
(Member)

Dr Sang-Joong Jung,
(Member)

Professor Boon-Giin Lee,
(Member)

Professor Wan-Young Chung,
(Member)

February, 2016

Table of Contents

4.1.3	Gyroscope Module.....	- 50 -
4.2	CA Sensory Processing Unit.....	- 51 -
4.2.1	On-chip Signal Processing.....	- 54 -
4.2.2	Bluetooth Low Energy.....	- 57 -
4.3	Transcranial Direct Current Stimulation (tDCS)-based Neuromodulation Unit	- 60 -
4.3.1	tDCS Electrodes.....	- 61 -
4.3.2	tDCS Circuit	- 63 -
4.4	Fabricating Headset case using 3D Printer	- 64 -
4.5	Chapter Summary	- 67 -
5	Design of Android WearTM-based BMI Terminal Device.....	- 68 -
5.1	What is Android Wear TM ?.....	- 69 -
5.2	Android Studio TM	- 71 -
5.2.1	Android Studio TM Interface.....	- 73 -
5.2.2	Android Studio TM SDK Manager.....	- 74 -
5.2.3	Android Virtual Device	- 75 -
5.2.4	Android Device Monitor.....	- 76 -
5.2.5	Logcat	- 76 -
5.3	Smartwatch-based BMI Application.....	- 77 -
5.3.1	Application Initialization.....	- 79 -
5.3.2	Feature Collection.....	- 80 -
5.3.3	Support Vector Machine-based Drowsiness Classification	- 81 -
5.3.4	Warning Signal	- 90 -
5.3.5	User Interface.....	- 91 -
5.4	Chapter Summary	- 92 -
6	Design of Closed-Loop DDD Algorithm.....	- 94 -
7	Experiment and Results.....	- 97 -
7.1	Verification of Basic BMI Functions.....	- 98 -
7.1.1	Sampling rate	- 98 -

7.1.2	Real-time FFT performance	- 98 -
7.1.3	Real-time SVM performance.....	- 100 -
7.1.4	EEG Signal Quality	- 100 -
7.1.5	Gyroscope Signal Quality.....	- 109 -
7.1.6	Proof-of-Concept Study on tDCS	- 111 -
7.2	Aging Test.....	- 115 -
7.2.1	Power consumption and battery life	- 115 -
7.2.2	Battery Life Comparison with Prior Work	- 116 -
7.3	Simulated Driving I: Evaluating CA and SVM-based DDD	- 117 -
7.3.1	Experiment Paradigm Design	- 118 -
7.3.2	Experiment Environment Setup.....	- 120 -
7.3.3	Experiment Analysis.....	- 121 -
7.3.4	Experiment Results.....	- 122 -
7.3.5	Discussion.....	- 129 -
7.4	Simulated Driving II: Evaluating Closed-Loop DDD Algorithm.....	- 148 -
7.4.1	Experiment Paradigm Design	- 148 -
7.4.2	Experimental Environment Setup.....	- 150 -
7.4.3	Experiment Analysis.....	- 150 -
7.4.4	Experiment Results.....	- 150 -
7.4.5	Discussion.....	- 154 -
7.5	Chapter Summary	- 161 -
8	Conclusions and Future Work.....	- 162 -
Reference.....		- 164 -
List of Publications (SCI (E) Journal Only).....		- 185 -
List of Publications (International Conference).....		- 186 -
Awards.....		- 187 -
Media Report.....		- 187 -
Appendix.....		- 188 -

List of Figures

- Fig 2-1 A commercial EEG-based DDD product, named Smartcap. Driving workers can wear the cap and have their brains monitored in the workplace
- Fig 2-2 An example of typical EEG signal (line chart) with its frequency spectral analysis result (pie chart). For the line chart, X-axis indicates the time (second). Y-axis indicates the amplitude of the digitalized EEG samples which are already filtered by band-pass filter (4-30Hz). For the pie chart, the X-axis indicates the frequency ranged from 0 to 64Hz (the half of the sampling rate 128Hz). Y-axis indicates the magnitude of Fast Fourier Transform (FFT) power.
- Fig 2-3 (a) The different brain cortices (b) The widely used EEG International System which is adapted from EEGLAB Toolbox using the built-in official location file (ver. 7.1.3.13b) [78].
- Fig 2-4 The type of EEG channels. Bipolar type (The top) and unipolar type or monopolar (The bottom)
- Fig 2-5 Example of conventional wet Ag/AgCl sensors (left side: Courtesy of [46]) and the finger-type dry sensors (right side: Courtesy of [45])
- Fig 2-6 Hierarchical taxonomy for EEG-based DDD studies containing six different tasks: data sensing, data processing, data-to-knowledge, wireless transmission, arousing feedback and appearance design.

- Fig 2-7 The percentages of number of studies that adopt different channel locations and electrode input types for single and two-channel EEG-based DDD.
- Fig 2-8 The percentages of number of studies that adopt different feature extraction methods and their lengths of time windows for EEG-based DDD.
- Fig 2-9 Commonly-used DM models in EEG-based DDD
- Fig 2-10 The trend of EEG acquisition devices used in DDD applications. The averaged year refers to the averaged publication year of those cited studies. For example, the publication year of cited studies for commercialized wBMI category is 2014, 2011, 2014 and 2014 respectively
- Fig 2-11 Various designs of BCI systems: (a) A single-channel wireless occipital EEG acquisition headband [61]. (b) A four-channel wireless occipital EEG acquisition headband [95]. (c) A baseball cap-based EEG acquisition device [30]. (d) A commercialized single-channel wireless frontal EEG acquisition headset (Neurosky Mindset®) [102]. (e) A commercialized 14-channel wireless EEG acquisition headset (Emotiv®) [19]. (f) A traditional wired BCI system [66].
- Fig 2-12 An example of a low-cost DDD system based on EEG headband and smartphone [94]. (a) The driving simulation experimental settings. (b) The screenshot of smartphone indicating the raw EEG data, real-time RPB features and PERCLOS reference.
- Fig 3-1 (a) Block diagram of the proposed system. (b) The fabricated headset prototype. (c) The demo for this fully wearable BMI system.

- Fig 4-1 (a) Schematic design, (b) PCB layout design (the upper left: top layer; the upper right: inner layer (active shield); the bottom: bottom layer) and (c) implementation of the driver circuit for EEG dry sensors.
- Fig 4-2 (a) Structure design, (b) Schematic design, (c) Circuit simulating (amplitude-frequency response) result, (d) PCB layout design and implementation of the EEG bio-potentials conditioning circuit
- Fig 4-3 The integrated 3-axis gyroscope and its direction.
- Fig 4-4 (a) Structure design, (c) Schematic design, (b) PCB layout design and implementation of the EEG bio-potentials conditioning circuit.
- Fig 4-5 The on-chip feature extraction algorithm
- Fig 4-6 The implementation of on-chip digital LPF
- Fig 4-7 The comparison of Bluetooth stack between BBR and BLE
- Fig 4-8 The BLE data payload packet format
- Fig 4-9 Self-adhesive electrodes (the left); Sponge electrodes (the right)
- Fig 4-10 (a) Schematic design (the left), PCB layout design (the right), (b) implementation of the tDCS-based neuromodulation unit.
- Fig 4-11 The working flowchart of BMI headset fabrication using 3D printer
- Fig 4-12 Appearance design including (a) part design and (b) overview design
- Fig 4-13 3D printer preparation using Creatork software
- Fig 4-14 Implementation of fabrication of headset case using 3D printer
- Fig 5-1 Examples of various wrist-worn device based applications
- Fig 5-2 The history of Android development tools: From Eclipse ADT to Android Studio v1.0+

- Fig 5-3 Android Studio interface for Android Wear™ project
- Fig 5-4 An example of the interface of Android SDK Manager
- Fig 5-5 An example of creating an Android Wear™ OS based virtual smartwatch
- Fig 5-6 An example of the interface of ADM
- Fig 5-7 An example of the automatic/“TAG” debugging using Logcat
- Fig 5-8 The working flowchart of smartwatch application
- Fig 5-9 The screenshot of the initialization procedure of the proposed wearable application, including start-up display (the top left), scanning BLE device (the top right) and pop-up window of the BLE device list (the bottom)
- Fig 5-10 The classification model building chain containing three different tasks: data collection, classification validation and classification optimization
- Fig 5-11 An example of the two-class (+1 & -1) classification problem with optimal decision surface. The circles and stars represent samples of class +1 and -1, respectively. (a) multiple decision surfaces (b) optimal decision surface.
- Fig 5-12 The procedure of LOSO cross-validation and optimization, where Si means the ith subject and Accuracy_i means the classification accuracy for ith Round.
- Fig 5-13 The implementation procedure of smartwatch-based SVM classification
- Fig 5-14 Pushing well-trained SVM model onto the smartwatch by using ADV tool
- Fig 5-15 Porting LibSVM to smartwatch and implement SVM functions in smartwatch
- Fig 5-16 The use of built-in vibration sensor of the smartwatch

- Fig 5-17 Smartwatch screen showing the designed UI for this wearable application termed “Brainwatch”. Green, Yellow and Red lights are placed at left side to right side.
- Fig 6-1 Flowchart of proposed closed-loop DDD algorithm
- Fig 7-1 A comprehensive experiment paradigm containing four different tasks.
- Fig 7-2 The comparison of FFT series between on-chip calculation and PC-based calculation
- Fig 7-3 The evaluation of the real-time performance of on-chip FFT
- Fig 7-4 EEG signals (line chart) and EEG band power (pie chart) comparison between wet electrodes (the top) and dry electrodes (the bottom). For the line chart, the X-axis indicates the time in seconds. The Y-axis indicates the amplitude of the digitalized EEG samples which are already filtered by the digital LPF in SPU. For the pie chart, the X-axis indicates the frequency range from 0 to 64Hz (the half of the sampling rate 128Hz). The Y-axis indicates the magnitude of FFT power.
- Fig 7-5 (a) A group of EEG signals and (b) its FFT results with the reduction of eye closure degree
- Fig 7-6 EEG signals under simulated driving environment. The female subject shown in the left bottom was too drowsy to keep her eyes open. At that moment, the EEG signals from the developed headset show obvious alpha rhythmicity, as marked by the two red circles. The two channel plots in yellow and blue were not EEG signals and not used in this study.
- Fig 7-7 A commercial wireless EEG headset (Emotiv)
- Fig 7-8 The extracted 14 ICA components from Emotiv EEG. Component#1 is the typical components of eye blinks.

- Fig 7-9 The time series of 14-channel Emotiv EEG. Blue series are original EEG data. Red series are eye-blanks-removed EEG data.
- Fig 7-10 Comparison of EEG signals (line chart) and EEG band power (pie chart) under EO and EC condition for our device. For the line chart, the X-axis indicates the number of EEG samples. The Y-axis indicates the amplitude of the digitalized EEG samples which are already filtered by the digital LPF in SPU. For the pie chart, the X-axis indicates the frequency range from 0 to 64Hz (the half of the sampling rate 128Hz). The Y-axis indicates the magnitude of FFT power. The EEG signal here is collected by our device from a representative subject.
- Fig 7-11 Comparison of EEG signals (line chart) and EEG band power (pie chart) under EO and EC condition for a commercial EEG device. For the line chart, the X-axis indicates the number of EEG samples. The Y-axis indicates the amplitude of the digitalized EEG samples which are already filtered by the digital LPF in SPU. For the pie chart, the X-axis indicates the frequency range from 0 to 64Hz (the half of the sampling rate 128Hz). The Y-axis indicates the magnitude of FFT power. The EEG signal here is collected by a commercial device from a representative subject.
- Fig 7-12 Gyroscope signal quality test including (a) normal drowsy situation; (b) yawning; (c) moving restlessly on chair
- Fig 7-13 The paradigm of the proof-of-concept study on the arousing effect of tDCS
- Fig 7-14 A representative experimental results of the proof-of-concept study on the arousing effect of tDCS. The EEG RBP features of

before, during and after the tDCS are shown in (a), (b) and (c) respectively.

- Fig 7-15 Example of experimental setup for evaluating drowsiness detection
- Fig 7-16 Experiment analysis chain
- Fig 7-17 Box-Whiskers plots of (the top) EEG and (the bottom) Gyroscope features extracted from labeled alert and drowsy datasets
- Fig 7-18 The typical three slightly drowsy symptoms captured by video as well as EEG and gyroscope from a representative subject. (a) Rubbing eyes (b) Moving restlessly on chair (c) Yawning. The blue line charts for each figure represent EEG raw signals, X-axis, Y-axis and Z-axis signal of gyroscope respectively. The two bars on the right side of the line charts represent the EEG RBP features (the top) and the gyroscope MP features (the bottom).
- Fig 7-19 The comparison of ROC_{area} of extracted features in this work and features proposed by previous works. (a) and (b) show the comparative results of the EEG and gyroscope feature groups, respectively.
- Fig 7-20 Flowchart of estimation of driver drowsiness using SVM-based posterior probabilistic model.
- Fig 7-21 The histogram of estimated posterior probability for each subject (#1~#15) in training phase for alert group (a) and drowsy group (b). The X-axis indicates the drowsiness level (0~1). The Y-axis indicates the number of dataset that falls into the corresponding bins of estimated drowsiness levels.

- Fig 7-22 Bland-Altman plot for the relationship of the difference between the observed PERCLOS vs. the estimated probability vs. their average values. Mean bias, +1.96SD, and -1.96SD lines are shown. SD = standard deviation.
- Fig 7-23 The threshold probabilities for each subject in training phase for (panel A) alert group with X-axis 1~15 and (panel B) drowsy group with X-axis 16~30. The threshold probabilities for each subject refer to the maximum probability in alert group and minimum probability in drowsy group.
- Fig 7-24 Posterior probability estimate $P(y=+1|f(x))$ calculated for each class for (a) subject #16 and (b) subject #18.
- Fig 7-25 Screenshots of the smartwatch that show the estimated driving status by real-time EEG power percentage features and a virtual traffic light. a) green: safe driving; b) yellow: early warning; c) red: fully warning).
- Fig 7-26 An example of real and sham tDCS procedure during 2-hour driving experiment
- Fig 7-27 The comparison of the number of traffic accidents between condition 1 (closed-loop DDD) and condition 2 (open-loop DDD)
- Fig 7-28 The duration of after-effect and EEG RBP features under condition 1. The left column and right column show RBP (β) and RBP(α) respectively
- Fig 7-29 The comparison of EEG RBP features between each tDCS sessions for the whole 2-hour driving simulation from a representative subject.
- Fig 7-30 The comparison of EEG RBP features and gyroscope MP features between before, during and after tDCS session. The X-

axis indicates the time in min. The Y-axis indicates the feature values. For example, 50% for RBP features and absolute value 50 for MP.

- Fig 7-31 Examples of the parking area or so-called drowsiness shelter in the highway in South Korea
- Fig 7-32 The screenshot of a self-developed smartphone-based SSVEP source (the top) and the experiment setup of pilot study on SSVEP-based arousing effect for driver drowsiness (the bottom)
- Fig 7-33 Comparison of SSVEP power spectral between alert and drowsy status (The data is from a representative participant)
- Fig 7-34 The smartphone application used to play β tone. All β tones surrounded by red box were used in this pilot study.

List of Tables

- Table 2-1 Brief comparison of existing DDD technologies
- Table 2-2 Brief comparison of EEG and other physiological signals in DDD application
- Table 2-3 Overviews of specific EEG frequency bands and their associated state of consciousness
- Table 2-4 Comparison of dry EEG systems
- Table 2-5 The FFT-based band power equations used in EEG-based DDD
- Table 2-6 Ground truths used in EEG-based DDD
- Table 2-7 Summaries of power consumption and estimated battery life for wireless single-channel EEG circuit
- Table 2-8 Summary of power consumption of several commercialized wireless chips
- Table 2-9 Summaries of advantages and disadvantages using different wireless technologies for DDD application
- Table 4-1 Time and Frequency-Domain Features Extracted From EEG and Gyroscope Signals
- Table 4-2 Comparison of technical specification between BBR and BLE
- Table 5-1 Comparison of Eclipse ADT and Android studio
- Table 7-1 The means and standard deviations of EEG features obtained from commercialized device and our device
- Table 7-2 Experimental results of the proof-of-concept study on the arousing effect of 10-min tDCS
- Table 7-3 Comparison of power consumption and battery life of the headset and smartwatch under remote and local feature extraction conditions
- Table 7-4 Comparison of Battery life of Bluetooth-enabled and EEG-based DDD systems

- Table 7-5 Comparison of ROC_{area} of EEG features and gyroscope features under one-to-one drowsiness level condition
- Table 7-6 Results of the LOSO cross-validation experiments using EEG feature, gyroscope feature and the combined feature
- Table 7-7 Results of the final test using EEG feature, gyroscope feature and the combined feature
- Table 7-8 Comparison of means of EEG features and gyroscope features under different head movements conditions
- Table 7-9 Comparison of ROC_{area} of EEG features and gyroscope features under different head movements conditions
- Table 7-10 LOSO Classification Accuracy of SVM Classifier with Different input feature sets and Different Kernels
- Table 7-11 Rules (Thresholds for DDD)
- Table 7-12 Results of final test using proposed wearable BMI system

List of Abbreviations

BMI	Brain Machine Interface
DDD	Driver Drowsiness Detection
ECG	Electrocardiogram
EEG	Electroencephalogram
EMG	Electromyogram
ESS	Epworth Sleeping Scale
EOG	Electrooculogram
FFT	Fast Fourier Transform
KDS	Karolinska Drowsiness Scoring
KSS	Karolinska Sleepiness Scale
LBP	Log Band Power
LDS	Lane Departure System
MP	Movement Power
PBP	Pure Band Power
PERCLOS	Percentage of Eye Closure
PPG	Photoplethysmogram
RBP	Relative Band Power
RK	Rechtschaffen and Kales
ROC	Receiver Operating Characteristics
SVM	Support Vector Machine
SWM	Steering Wheel Movement

Acknowledgement

First and foremost, I would like to express my sincere gratitude to my research supervisor, Professor Wan-Young Chung for guiding and encouraging me patiently throughout the completion of this dissertation. He had given me the freedom to explore the research topics I am interested in, meanwhile he always ensured that I was progressing steadily and progressing on the right way. Also, he had given me the deep insights into how to write well-structured international journal articles. His teaching, supervision, and attitude will remain forever grateful to me.

Thanks are also attended to my fellow ubiquitous sensor network laboratory members for their helping in providing an excellent research environment which made this research possible. Their sharing and comments have meant a lot to me. I am privileged to have great enthusiastic, dedicated, knowledgeable and meticulous seniors and other lab members for supporting my research, namely: Dr Boon-Giin Lee, Dr Sang-Joong Jung (정상중), Mr Tran Viet Thang, Boon-Leng Lee, Hyeon-Seok Lee (이현석), Zhenyang Ong and Yubing Jiang. Also, for those who attended to the recruited participants for this research, Young-Eun Jeon (전영은), Ha-Rim Seo (서하림), Sang-Jun Kim (김상준), Jong-Beom Jeon (전종범) and Hye-In Song (송혜인) in particular, thanks for their positive participation and friendly cooperation.

Special thanks to my family, my cousin Wei Li and my friend Mandy Yang for supporting me throughout this research work. This research is benefited a lot from their understanding and encouragement.

상황인식 및 신경 조절술 기반의 페루프 운전자 줄음 감지를 위한 웨어러블 노 기계 인터페이스 시스템

A horizontal row of six empty square boxes, intended for children to draw or write in.

부경대학교 대학원 전자공학과

요약

Chapter 1

1 Introduction

Driver drowsiness is a major cause of mortality in traffic accidents worldwide. The U. S. National Highway Traffic Safety Administration (NHTSA) reports that drowsy driving is the cause of an estimated 40,000 injuries and 1,550 deaths in car crashes per year [1]. Also, the Korean Expressway Cooperation reports that, from 2010 to 2013, 1,223 people died in Korean highway traffic accidents, 31% of which could be attributed to driver drowsiness [2, 3]. Many of these deaths could be avoided if driver drowsiness was properly monitored and drivers were given early warnings. Therefore, cooperative efforts between government and private sectors have been done to reduce the number of drowsiness-related traffic accidents by proposing numerous types of algorithm-level and system-level approaches.

Among the numerous driver drowsiness detection (DDD) approaches, Electroencephalographic (EEG) signal, which reflects the brain activities, is more directly related to drowsiness [4]. Thus, many EEG-based DDD models that combine brain-machine-interface (BMI) system together gained more and more attention in recent years [5-9]. However, the existing methods are not robust enough to recognize the drowsy driver's early features, when drowsy warning might be the most effective, if compared to mid- or late-stage warning. In addition, most of the existing BMI-based DDD solutions are open-loop without any arousing feedback algorithm. Regarding the few solutions containing the auditory arousing feedback [10], the arousing effect is too short to allow drivers drive to nearby drowsiness shelter or service area (if assume drowsy driving occurred on the highway).

Practical utility of BMI-based DDD systems are being improved with the development of low-power integrated circuits, wireless communications technologies and dry electrodes. However, several unresolved problems in previous studies need to be overcome in this dissertation (e.g, the side-effect of distracted driving caused by DDD systems and the high-power consumption caused by data-stream-centric wireless transmission)

This chapter introduces in detail the motivation, research objectives, contribution and organization of this dissertation.

1.1 Motivation and Research Objectives

Due to the importance of driver drowsiness, this dissertation proposed a context-aware and neuromodulation -based BMI system. This system is a brain signal (EEG) based system combining the contextual information of head-movements and the neuromodulation technology of transcranial direct current stimulation (tDCS) together. The ultimate goal of this system is creating a closed-loop DDD solution by which drivers can detect drowsiness timely and boost their alertness by themselves, as opposed to the use of coffee, energy pills and etc. Considering the practical utility, the smartwatch is included in this system serving as a wearable user interface. Also, the arousing feedback method is developed based on forehead non-hairy tDCS instead of conventional hairy region. In addition, the system is carefully designed for low-power consumption, with on-chip feature extraction and Bluetooth Low Energy (BLE) technology. To achieve these goals, this study uses the following strategies:

- ①. Design and implement a wireless and context-aware BMI headset with an integrated feature extraction processor and BLE module;

- ②. Propose an effective driver drowsiness assessment model according to the EEG signals and contextual information which are collected from BMI headset.
- ③. Propose an effective arousing feedback algorithm according to forehead non-hairy tDCS-based neuromodulation technology.
- ④. Design and implement a wearable application using smartwatch;
- ⑤. Test the wearable application by driving simulation experiment.

1.2 Contributions

We reviewed studies about EEG-based DDD in the past decade from well-known literature pools including IEEE Xplore, ScienceDirect, and SpringerLink. To the author's best knowledge, this is the first study attempting to detect driver drowsiness using EEG signals enriched with contextual information of head-movement. Also, this is the first study attempting to boost drivers' alertness using forehead non-hairy tDCS-based neuromodulation method. In addition, it is the first study attempting to implement a fully wearable BMI system. Thus, the contributions of this work are fourfold:

- ①. The full design of a wearable and context-aware BMI system is described;
- ②. The practical utility of early detection of drowsy driving using contextual-information-enriched EEG is evaluated and confirmed;
- ③. The arousing effect using forehead non-hairy tDCS-based neuromodulation technology is evaluated and confirmed;
- ④. The real-time DDD performance of a commercial smartwatch is investigated, including system computational cost and battery life.

1.3 Dissertation Organization

The rest of this dissertation is organized as follows:

An introduction to related works in DDD is presented in Chapter 2, involving the measurement methodologies, prediction methodologies and arousing feedback methodologies. Particularly, the EEG-based DDD will be reviewed in detail including the basic theory of EEG signal, EEG montages, EEG spectral analysis. Finally, the limitations of previous approaches will be presented. In addition, overview of BMI system will be introduced including EEG sensors, wireless technologies and physical design of BMI. The original contribution of this dissertation will be described starting from Chapter 3.

Chapter 3 focuses on the design and implementation of the hardware platform of the sensing device of the proposed system including the context-aware sensory input unit, sensory processing unit and neuromodulation unit.

Chapter 4 describes the design and implementation of the wearable terminal device of the proposed system including the introduction of used Operating System (OS), the OS development environment and the developed wearable application.

Chapter 5 focuses on the design of closed-loop DDD algorithm involving the design of driver drowsiness prediction model and the integrated algorithm.

The experiments and results are depicted in Chapter 6 including the experimental paradigm design, environment setup and data analysis. Discussion on the principle results are also presented in Chapter 6.

Chapter 7 proposes future work and concludes this dissertation.

Chapter 2

2 Related Works and Theory

2.1 Driver Drowsiness Detection (DDD)

Driver drowsiness, that is, excessive sleepiness, is more likely to happen when a person is driving for extended periods in monotonous environments, such as on a highway. The standard clinical tests for measuring sleepiness are the Multiple Sleep Latency Test (MSLT) and the Maintenance of Wakefulness Test (MWT), combined with polysomnography datasets [4]. These measurements are very expensive and cumbersome to perform (at least eight channels are needed: four EEG, two electrooculogram (EOG), one electromyogram (EMG), and one electrocardiogram (ECG) [4]); it would be practically impossible to use these methods to detect driver drowsiness in an actual driving environment. For instance, the use of multiple sensors would be uncomfortable for the driver and could even impede his or her movement. Thus, there is a strong demand for an easy-to-use DDD system.

To enable the detection of driver drowsiness both simply and inexpensively, many methods have been proposed, including vehicle-based methods (such as the lane departure warning system (LDWS) [11, 12] and the steering wheel movement (SWM) system [13-15]), video-based methods (such as the detector of the degree (percentage) of eyelid closure over the pupils over time (PERCLOS) [16-18]), and physiological-signal-based methods (such as those based on the ratio of low frequency to high frequency of heart rate variability (HRV) derived from ECG or Photoplethysmogram (PPG) [19, 20] and EEG (brain waves) [21]). Table 2-1 summarizes the existing DDD technologies together with their advantages and disadvantages.

Table 2-1 Brief Comparison of Existing DDD Technologies

Examples	Vehicle-based	Behavioral-based	Physiological-based
	LDWS and SWM system	PERCLOS	PPG, ECG, EEG, EOG and EMG
Merits	Non-contact, easy to use and commercialized	Non-contact and partially commercialized	Clinical standard and reliable
Drawbacks	Unreliable (Not directly related to drowsiness)	Lighting limitation (Cannot work properly at night or when driver is wearing glasses)	Expensive and cumbersome

LDWS: lane departure warning system

PERCLOS: eyelid closure over the pupils over time

Williamson *et al.* and M. Golz *et al.* undertook a comprehensive review of on-road fatigue monitoring technologies in 2005 and 2010, respectively [22, 23]. In 2012, A. Sahayadhas *et al.* reviewed existing sensor-based DDD systems [24]. They believed that physiological sensor-based signals offer the most reliable means of detection as these signals provide an indication of the true internal state of the driver. In a more recent study, T. Brown *et al.* detailed and reviewed vehicle-based sensor technologies for DDD [25]. A major limitation of these reviews is that they paid very little attention to the EEG. EEG is a non-invasive physiological means of measuring brain activity and has the closest relationship with drowsiness [4]. Particularly, under the same conditions, the performance using EEG alone is proved to be better than using other physiological signal alone [26]. Table 2-2 shows a comparison of EEG and other physiological signals that are commonly applied to DDD.

Table 2-2 Brief Comparison of EEG and other physiological signals in DDD application

	EEG	ECG, PPG	EMG, EOG
Advantages	Direct relationship to drowsiness, shorter data-processing time window (clinical use: 30 s [27])	Simple-to-use; strong wearable ability	
Disadvantages	Cumbersome	Indirectly related to drowsiness, longer data-processing time window (3 to 5 min) [28]	Assistive signals [27,29]; Not comparable with EEG, ECG and PPG



Fig. 2-1. A commercial EEG-based DDD product, named Smartcap. Driving workers can wear the cap and have their brains monitored in the workplace [30].

We can assume that, in the past, EEG was not widely applied to practical DDD systems because it would be difficult to obtain EEG recordings under day-to-day driving conditions due to the size of the equipment and the inconvenience of wet scalp electrodes. Nowadays, however, with the development of low-power integrated circuits, wireless

communications technologies and dry electrodes, low-cost and wireless BMI systems are allowing EEG-based DDD to make the transition from the research stage to practical use. Particularly, an Australian start-up company named Smartcap [31] (as shown in Fig. 2-1), has already proved this point.

2.2 Electroencephalogram (EEG) Signal

EEG is the measurement of electrical activity produced by the brain as recorded from electrodes placed on the scalp. It is a readily available test that provides evidence of how the brain functions over time. The EEG is a particularly powerful clinical tool and has been taken as the gold standard for neurology and psychology research for decades. It is a relatively simple, inexpensive and completely harmless method for analyzing the brain activity. Moreover, EEG signals recorded from the scalp have small amplitude of approximately 10~100 uV with the frequency range from 0.5 to 100 Hz. Generally, based on different frequency bands, EEG signals can be categorized into five specific categories of brain activity, which have commonly discussed in EEG literature: delta (δ), theta (θ), alpha (α), beta (β) and gamma (γ) waves as shown in Table 2-3.

Table 2-3 Overviews of specific EEG frequency bands and their associated state of consciousness

EEG Bands	State of Consciousness
γ (above 30Hz)	History of idea, Role in attentive focus, Relation to meditation
β (13-30Hz)	Fully awake, Alert, Excitement, Tension
α (8-12Hz)	Deeply relaxed, Passive awareness, Composed
θ (4-7Hz)	Drowsiness, Unconscious, Deep tranquility, Optimal meditative state
δ (below 4Hz)	Sleep, Unaware, Deep unconsciousness

A typical EEG signal (6-second digitalized EEG samples) with abundant α rhythmicity is shown in Fig. 2-2.

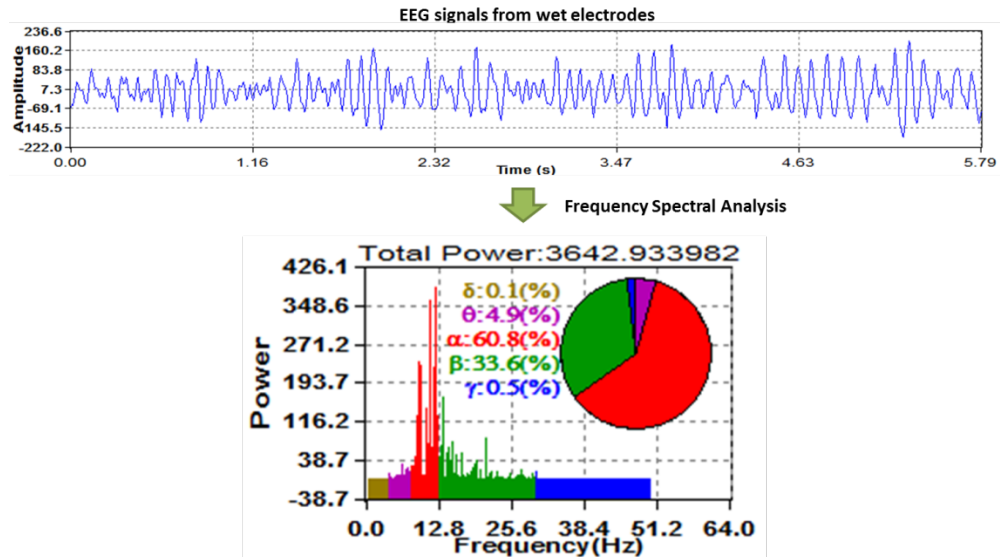
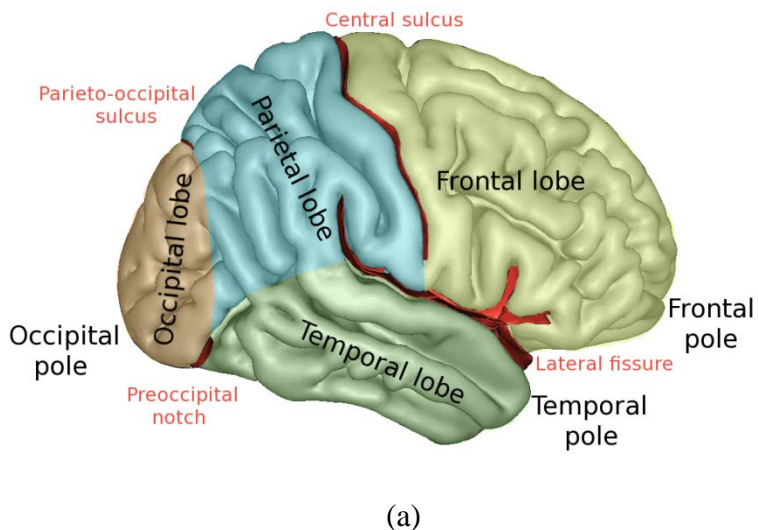


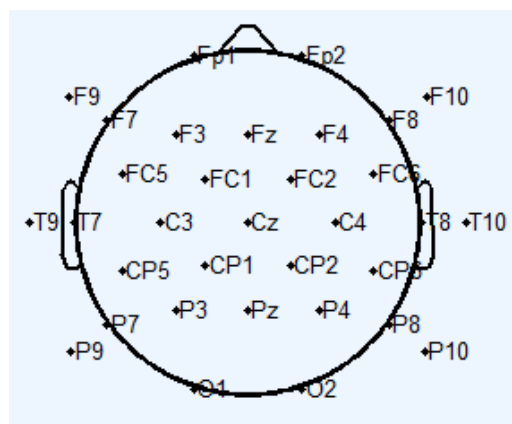
Fig. 2-2. An example of typical EEG signal (line chart) with its frequency spectral analysis result (pie chart). For the line chart, x-axis indicates the time (second) and y-axis indicates the amplitude of the digitalized EEG samples which are already filtered by band-pass filter (4-30Hz). For the pie chart, the x-axis indicates the frequency ranged from 0 to 64Hz (the half of the sampling rate 128Hz) and y-axis indicates the magnitude of Fast Fourier Transform (FFT) power.

The brain consists of different functional cortices as shown in Fig. 2-3 (a). Frontal cortices are usually used for emotion recognition [32], such as stress assessment. Central cortices are commonly used for motor imagery research for the disabled [33]. Occipital cortices are highly correlated with vigilance level and thus are widely used in DDD study [34]. Therefore, selection of measurement locations is the indispensable procedure before applying EEG to any brain-related research. Fig 2-3(b) shows the EEG 10-20

International System which is the map for 33 commonly-used EEG measurement locations.



(a)



(b)

Fig 2-3 (a) The different brain cortices (b) The widely used EEG 10-20 International System which is adapted from EEGLAB Toolbox using the built-in official location file (ver. 7.1.3.13b) [35].

In addition to selection of measurement locations, the selection of measurement types are also important. The EEG measurement types can be

classified into unipolar and bipolar measurement (as shown in Fig. 2-4). In the unipolar case, each electrode records the potential difference, compared to a neutral electrode connected to an ear lobe or mastoid. Bipolar measurements show the potential difference between two paired electrodes.

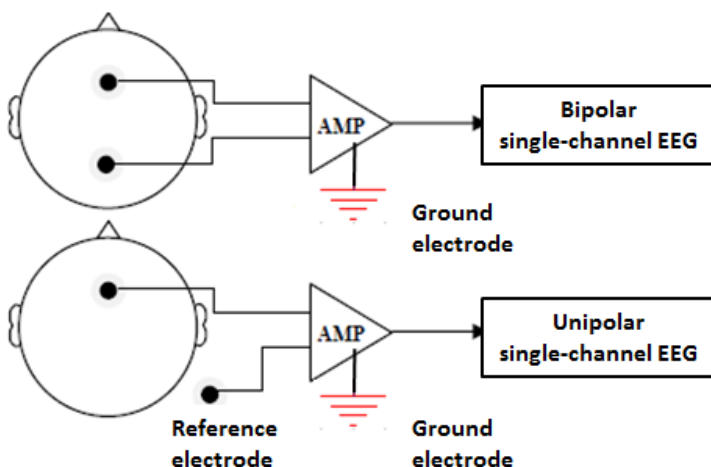


Fig. 2-4. The type of EEG channels. Bipolar type (The top) and unipolar type or monopolar (The bottom)

2.3 EEG-based Brain Machine Interface (BMI) System

Over the past two decades, the study of the BMI has grown dramatically. According to IEEE Xplore search engine, a search result with the keyword “Brain Machine Interface” returns zero paper for year 1995. But, the same query returns 906 journals and conference papers for year 2015 (date of search: August 26, 2015).

BMI systems measure neurophysiological signals of the human, EEG in particular. EEG-based BMI provides a feasible and noninvasive way for the communication between the human brain and external devices (e.g., TV,

video tape recorders, air-conditioners and wheelchairs) [5]. EEG-based BMI can also apply to long-term medical monitoring (e.g., epilepsy) [36]. As an emerging application, a real-time drowsiness detection algorithm can be implemented in EEG-based BMI system for DDD [5-10].

EEG-based BMI has become the mainstream of BMI system because of its much fine temporal resolution, ease of use, portability and low set-up cost [7]. Traditionally, the variations of brain waveforms are measured and analyzed by personal computers (PCs). Due to the inconvenience of PC-based BMI that limits the user's mobility, portable and inexpensive BMI platform, such as proprietary embedded devices with small size and the mass consumer electronics (e.g. smartphone and tablet)-based BMI systems have been proposed [9, 10]. The following sections introduce in detail the most fundamental components of the EEG-based BMI system including EEG biopotential sensors, EEG biopotential conditioning circuit and EEG digital subsystem.

2.3.1 EEG Biopotential Sensors

EEG-based BMI system measures brain electric potentials over the scalp. Therefore, EEG biopotential sensors are the most important components for EEG-based BMI systems. Traditionally, Ag/AgCl sensors are used for EEG biopotential recordings. With proper hair preparation and the use of conductive gels or glues for better attachment and higher conductivity, the recorded EEG signal is excellent for both medical and research use [37]. However, these preparations are time consuming, uncomfortable and even painful for participants [37]. Furthermore, the conductive gels easily desiccate and lose their adhesion. These problems

limit wet Ag/AgCl sensors' success in the application of long-term EEG monitoring in a real-life environment.

Recently, to overcome the weakness of wet EEG sensors and make EEG recording more feasible in real-life applications, many researchers have studied dry EEG sensors. By using dry EEG sensors, the participants do not require the use of conductive gels or glues. They can conveniently attach the sensors to their scalp without any hair arrangement. To make dry contact at the sensor-skin interface, researchers employ special materials or shapes in the design of dry sensors including conductive rubber [38], comb-like electrode [39], gold-plated electrode [40], bristle-type electrode [41], and foam-based sensor [42] and spring-loaded fingers [43, 44].

The most widely used dry electrode design is a set of contact posts which look like fingers [43, 44, 45]. This design has an advantage in contact ability because it is easy to penetrate into the scalp through the hair without an extended hair arrangement. Fig. 2-5 shows the conventional wet Ag/AgCl sensors and the finger-type dry sensors respectively. Table 2-4 lists some commercially available EEG systems. Most of these dry sensors are useful for hairy sites, which indicate that EEG biopotential recordings in hairy occipital region are available.



Fig 2-5 Example of conventional wet Ag/AgCl sensors (left side: [46]) and the finger-type dry sensors (right side: [45])

Table 2-4 Comparison of Dry EEG Systems

Dry EEG system	Mindo-4 [9]	Cognionics [47]	Imec [48]
Sensor Type	Dry	Dry	Dry
Bandwidth	0.23-125Hz	0-50Hz	0.5-100Hz
Resolution	24bits	24bits	12bits
Number of Channel	4	16/24/32/64	8
Sampling rate	128/256/512Hz	300Hz	1024Hz
Signal quality compared with wet EEG systems	Correlation coefficient:>92% [44]	Correlation coefficient:>90% [49]	Correlation coefficient:81-92% [48]

2.3.2 EEG Biopotential Conditioning Circuit

As mentioned in Section 2.2, EEG signals are usually weak and prone to interference by undesired noises. Therefore, both amplifying and filtering are required for further signal processing. In addition, human skin typically provides source impedance in the order of 1-5Mohm. Thus, in order to acquire the EEG signals, the amplifiers must match the source impedance or have greater input impedance than the source skin impedance. For these

reasons, the output of the bipotential sensors is transferred to an EEG biopotentials conditioning circuit where it is amplified by an instrument amplifier (IA). The IA features a high differential input-impedance of and a high common mode rejection ratio (CMRR). Therefore, the IA can balance the sensor-skin impedance well and reject common mode noise as much as possible. Additionally, in order to acquire the useful EEG bands, the output signal from the IA is transferred to the High Pass Filter (HPF), and then filtered by the Low Pass Filter (LPF). Next, the signal is amplified by the amplifiers to meet the input requirement of analog-to-digital converter ADC. Finally, the EEG biopotential signals can be converted to digital signals which can be read and recorded by electronic terminal devices, such as PC, smartphone, tablets and etc.

2.3.3 EEG Digital Subsystem

For EEG digital subsystem, four integrated circuits are included: a multiplexer, an ADC, a microcontroller unit (MCU), and a transmission unit (e.g., a RS232-based transmission unit for wired BMI and a Bluetooth-based transmission unit for wireless BMI (wBMI)). It is important to note that most of today's mainstream MCU has built-in multiplexer and ADC. The multiplexer here is used to measure multi-channel EEG signals simultaneously. The ADC here is used to transform the EEG analog biopotential signals into discrete digitized data with a specific sampling rate. Technically, the sampling rate is determined by the speed of the microprocessor, transmission unit, and the speed of terminal device. For specific application, the sampling rate is determined by the frequency region of interest (ROI). For example, if the frequency ROI is 0-60Hz. The minimum sampling rate should be 120Hz, according to Nyquist sampling

law. In addition, considering the following advanced signal processing, such as FFT, formally, researchers and system developers choose the sampling frequency as the power of 2, such as 128Hz, 256Hz, 512Hz and 1024Hz. For ADC resolution, there is no gold standard. The use of minimum 8bits and maximum 24bits can be found in previous studies. However, according to a standard of EEG open-source project, the recommended minimum resolution is 10bits [50]. It is also important to note that the more the ADC resolution is used the more data would be made. Researchers and system developers should fully take into account its impact on the system computational load.

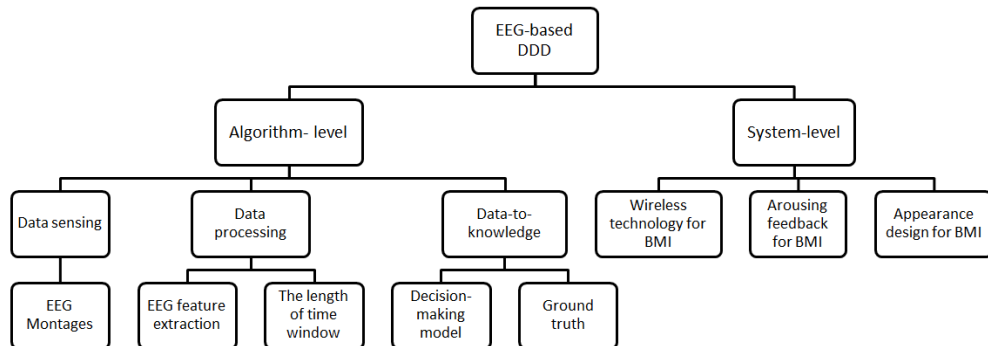


Fig. 2-6. Hierarchical taxonomy for EEG-based DDD studies containing six different tasks: data sensing, data processing, data-to-knowledge, wireless transmission, arousing feedback and appearance design.

2.4 Systematic Review of EEG-based DDD

This subsection focuses on the systematic review of EEG-based DDD [171]. To facilitate this systematic review, the EEG-based DDD are organized into a tree-structure taxonomy (as shown in Fig. 2-6), in which two main categories are identified, namely algorithm-level problems (e.g., data sensing, data processing, data-to-knowledge) and system-level problems

(e.g., wireless technology, arousing feedback, appearance design). This review aims at synthesizing a system infrastructure to unify implementation principles, find out the advantages and unresolved problems, and highlight our original contributions which are depicted from Chapter 3.

We make the following distinction for the major components of this taxonomy.

- ①. *Data sensing*: EEG data sensing involves three stages, including EEG bio-potential sensing, conditioning and ADC processing. These general contents have been introduced in Section 2.3. Our focus here is the EEG montages (e.g., the number, location and type of the EEG channel to be used in DDD. The significance of this focus is that, unlike the well-documented three-unipolar-channel methods (e.g., F4, C4, O2) in a clinical sleep-scoring system [27], there is no standard channel-selection document for EEG-based DDD. Therefore, there is a demand to provide a primary channel-selection reference.
- ②. *Data processing*: One focus here is the feature extraction methods which are used to generate a set of features from the raw EEG signals. The other one is the length of time window. The goal is to explore how often the EEG features are generated, which is very important to the timeliness of the proposed algorithm or system.
- ③. *Data-to-knowledge*: This problem involves the understanding of the generated features, so decision-making (DM) models are indispensable here. However, unlike the application-dependent problems (e.g., data sensing and processing), DM methods are more general, i.e., DM algorithms can be used for a wide range of

features. Therefore, instead of focusing on the mathematical model, we focus on the detection accuracy and the type of the DM model (i.e., two-class classification, multi-class classification or probability estimation). The significance of examining the type of the DM model is that it can directly indicate the effectiveness of the DDD system. For example, a two-class classification system is not capable of determining the driver's degree of drowsiness. However, the estimation of the degree of drowsiness is the focus of a multi-class classifier and thus could provide drivers with an earlier warning of drowsiness. The other focus here is the ground truth which is usually used to verify the developed models.

- ④. *Wireless technology*: Generally, wireless transmission is the most power-demanding component for wireless sensor nodes [51]. So, how to design a low-power wireless BMI (wBMI) system is a critical problem for DDD application which needs long-term EEG monitoring. In this section, the power consumption of wireless single-channel EEG circuit is calculated based on twelve system-level wBMI studies.
- ⑤. *Arousing feedback*: A DDD system which includes arousing feedback function is called closed-loop DDD system, which has strong practical utility because it not only detects drowsiness, but also tries to arouse the driver via effective warning.
- ⑥. *Appearance design*: For real-life application, the available physical designs of the EEG sensing parts of wBMI systems are reviewed here.

Totally, 126 references comprising 111 studies and 15 other references (e.g., the links of driver's handbooks, chip datasheet and

commercial products) were included in this review article. The majority of the studies (93%, 103 out of 111) were taken from well-known literature pools including IEEE Xplore, ScienceDirect, and SpringerLink by using “EEG or Electroencephalogram” and “driver drowsiness or drowsiness” as searched term.

2.4.1 Algorithm-level problems

2.4.1.1 Data Sensing (EEG Montages)

Fig. 2-7 shows that bipolar single-channel in occipital region is the most commonly-used EEG montages for DDD research based on 54 studies published in past decades. The publication list and related montages information are shown in Table 1 in Appendix).

The more the sensing channels are used, the more the power consumption would be depleted. Based on the survey results, we know that a single-channel EEG is the most popular configuration among EEG-based DDD studies. This result confirms the feasibility of using battery-powered wBMI to implement an EEG-based DDD.

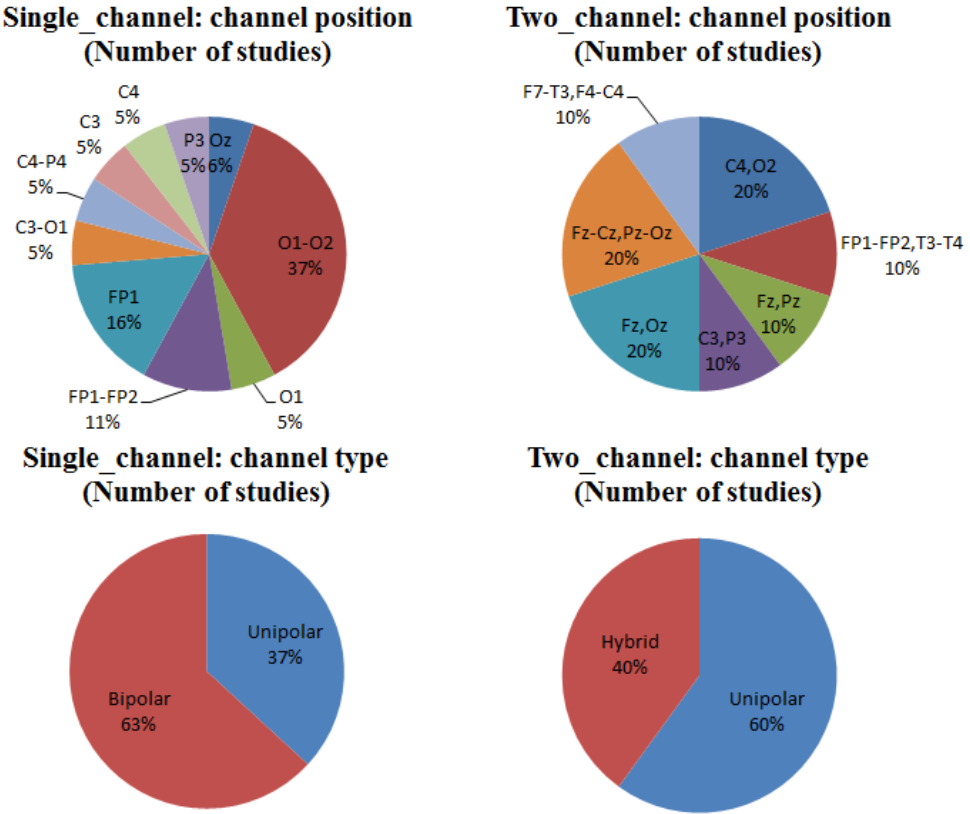


Fig. 2-7. The percentages of number of studies that adopt different channel locations and electrode input types for single and two-channel EEG-based DDD.

Ten years ago, C. T. Lin *et al.* pointed out that the EEG changes at occipital and central region have a strong correlation with driver drowsiness [52]. During the ten years, numeric EEG-based DDD approaches have been proposed. Our survey results indeed found that the most popular EEG channel for DDD is located in occipital region, which is further confirmed by C. T. Lin *et al.* again in 2012: the occipital EEG is highly correlated to the driver's level of vigilance [34]. The physiological reasoning behind the

“success” of occipital region should be associated with our visual cortex. For human being, our visual cortex, which is responsible for processing visual information, is just located in the occipital region of the brain. When drivers are transiting from alert to slightly drowsy, moderately drowsy, even significantly drowsy or extremely drowsy status, their eyes will successively experience following steps: increase in duration and frequency of sideway glance, glazed-eye, reduction on degree of eye opening, almost complete eye closure, and significant increase in duration of eye closure [104]. All these drowsiness-related eye movements will blur visual field and reduce visual input, which will further cause EEG changes (e.g., the increased α wave) [105]. Actually, the relationship between occipital EEG changes and visual cortex is more than drowsiness detection. Dewan et al. [106] even used the EEG changes there to produce Morse code.

One challenge for occipital EEG is that occipital region is hairy. For real-life application which involves the usage of dry electrodes, the artifacts caused by drivers, such as rubbing eyes and face, yawning, moving restlessly on chairs [104], would significantly influence the EEG signal quality and result in unreliable measurements.

DDD research focuses on the EEG difference between alert and drowsy status and few study reported the hemisphere superiority research on EEG-based DDD [105]. Therefore, the bipolar channel may provide sufficient information. This point has been already proved by our survey result, particularly for the single-channel EEG methods. However, for emotion recognition research for example, the unipolar channel is necessary to compare the EEG changes between right and left hemisphere [107].

2.4.1.2 Data Processing

For EEG-based DDD, the foremost step for measured EEG raw signal is the extraction of a set of features that correlated with drowsiness. However, similarly, there is no standard DDD document for feature extraction. Therefore, we reviewed a wide range of EEG features from 59 studies published in past decades [4, 21, 26, 52-103, 108-111]. Fig. 2-8 shows that these features can be classified into six categories: pure time-domain-based features, FFT-based features, Higher-Order-Statistics (HOS)-based features, wavelet-based features, other time-frequency-based features, and hybrid features. FFT-based features are found to be the most common. In addition, due to the importance of the timeliness of the DDD system, the length of time window for feature extraction is reviewed at the same time. The length of 1-minute is found to be the most common.

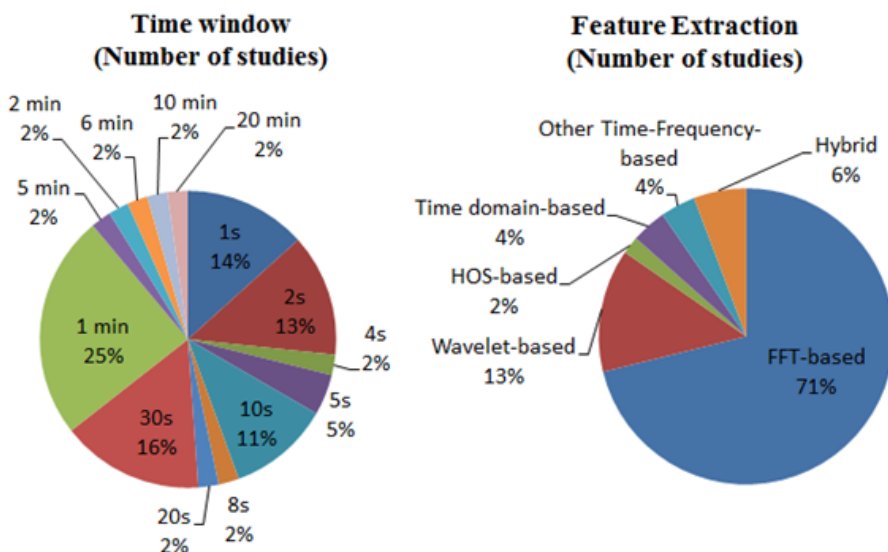


Fig. 2-8. The percentages of number of studies that adopt different feature extraction methods and their lengths of time windows for EEG-based DDD.

FFT-based features are generally FFT power features from different EEG frequency bands including the δ , θ , α , β and γ band. These band power features can be directly fed to a DM model to detect driver drowsiness. Alternatively, various band power equations (as shown in Table 2-5) and the relative band power can also be used. “Relative band power (RBP)” implies that the authors use EEG power percentages instead of the absolute EEG power values as the input features for DDD [21, 79, 84, 100]. The RBP is calculated by dividing the FFT power of one EEG band by the sum of the FFT power of all the employed EEG bands, as shown in Equation 11, where, $Z_i = \{ \delta, \theta, \alpha, \beta, \gamma \}$.

Table 2-5 The FFT-based band power equations used in EEG-based DDD

No.	Equation	Reference
1	θ/β	[62, 68, 70]
2	$\theta/(\alpha+\beta)$	[65]
3	$(\theta+\alpha)/\beta$	[62, 65]
4	$(\theta+\alpha)/(\alpha+\beta)$	[62, 65]
5	θ/α	[91, 97]
6	δ/α	[94]
7	α/β	[62, 76, 103]
8	$(0.6*\theta+0.4*\alpha)/(0.5*\beta)$	[70, 87]
9	$(\alpha+\beta)/\delta$	[63]
10	$(\delta+\theta)/(\alpha+\beta)$	[66]

$$RBP(z_i) = \frac{Power(z_i)}{\sum_{i=1}^5 Power(z_i)} \times 100\% \quad (11)$$

It is very important to note from Table 2-5 is that among the five EEG frequency bands, the θ , α , and β bands are more popular than the δ and γ bands for detecting drowsiness. The physiological background behind this is as follows [29]: 1) when a driver transitions from the alert to the sleepy state, the β power decreases; 2) when a driver is relaxed with his or her eyes

closed, the α power increases and becomes abundant; 3) when the driver enters the standard sleep state, the β and α power gradually diminish and give rise to θ power.

The length of time window for feature extraction has direct relationship to the timeliness of the DDD system. For example, HRV is the widely-used drowsiness indicator for ECG or PPG signals [19]. The minimum and regular time window for HRV analysis is 3 minutes and 5 minutes respectively [28]; while we found that 1 minute is the most popular length of time window for EEG-based DDD methods. Clearly, from the point view of timeliness, EEG signal is more suitable for DDD application as its detection result could be delivered to drivers as early as possible. The physiological reasoning behind the shorter time window for EEG analysis should be its direct relationship to drowsiness.

2.4.1.3 Data-to-Knowledge (DM model and ground truth)

In this section, we review the ground truth and DM models based on the same studies as those mentioned in Section Data Processing.

For DM models, Fig. 2-9 shows that the threshold-based approach and binary classification methods are predominant, accounting for 61% of all of the reviewed papers. The multi-class classification models constitute nearly 30%, followed by the regression and probabilistic models, which correspond to 4% and 6%, respectively.

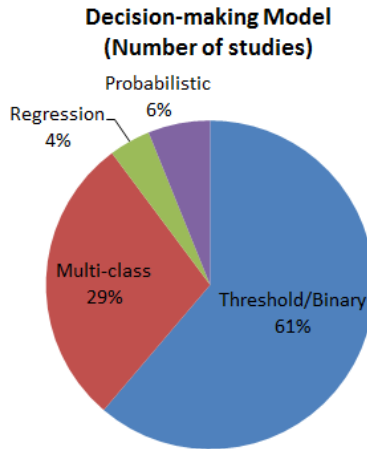


Fig. 2-9. Commonly-used DM models in EEG-based DDD

Ground truth is used to label true alert and drowsy events. So, the reliability of ground truth is very important to develop a DM model for DDD. Table 2-6 lists all the ground truths when building these DM models, where KDS, KSS, ESS and RK stand for Karolinska Drowsiness Scoring, Karolinska Sleepiness Scale, Epworth Sleeping Scale and Rechtschaffen and Kales. The ground truth #1~3, #11 and #22 are perhaps effective to recognize general-purpose inattentive driving patterns including drunk driving, stressful driving and distracted driving, but maybe not professional enough and accurate enough for DDD if compared to ground truth #10, #14, #15 and #17. The ground truth #8 is too dangerous to implement. The ground truth #9 and #19 are well-known standard for scoring sleep stage, which is not directly to drowsiness. Other ground truths listed in Table 2-6 are self-assessment-based, which is relatively not reliable. To authors' best knowledge, among the ground truths listed in Table IV, PERCLOS is the only one method that experienced sufficient verification in real life application [10-12].

Table 2-6 Ground Truths used in EEG-based DDD

DM model	No.	Ground truth
Threshold/ Binary	1	Subjects' response time to lane departure event [61, 85, 109]
	2	Subjects' response time to sound simulation [60]
	3	Subjects' collision rates with time [76]
	4	Subjects' self-assessment [70, 86] (Subjects press a button placing next to them when feeling drowsy)
	5	Subjects' self-assessment [87] (Alert: KSS < 8 and KDS = 0; Fatigue: KSS ≥ 8 and KDS ≥ 50)
	6	Subjects' self-assessment [71] (Alert: KSS < 8.5; Drowsy: KSS ≥ 8.5)
	7	Subjects' self-assessment [57] (Alert: KSS < 7; Drowsy: KSS ≥ 7)
	8	Subjects aborted to drive due to severe fatigue [71, 103]
	9	RK (Wake, Stage I) [64, 84, 93, 98]
	10	Facial features that are manually identified by video recording [72] (Drowsiness: Wierewille scale>=3)
	11	The accuracy of counting the number of times that a visual stimulus was shown [54]
	12	Authors' self-assessment based on the experimental video recording and the subjects' self-assessment [62]
	13	Authors' self-assessment based on subjects' eye and head movements [53]
	14	Assessment of Driver Vigilance and Warning According to Traffic Risk Estimation (AWAKE): Index>=1 represents drowsiness [79]
	15	PERCLOS [97]
Multi-class	16	Subjects' self-assessment (ESS) [73, 77] (Alert: ESS<8; Drowsy: 8≤ESS≤11; Severe drowsy: ESS≥24)
	17	Facial features that are manually identified by video recording (Wierewille scale) [46, 88, 97]
	18	Self-assessment (KSS) [63]
	19	RK(Wake, Stage I, Stage II) [90]
	20	Authors' self-assessment based on their own experience [91]
Regression	21	Unknown sleep scoring standard [58]
	1	Subjects' response time to lane departure event [80, 95]
	17	Facial features that are manually identified by video recording [68] (Wierewille scale)
Probabilistic	22	Subjects' driving error index [52]
	23	Self-assessment [75, 102] (Subjects press buttons on the steering wheel when feeling arousal, a little bit drowsy and drowsy)

Timeliness is a big challenge of DDD. To address this problem, not only the shorter length of data-processing time window should be adopted, but also a smart DM model that could timely estimate driver drowsiness should be used. We have reviewed DM models of EEG-based DDD

proposed in previous studies and found that they could be classified into five categories: pure threshold-based models, binary classification models, multi-class classification models, regression models and probabilistic models. Clearly, multi-class classification models which aim to detect driver drowsiness early by classifying driver drowsiness into several levels are better than threshold-based or binary classification models. However, they are still inferior than probabilistic models (or regression models) which aim to transform the drowsiness level to any value of 0~1 (or a continuous variable) instead of discrete labels. However, from the perspective of real-life application, the higher the resolution of DDD could be achieved, the more intensive system computation (thus the more power consumption) would be suffered. In addition, there is no ground truth which outputs non-discrete labels. Therefore, direct validation of probabilistic or regression models to another technique are currently impossible. Thus, relatively speaking, multi-class models are the best models for EEG-based DDD.

2.4.2 System-level problems

2.4.2.1 Wireless Technologies

Traditional wired BMI systems were commonly seen in EEG-based DDD studies, such as [21, 26, 66, 96, 110]. These systems could be acceptable for research purposes, but essentially impossible for practical use due to their being so cumbersome. Fortunately, this limitation can be overcome by recently developed wBMI systems. wBMI systems eliminate the wire connection between the EEG sensing part and the data-to-knowledge part, using various wireless transmission technologies. In this case, wBMI systems can be manufactured easily and offer several desirable

advantages, such as their small size (fewer sensing channels from the perspective of power consumption) and light weight. These desirable aspects of wBMI systems make them very suitable for real-life DDD applications. The trend for EEG sensing devices to move from wired BMI to wBMI for DDD applications is as shown in Fig. 2-10.

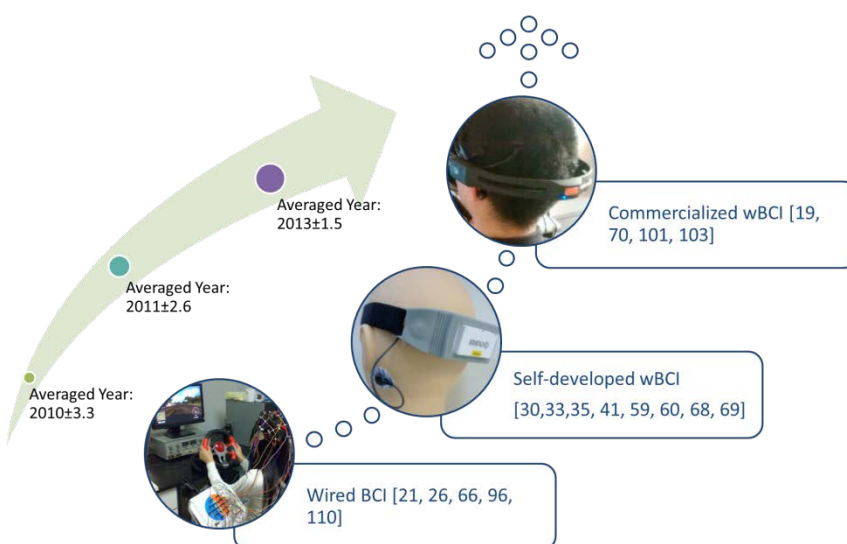


Fig 2-10. The trend of EEG acquisition devices used in DDD applications. The averaged year refers to the averaged publication year of those cited studies. For example, the publication year of cited studies for commercialized wBMI category is 2014, 2011, 2014 and 2014 respectively

Regarding the protocol of wireless transmissions, various communication modules are employed including proprietary radio frequency (RF), IEEE 802.15.4 Zigbee and Bluetooth modules. Generally, wireless transmission is the most power-demanding component of wireless sensor

nodes [51]. Therefore, the power consumption for each type of wireless technology is compared and summarized in Table 2-7, where the multi-channel power consumption is normalized to single-channel power by Equation 12, in order to make a reasonable comparison.

Table 2-7 Summaries of Power Consumption and Estimated Battery Life for Wireless Single-channel EEG Circuit

Wireless protocol	Averaged $CC_{single-ch}$ (mA)	Module	Chip	Estimated Battery life (using 100mAh button cell)
Zigbee	1 [112], 7.1 [113]	MICAz [114]	CC2420 [115]	14~100 hours
	5.5 [116]	TelosB [117]	CC2420	
	4.9 [118]	Self-developed	CC2430 [119]	
Bluetooth (v2.0+EDR)	31 [7, 61, 120]	Self-developed	-	3 hours
RF	ISM: 2.4GHz	0.16 [121]	Self-developed	43~1000 hours
	ISM: 2.4GHz	0.5 [123]	Self-developed	
	ISM: 2.4GHz	0.1 [125]	Self-developed	
	MICS:402 -405MHz	0.78 [127]	Self-developed	
	ISM: 433MHz	2.3 [76]	Self-developed	

$$\begin{aligned}
 P_{single-ch} &= \frac{P_{total}}{m} \\
 CC_{single-ch} &= \frac{P_{single-ch}}{voltage} \\
 P_{total} &= bit_rate \times energy / bit \\
 &= f_s \times n \times m \times energy / bit \\
 &= voltage \times CC_{single-ch} \times m
 \end{aligned} \tag{12}$$

Where, n , m and P_{total} , denote the ADC resolution in bits, the total number of sensing channels, and the total power consumption, respectively. $P_{single-ch}$ and $CC_{single-ch}$ stand for the single-channel power consumption and single-channel current consumption. In Equation 12, the calculation of P_{total} is adapted from Table 1 in [125]. The data comprising n , m and P_{total} was derived from twelve system-level wBMI studies (see the second column in Table 2-7).

Table 2-8 Summaries of Power Consumption of Several Commercialized Wireless Chips

Chips					
nRF2401A	BRF6150	CC2560	CC2540	CC2420	ZL70100
Wireless protocols					
ISM	Bluetooth v1.2	Bluetooth v2.0+EDR	Bluetooth Low Energy	Zigbee	MICS
TX power (mA)					
Max:10.5 [124]	Typical: 25 [130]	Max: 40 [131]	Max: 18.6 [132]	Max: 17.4 [115]	Max:5 [128]

We can clearly see that RF-transmitter-based systems, Zigbee-based systems, and Bluetooth-based systems have the low, medium, and high power consumptions, respectively. This survey result was also confirmed from the related datasheets shown in Table 2-8.

The comparison result is as we expected because the RF protocols are usually proprietary and do not conform to any IEEE standards, are computationally lightweight, and are optimized for specific applications. Bluetooth and Zigbee are IEEE wireless standards. While they provide users with the benefit of interoperability, they also introduce complexities and

overheads that an application may not require, resulting in a higher power consumption and system cost. The advantages and disadvantages of using wBMI with different wireless technology are summarized in Table 2-9.

Table 2-9 Summary of advantages and disadvantages using different wireless technologies for DDD application

Wireless protocol	Advantages	Disadvantages
RF	Longest battery life	Cannot combine with existing smart devices; Need to develop proprietary terminal devices
Zigbee	Longer battery life	
Bluetooth	Seamless connection to commercial smart terminal devices; higher transmission rate	Shortest battery life

Regarding the battery life, two hours should be the minimum for a real-life application. This is because the recommended maximum continuous driving period is just two hours, according to worldwide driver's handbooks [133-135]. In this case, the battery life estimated for a 100-mAh button cell battery and Bluetooth wireless protocol (up to 3 hours) is acceptable. A longer battery life can easily be achieved by using a high-capacity battery (such as the 750-mAh [95], 1100-mAh [61], or 16,000-mAh [56] batteries used in the studies instead of the 100-mAh one used in Table 2-9). Thus, relatively speaking, Bluetooth models are the best modules for EEG-based wBMI system for DDD.

2.4.2.2 Arousing Feedback

Here, we review the arousing feedback methods used to maintain drivers' attention. These methods include visual, vibrational, auditory and non-invasive electronic current-based brain-stimulation techniques.

Specifically, for visual feedback, the display of an alert icon was proposed [136]. However, Belz et al. [137] found that drivers were less sensitive to visual feedback since they needed to pay attention to road conditions and dashboard. For vibrational feedback, a concept of the usage of the built-in vibration sensor of the wristband device (e.g., smartwatch) was proposed [136], but no any experimental evidence was shown. For auditory feedback, C. T. Lin et al. proposed a 1750Hz tone-burst after comparing with 500Hz and 3000Hz tone-burst [5]. They quantitatively showed that when drivers are drowsy the 1750Hz auditory feedback could effectively decrease the θ and α power in the occipital region based on simulated driving experimental results [138]. They further confirmed that this 1750Hz auditory feedback could maintain driver's attention up to 40 seconds [10]. We think that the time is long enough for drivers to have a safe stop on wayside and then take a nap there. However, for commercial drivers, it is unlikely that they are allowed for more time off for rest. Therefore, it is necessary to further investigate drowsiness countermeasures that can enhance alertness. For example, to achieve longer attention maintenance, neuromodulation -based methods are perhaps useful. Neuromodulation -based methods increase the attention and concentration by stimulating brain with small amounts of electronic current (including alternating current [139] and direct current [140-142]). The electrodes could be placed just below the temples [139] or F3 and F4 (in accordance with EEG 10-20 International System [141, 142]). For alternating current-based methods, such as cranial electrical stimulation, the attention maintenance could reach to maximum 4 hours [142]. For direct current-based methods, such as transcranial direct current stimulation (tDCS), the time could reach to at least 6 hours [140]. Both are longer than 2 hours of effect with caffeine [140]. Besides the long-lasting effect, another advantage of using neuromodulation methods is that drivers do not have any side-effect

[139]; while the side-effect of long-term coffee drinking is still controversial. One limitation of these studies is that they mainly focused on the effects on behavioral performance and did not explore EEG dynamics from the perspective of EEG power changes (just like the studies conducted by C. T. Lin's group above [85, 138]). Also, comparing to aforementioned feedback methods, several possible practical hurdles of using current-based neuromodulation are: 1) a slight tingling sensation at the source of the electrodes; 2) the inconvenience of using wet electrodes (usually saline-soaked sponge electrodes); 3) a relatively longer stimulation time to feedback (10~30 minutes).

2.4.2.3 Appearance Design

The available physical designs of a wired BCI system and the EEG sensing parts of wBCI systems are shown in Fig. 2-11. We can clearly see that the wBCI has been fabricated as a baseball cap [56], headband [59, 61, 67, 86, 94, 95], and headset [19, 70, 85, 101, 103]. We think the cap-type and headband-type EEG sensing devices could be more suitable for real-life application because they have better wearable performance (thus better (tighter) contact between EEG electrodes and scalp could be achieved). A complete wBCI system example in a DDD application is shown in Fig. 2-12. This system, which was proposed by our laboratory, consists of an elastic-headband-based EEG sensing device and smartphone-based data-to-knowledge device [97].

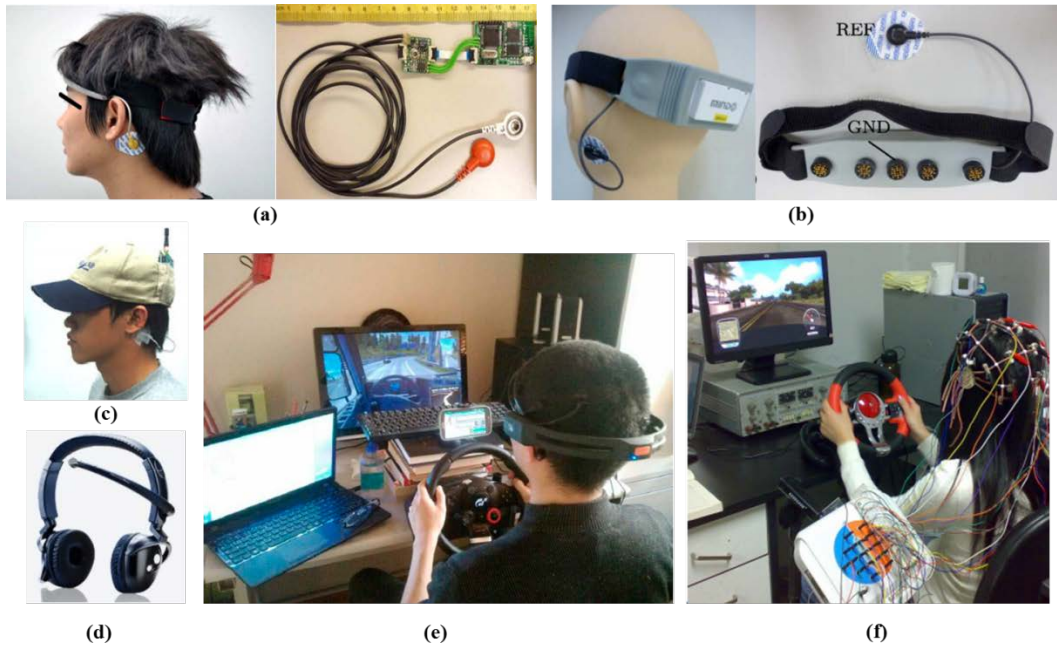
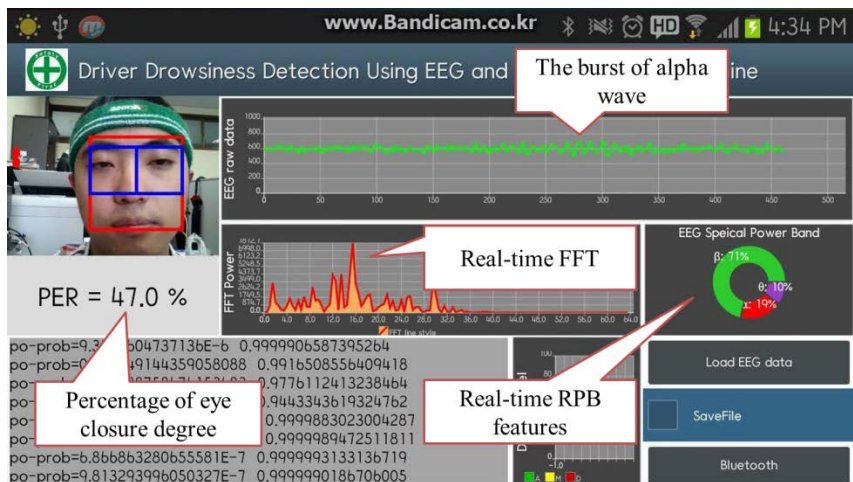


Fig 2-11. Various designs of BCI systems: **(a)** A single-channel wireless occipital EEG acquisition headband [61]. **(b)** A four-channel wireless occipital EEG acquisition headband [95]. **(c)** A baseball cap-based EEG acquisition device [30]. **(d)** A commercialized single-channel wireless frontal EEG acquisition headset (Neurosky Mindset®) [102]. **(e)** A commercialized 14-channel wireless EEG acquisition headset (Emotiv®) [19]. **(f)** A traditional wired BCI system [66].



(a)



(b)

Fig 2-12. An example of a low-cost DDD system based on EEG headband and smartphone [94]. (a) The driving simulation experimental settings. (b) The screenshot of smartphone indicating the raw EEG data, real-time RPB features and PERCLOS reference.

2.4.3 Limitation of Existing EEG-based DDD Approaches

Over the years, many EEG-based approaches have been proposed to combat driver drowsiness. These approaches not only include algorithm-level solutions, but also contain system-level solutions with an aim to apply for real-life driving. However, several unresolved problems in previous studies need to be overcome in this dissertation.

Firstly, the lack of integrated context-aware sensing mechanism. As mentioned in Section 2.4.1.1, for real-life applications, a possible drawback of the aforementioned studies is that inevitable head movements caused by yawning, rubbing of the face or eyes, and moving restlessly on the chair when drivers are slightly drowsy [104], would significantly influence the EEG signal quality and result in unreliable detection results. Therefore, the use of the EEG method alone is not robust enough to recognize a drowsy driver's early features, particularly under real-life application environments with dry EEG sensors.

If EEG data is used as the main signal for DDD, then the head movement data can be regarded as contextual information that could be easily captured by motion sensors. For example, E. Vural *et al.* [143] proposed to use accelerometer to measure the head movements. They mentioned that head motion increased as the driver became drowsy and the head would become still just before falling asleep. One limitation of this study is that they used accelerometer alone instead of the combination of EEG and accelerometer. In addition, the head motion was measured using only one dimension of the accelerometer, which limits the system to a low-directional-resolution output. S. O. Regan *et al.* [144, 145] proposed to use gyroscope to measure head movements. Based on a commercial device with integrated two-dimension gyroscope [146], they successfully recognized the

head-movement-related artifacts in EEG signals. Nevertheless, the head movements mentioned were intentional, as instructed by researchers, as opposed to the natural movements that would occur in real-life applications.

Both accelerometer and gyroscope are commonly used motion sensors. The accelerometer senses gravity as the external references. However, the gyroscope differs significantly. It senses its own rotation without the need for any external reference. Thus, its sensory value goes to zero when head movement ceases, which makes it suitable for detecting the intensity of head movement. Therefore, in this dissertation, we propose to enrich the EEG data with the intensity of head-movement from a simulated driving environment by integrating three-axis gyroscope sensors into the EEG headset.

Secondly, the lack of research on the simultaneous measurements of neuromodulation (tDCS) and EEG for DDD. As mentioned in Section 2.4.2.2, tDCS technology is the most effective alertness boosting solution. It has long-lasting effect compared to visual, vibrational, auditory feedback and even caffeine. However, there was no direct validation of the arousing effect to another technique, such as EEG. Therefore, the integration of tDCS and EEG should be done in this dissertation. Also, a novel closed-loop DDD algorithm should be developed based on this integrated BMI system platform.

Thirdly, the lack of fully wearable wBMI-based DDD system. Previous studies have made great effort to improve the practical utility of wBMI-based DDD system, such as Android smartphone [10] and tablet-based system [9]. These portable smart devices based wBMI system might lead to low-cost and simple-to-use in-vehicle DDD solutions. However, for practical purpose, these in-vehicle devices have the higher risk for producing distracted driving. For example, the authors in [147] mention that drivers

who read, text, watch in-vehicle digital multimedia broadcasting, or use their smartphones are inherently distracted while driving and thus more susceptible to accidents. Particularly, in U.S., 3,154 were killed in distracted driving crashes in 2013. The U.S. government is leading the effort to stop texting and cell phone use behind the wheel. The laws of 12 states even prohibit all drivers from using handheld cell phones while driving [148]. Therefore, to commit to distraction-free driving, a fully wearable wBMI system should be implemented in this dissertation.

Fourthly, the lack of remote monitoring functions. An Internet-enabled wBMI system could be considered in the future because these standalone DDD systems could be useless when installed in the vehicles of selfish drowsy drivers who would not admit that they are a menace on the road and deliberately continue to drive even if a warning alarm has been issued. This would shift DDD from a standalone, self-tracked system to a connected, fully-supervised driver safety technology. To create such a DDD system, Internet connectivity and cloud computing technologies should be applied to current wBMI systems. This may be resolved by using Bluetooth and Internet-enabled mobile smart devices, however, the increased amount of data to be transmitted could shorten the battery life of the overall system. Therefore, EEG data compression algorithms and energy harvesting technologies should also be integrated to future wBMI system.

2.5 Chapter Summary

We have structured this chapter according to algorithm-level studies and system-level studies, in order to facilitate a systematic review of EEG-based DDD approaches. We have further structured the algorithm-level

studies according to standard pattern recognition chain: data sensing, data processing and data-to-knowledge. Also, the system-level studies have been structured according to three important fields for real-life DDD applications: wireless technologies, arousing feedback methods and physical appearance designs.

Based on the techniques reviewed, we conclude the following:

- ①. Bipolar single-channel in occipital region is the most commonly-used EEG channel for DDD research.
- ②. Traditional EEG frequency bands based features are major features and widely used in real-time EEG-based BMI system for DDD application.
- ③. Given no suitable ground truth for continuous-output-type DM models (e.g., probabilistic models and regression models), multi-class classification models are the best models for DDD, in terms of detection resolution and timeliness.
- ④. Given the acceptable battery life, Bluetooth is the best wireless protocol for EEG-based wBMI for real-life DDD application, in terms of advantages such as higher transmission rates and wide accessibility.
- ⑤. tDCS technology is the most effective arousing feedback method. It has long-lasting effect compared to visual, vibrational, auditory feedback and even caffeine.
- ⑥. EEG has direct relationship to drowsiness if compared to other physiological signals. Thus, EEG-based DDD algorithms could achieve quick-detection with shorter data-processing window.
- ⑦. Several unresolved problems in previous studies have been found out. These problems directly correspond to the original

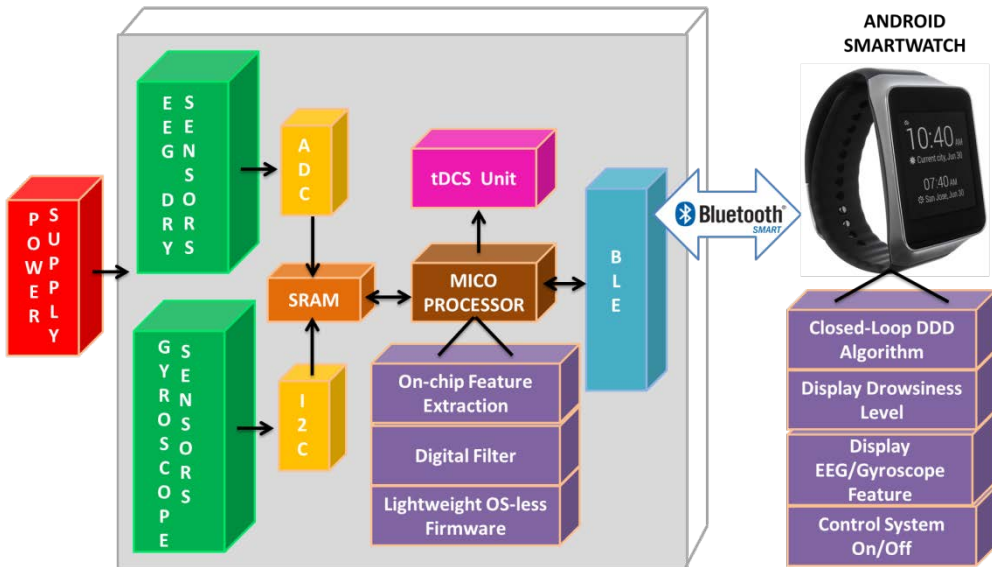
contributions of this dissertation which will be introduced in detail from Chapter 3.

Chapter 3

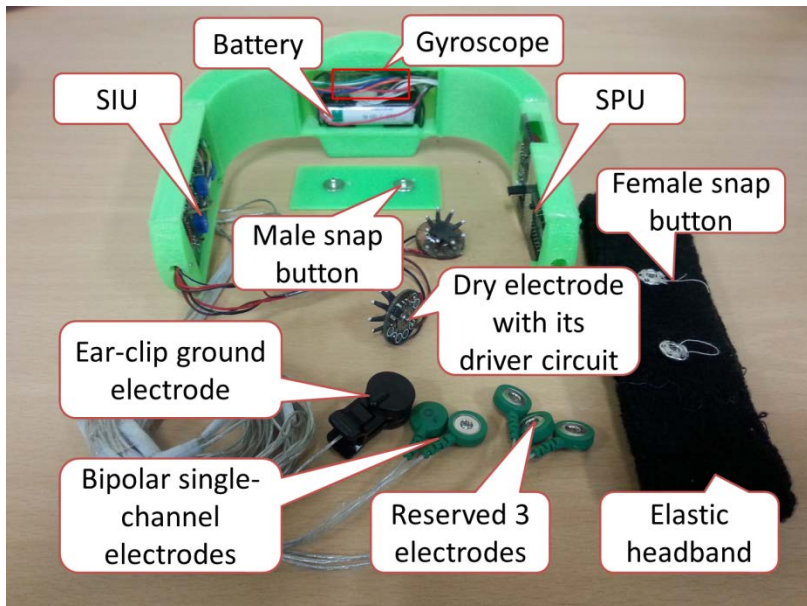
3 Overview of Proposed System

Fig. 3-1(a) shows the proposed DDD system, which consists of a smart BMI sensing headset and a smartwatch. The smart BMI sensing headset is powered by a 3.6 V 2600-mAh lithium-ion battery and incorporates a context-aware sensory input unit (SIU) as well as a sensory processing unit (SPU). The EEG signals from the SIU are converted to digital data by the SPU's 12-bit ADC and stored in the 20K static random access memory (SRAM), together with the digitalized gyroscope data. Then, the EEG and gyroscope features are directly extracted inside of the 32-bit MCU in the SPU. Then, the extracted features are wirelessly transmitted to the smartwatch via a Bluetooth Low Energy (BLE) module [149]. The smartwatch puts these features into a well-trained support vector machine classification model to automatically estimate the driver drowsiness level. If the drowsiness level exceeds a particular threshold, the built-in vibration sensor of the smartwatch would be activated. At the same time, according to the integrated closed-loop DDD algorithm, the tDCS-based neuromodulation module would start to boost driver's alertness with small amounts of electrical current.

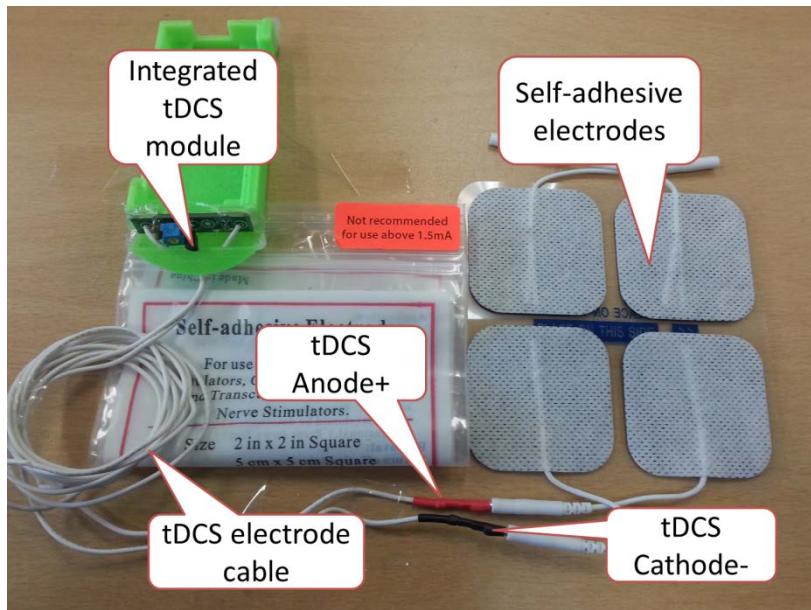
For real-life application, the developed system are put into a specifically designed case which is fabricated by 3D printer and then the case is connected to an elastic headband via two snap buttons (as shown in Fig. 3-1(b)). The following Chapters introduce in detail the major components of this system.



(a)



(b)



(c)



(d)

Fig 3-1. (a) Block diagram of the proposed system. (b) The fabricated headset prototype. (c) The integrated tDCS module. (d) The demo of this fully wearable BMI system.

Chapter 4

4 Design of Smart BMI Sensing Headset

Traditionally, wBMI headset simply gathers data and blindly and wirelessly transmits the data to a terminal device. The proposed smart wBMI headset is an extension of traditional wBMI headset with embedded feature extraction algorithm. The smart BMI headset therefore can extract features locally from sensed raw EEG and gyroscope signals. By the internal feature extraction, the amounts of wirelessly transmitted data and the power consumption of the whole system would be significantly reduced. Following sections introduce in detail the major components of the proposed smart wBMI sensing headset.

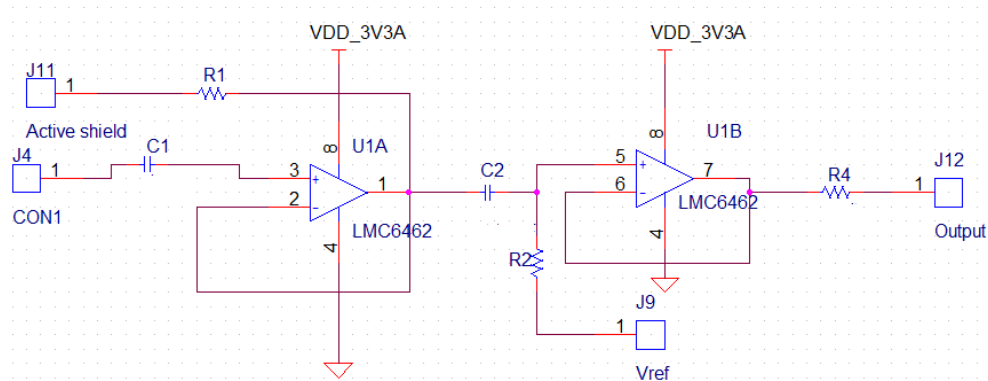
4.1 Context-Aware (CA) Sensory Input Unit

The sensory input unit consists of three EEG dry electrodes, an EEG bio-potentials conditioning circuit and a three-axis gyroscope module. To begin, therefore, we introduce the EEG dry electrodes first.

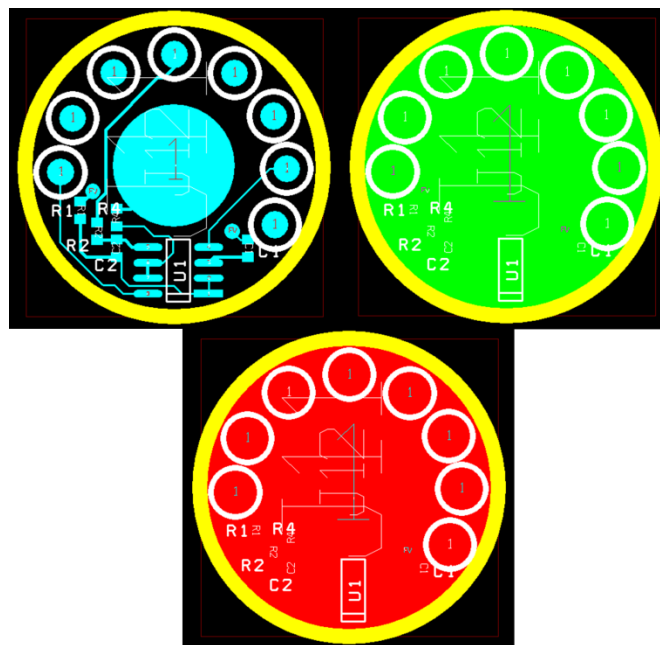
4.1.1 Dry EEG Sensors

One of the three EEG dry sensors is a one ear-clip sensor, from Laxtha Co., Ltd [150], which serves as a ground sensor. It is placed on the earlobe and given 1.65V bias to satisfy the required condition of the SPU's ADC, which is powered by a single positive reference voltage (+3.3V). Two dry sensors, from Cognionics Co., Ltd [46], are used as EEG signal sensors. They are specifically designed for placement in hairy regions. Thus, in this

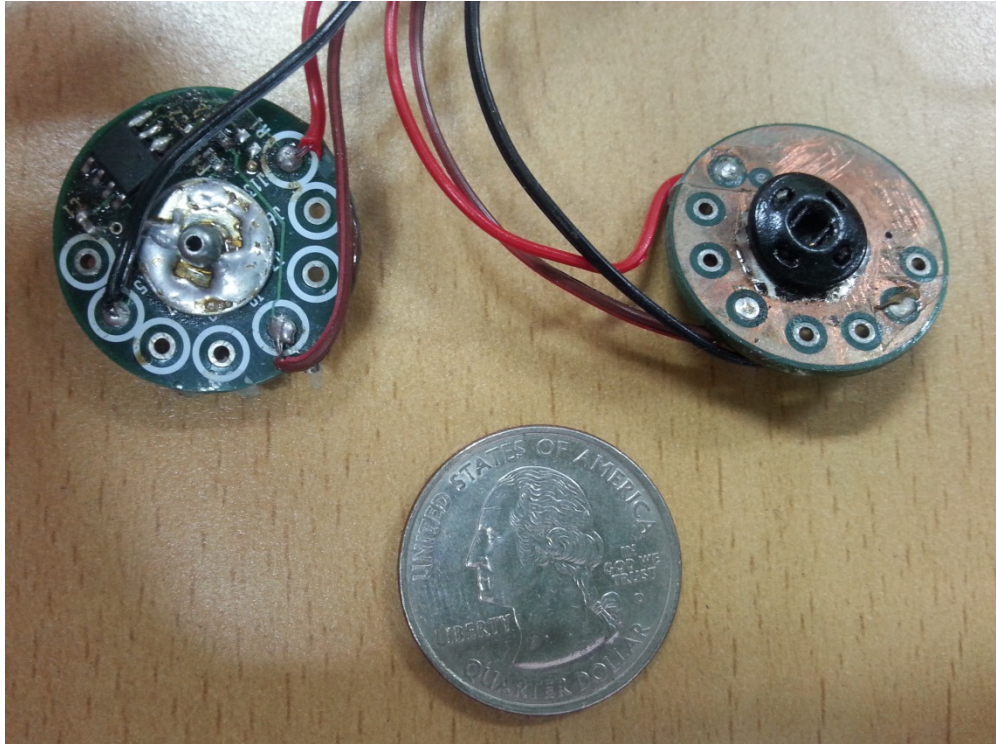
study, they are placed at occipital regions O1 and O2, which are highly correlated with the driver's vigilance level [34]. Before applying them to the EEG bio-potentials conditioning circuit, the driver circuit for the dry signal sensors, adapted from [151], is implemented (See Fig. 4-1). The comparison between conventional wet Ag/AgCl sensors and the dry sensors can be found in Chapter 7.



(a)



(b)



(c)

Fig 4-1 (a) Schematic design, (b) PCB layout design (the upper left: top layer; the upper right: inner layer (active shield); the bottom: bottom layer) and (c) implementation of the driver circuit for EEG dry sensors.

Fig 4-1(b) shows that this driver circuit is a standard 3-layer PCB comprising an onboard amplifier (top layer), active shield (inner layer) and a solid copper fill (bottom layer). The onboard amplifier is the Texas Instrument LMC6462, which is a rail-to-rail CMOS operational amplifier (opamp) in dual SOIC-8 package with an input structure suitable for high impedance instrumentation circuits. The first opamp in Fig. 4-1(a) is

configured as a unity-gain voltage buffer. The 10nF and 10k resistor are used to protect the input of the amplifier and isolate the output of the amplifier from the active shield. A passive RC HPF with a corner frequency of 0.7Hz is used to center the signal around V_{ref} (1.65V bias) and remove low frequency noise or drift. The second opamp in Fig. 4-1(a) is then buffers this high-passed signal and drives the cable connecting the circuit to the EEG bio-potentials conditioning circuit. A 100Ω resistor is used to isolate the cable capacitance from the amplifier's output. It is also important to note that two female snap buttons are included on the top and bottom layer for mechanical stability, as well as compatibility with the male snap button mounted dry EEG sensors and elastic headband.

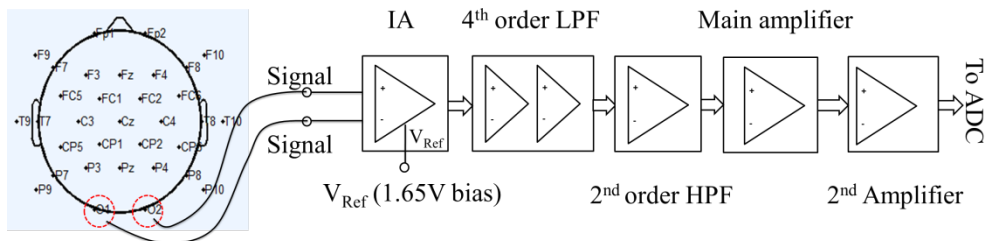
4.1.2 EEG Bio-potentials Conditioning Circuit

Fig. 4-2 (a) illustrates the structure of the designed EEG bio-potentials conditioning circuit, where we can see clearly that the output of the bipolar dry EEG sensors is firstly amplified by an IA (INA28, Texas Instruments) with 16.5X gains ($G_{IA}=1+\frac{50k\Omega}{R33+R34+R39}$, See Fig. 4-2 (b)).

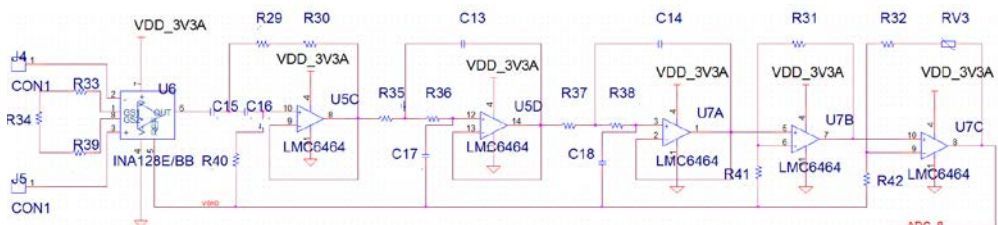
The INA128 is a low-power rail-to-rail IA which features a high differential input-impedance of $10Gohm \parallel 2pF$ and a high CMRR of 100dB when the gains are 10X. Therefore, INA128 can balance the sensor-skin impedance well and reject a large range of common mode signals. The ground dry sensor is given 1.65V bias and serves the reference voltage of the IA. The bias is used to satisfy the required condition of the SPU's ADC which is only powered by a single positive reference voltage (+3.3V). Additionally, in order to acquire the most useful EEG bands for DDD application (θ (4-7 Hz), α (8-13 Hz) and β (13-30 Hz)), the corner frequencies of the LPF and HPF

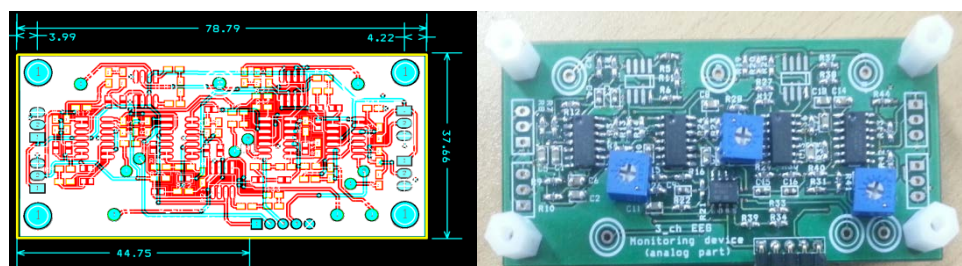
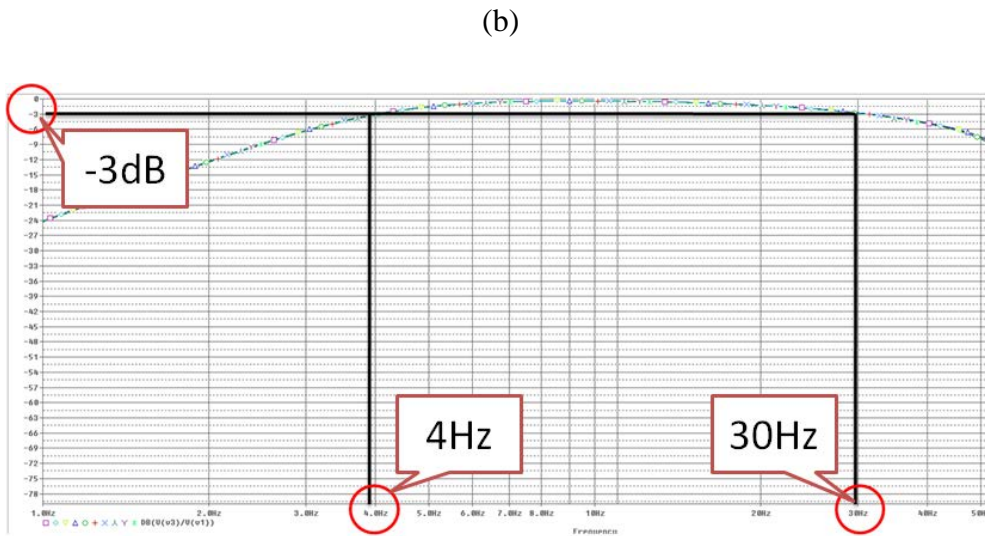
are set to 4Hz ($f = \frac{1}{2\pi C15\sqrt{R40(R29 + R30)}}$, where $R40=2(R29+R30)$ and $C15=C16$) and 30 Hz ($f = \frac{1}{2\pi R35C13}$, where $R35=R36=R37=R38$ and $C13=C14=C17=C18$), respectively. The output signal of IA is transferred to 2nd-order Butterworth HPF and then filtered by the 4th-order Butterworth LPF. Finally, the signal is amplified by the main and 2nd non-inverting amplifier with 151X ($G_{A1}=1+\frac{R31}{R41}$) and 12X gains ($G_{A2}=1+\frac{R32+RV3}{R42}$).

The significance of using non-inverting amplifier is that it features high input impedance and low output impedance, which is similar to voltage follower. The amplifier used here is LMC6464 from Texas Instruments, which is a low-power operation amplifier with rail-to-rail input and output. A notch filter for power-line noise was not included in this circuit because there are no main power outlets in the car environment. For indoor tasks, such as the driving simulation experiment, a digital notch filter was directly implemented on chip to remove 60 Hz power-line noise in real-time.



(a)





(d)

Fig 4-2. (a) Structure design, (b) Schematic design, (c) Circuit simulating (amplitude-frequency response) result, (d) PCB layout design and implementation of the EEG bio-potentials conditioning circuit

Fig. 4-2 (c) illustrates the result of Monte Carlo analysis under the condition of tolerance of resistance and capacitor is 1% and number of measurement is 10) using OrCAD tool ver 9.2. It is clear that the designed circuit works well with standard 3dB attenuation at 4Hz and 30Hz. Also, a

smooth band-pass field is obtained. In Fig. 4-2 (d), it is important to note that the EEG bio-potential conditioning circuit is designed for 3-channel EEG monitoring. In this dissertation, we used one of the 3 channels for DDD study. Two of them are reserved for future study. In addition, we can note that the output voltage of this EEG bio-potentials conditioning circuit ranges from approximate 300mV (minimum amplitude of EEG raw signal (10uV) gained by G_{total}) to 3V (maximum amplitude of EEG raw signal (100uV) gained by G_{total}), where $G_{total}=G_{IA}\times G_{A1}\times G_{A2} \approx 3\times 10^6$. This range matches well with the requirement of input voltage of SPU's ADC, which ranges from 275mV (power supply divided by ADC resolution) to 3.3V (the value of power supply).

4.1.3 Gyroscope Module

We use L3G4200D as the sensor platform for collecting the gyroscope data. The L3G4200D is from a ST semiconductor, which is a low-power three-axis digital output gyroscope. It integrates the LPF, HPF and 16-bit ADC and also supports the I2C and SPI digital output interface. In this study, the L3G4200D are integrated on the EEG headset (see Fig. 4-3). The 16-bit sensor readings are transferred directly to the SPU via the I2C connection. The directions of the three axes are shown in Fig. 4-3, where X, Y, Z axes direct to the right-left, up-down and front-rear directions, respectively. Therefore, the head-movements around the three axes can be captured. For example, the X axis is used to capture yield and look up head-movements, such as yawning; the Y axis is used to capture left-right head shaking movements; and the Z axis is used to capture left-right head swaying movements. The measurement range of this module is set as ± 250 degree/s.

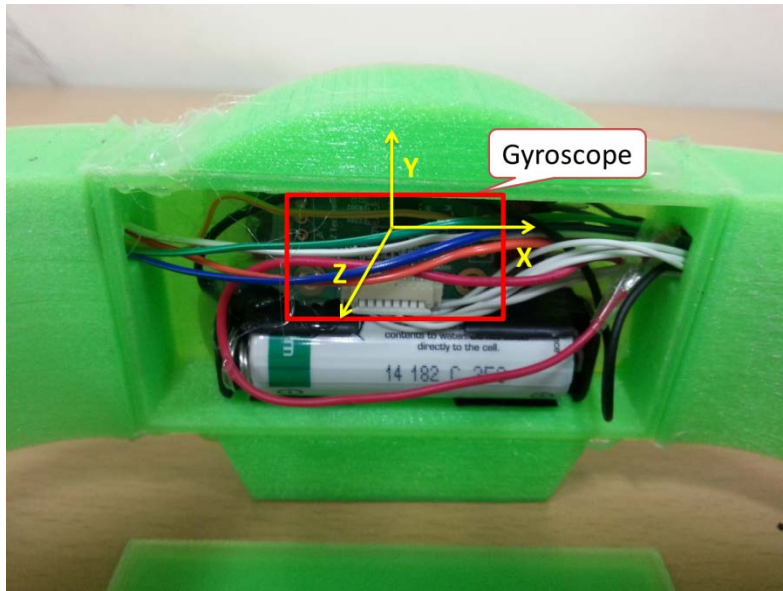


Fig 4-3. The integrated 3-axis gyroscope and its direction.

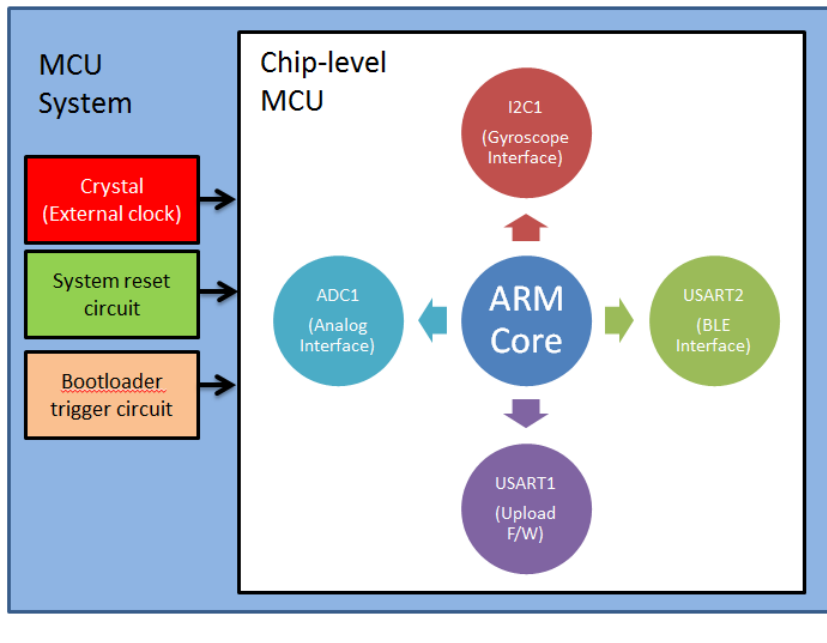
4.2 CA Sensory Processing Unit

The sensory processing unit (SPU) consists of a self-developed MCU system and a commercial BLE transmitter.

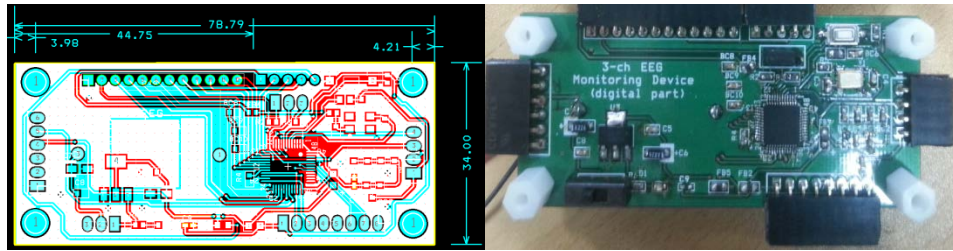
The MCU is STM32F103CB from a ST semiconductor. The STM32F103CB was chosen because it is ARM 32-bit Cortex-M3 based MCU with maximum 72MHz core frequency. It also provides 128KB flash, 20KB SRAM space, two DMA-enabled 8-channel 12-bits ADCs, two I2C interfaces and three USARTs. In fact, teardowns of many wearable products available today have already revealed wide use of Cortex-M class processors. These products include a Pebble smartwatch that integrates a STM32 Cortex-M3 MCU, accelerometer, magnetometer, and Bluetooth connectivity; the Fitbit Flex activity tracker which also integrates an STM32 MCU, plus accelerometer and Bluetooth.

With the highly successful ARM core and rich peripherals, STM32F103CB MCU is highly suitable for running real-time feature extractions on chip if compared to 8- and 16-bit MCU. In this study, it operates at 3.3 V with a clock speed of 8MHz. The MCU's state-machine loop repeats at an interval equivalent to the sampling rate of 128 Hz. The BLE is used because the smartwatch has embedded BLE microprocessors with capabilities for connecting wirelessly to external biomedical sensors by lower power consumption.

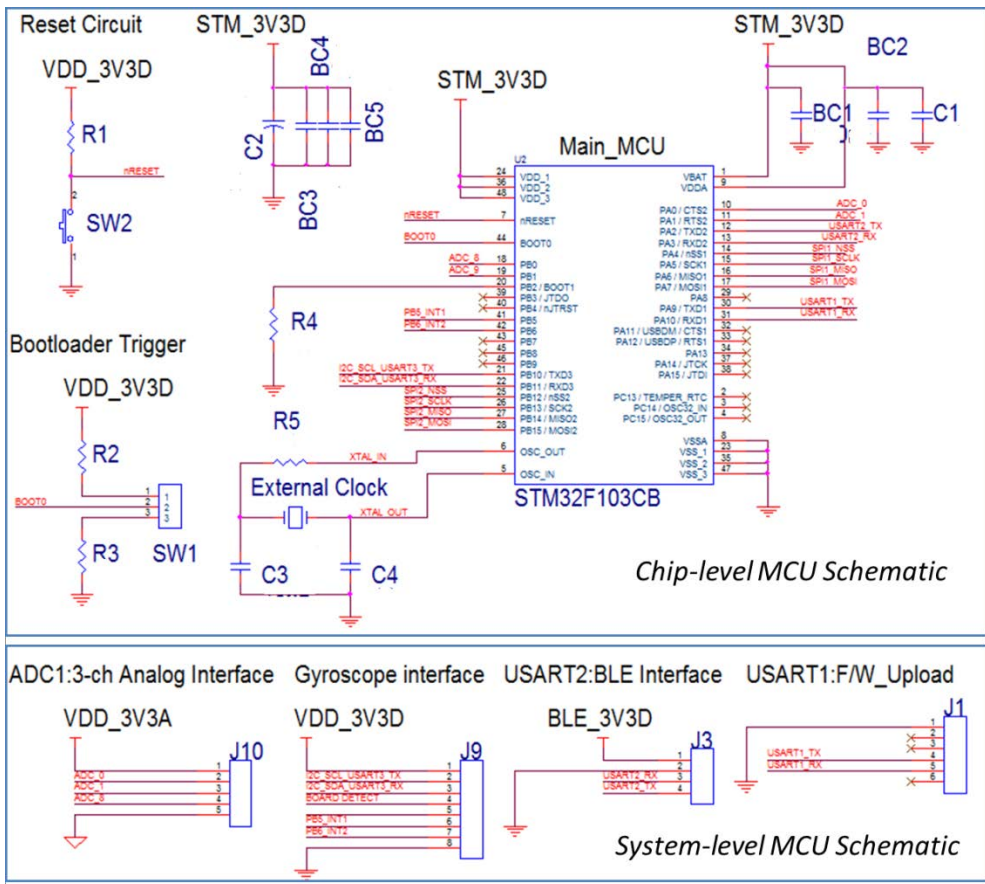
Generally, wireless transmission is the most power-demanding component of wireless sensor nodes [51]. Therefore, the combination of on-chip feature extraction and BLE in this study aims to reduce the transmitted data and the whole system power consumption. A self-developed lightweight OS-less firmware (F/W) is implemented on the 32-bit MCU to control the whole SPU. Fig. 4-4 demonstrates the developed MCU system.



(a)



(b)



(c)

Fig. 4-4 (a) Structure design, (b) PCB layout design and implementation, (c) Schematic design of the EEG bio-potentials conditioning circuit.

4.2.1 On-chip Signal Processing

A digital 4th order butterworth LPF (corner frequency=30Hz) is implemented in the SPU to further filter the EEG signals, particularly the power line noise (60Hz). Then, for each 2-second EEG and gyroscope epoch, the following feature extraction approaches are operated, respectively.

On-chip EEG Feature Extraction: Relative Band Power (RBP). First, FFT power is calculated as the sum of the squared FFT magnitude of the EEG signals; then, the RBP is calculated by dividing the FFT power of one EEG band by the sum of the FFT power of all three EEG bands, as shown in Equation 13, where $b_i=\{\theta, \alpha, \beta\}$.

$$RBP(b_i) = \frac{Power(b_i)}{\sum_{i=1}^3 Power(b_i)} \times 100\% \quad (13)$$

On-chip gyroscope Feature Extraction: Movement Power (MP). The MP was developed for the accelerometer by Da-Wei Chang *et al.* [152]. As in their work, the MP is applied to the gyroscope analysis in this study. First, the gyroscope magnitudes of the three axes are averaged; then, the standard deviation of the averaged gyroscope signals in one epoch, defined as the MP, is calculated as shown in Equation 14.

$$Gyro_{avg} = (Gyro_x + Gyro_y + Gyro_z)/3 \quad (14)$$

$$MP = STD(Gyro_{avg})$$

It is very important to note that before finally settling with RBP and MP on MCU, other EEG and gyroscope features shown in Table 4-1 were

compared using the area under receiver operating characteristics curve. The comparison result is summarized in Fig. 7-19 in Section 7.3.5.2.

Table 4-1 Time and Frequency-Domain Features Extracted From EEG and Gyroscope Signals

Signal	No.	Features	Reference
EEG	1	θ/β	[62]
	2	$\theta/(\alpha+\beta)$	[69]
	3	$(\theta+\alpha)/\beta$	[69]
	4	$(\theta+\alpha)/(\alpha+\beta)$	[69]
	5	θ/α	[110]
	7	α/β	[62]
	8	$(0.6*\theta + 0.4*\alpha)/(0.5*\beta)$	[70]
	9	Relative band power (RBP)	[84, 100]
Gyroscope	1	Movement power (MP)	current study
	2	Magnitude (Mag)	[144, 145]
	3	Total FFT power	[144,145]
	4	FFT power of X-axis	current study
	5	FFT power of Y-axis	current study
	6	FFT power of Z-axis	current study

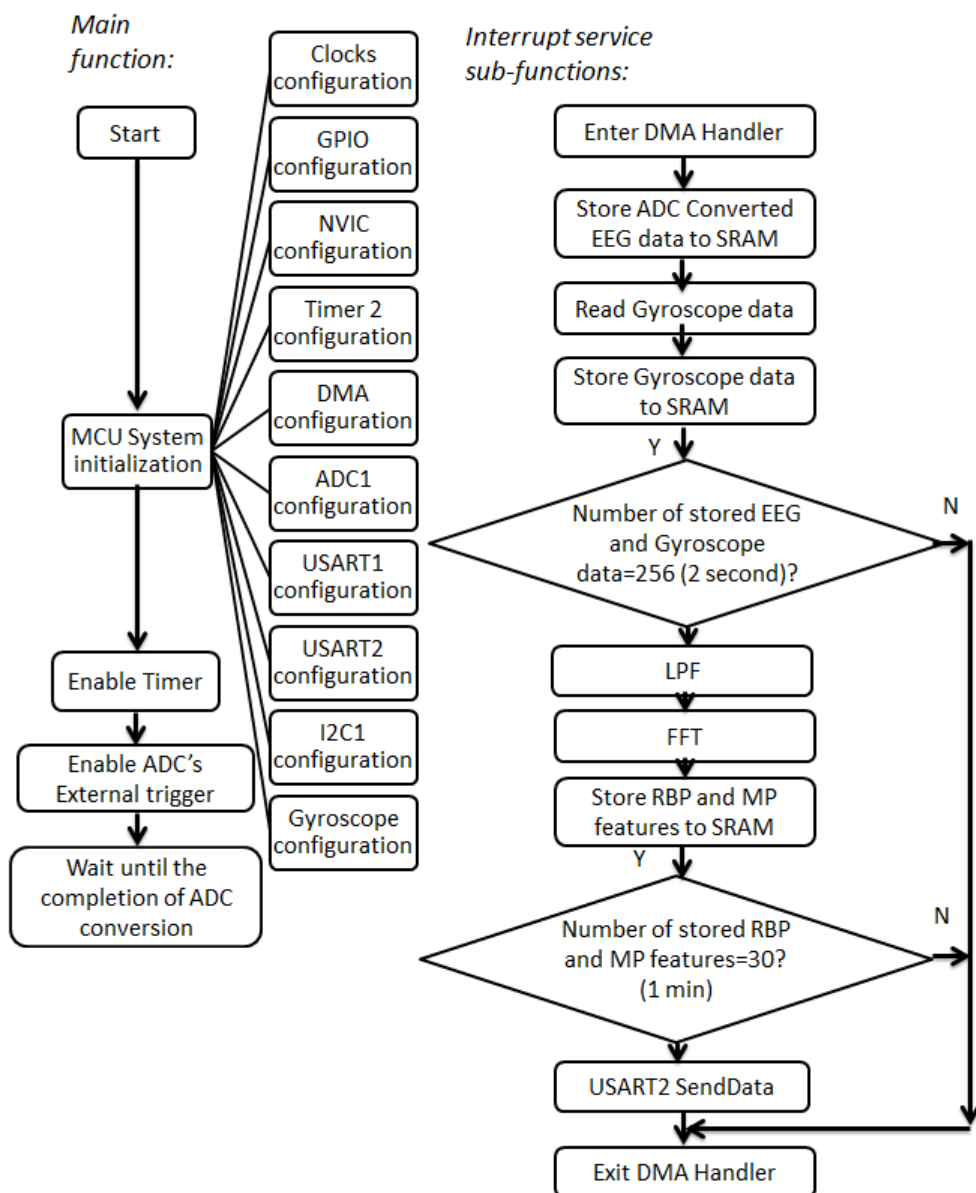


Fig. 4-5. The on-chip feature extraction algorithm.

Therefore, a set of four features (Per (θ), Per (α), Per (β) and MP) were extracted from each 2-s epoch. In order to synchronize the extracted features with the 1-min video-based ground truth (See Section 7.1), every

30th feature set was successively averaged before transmitting to smartwatch. The complete on-chip feature extraction algorithm is demonstrated in Fig. 4-5, in which the implementation of on-chip digital LPF is shown in Fig. 4-6.

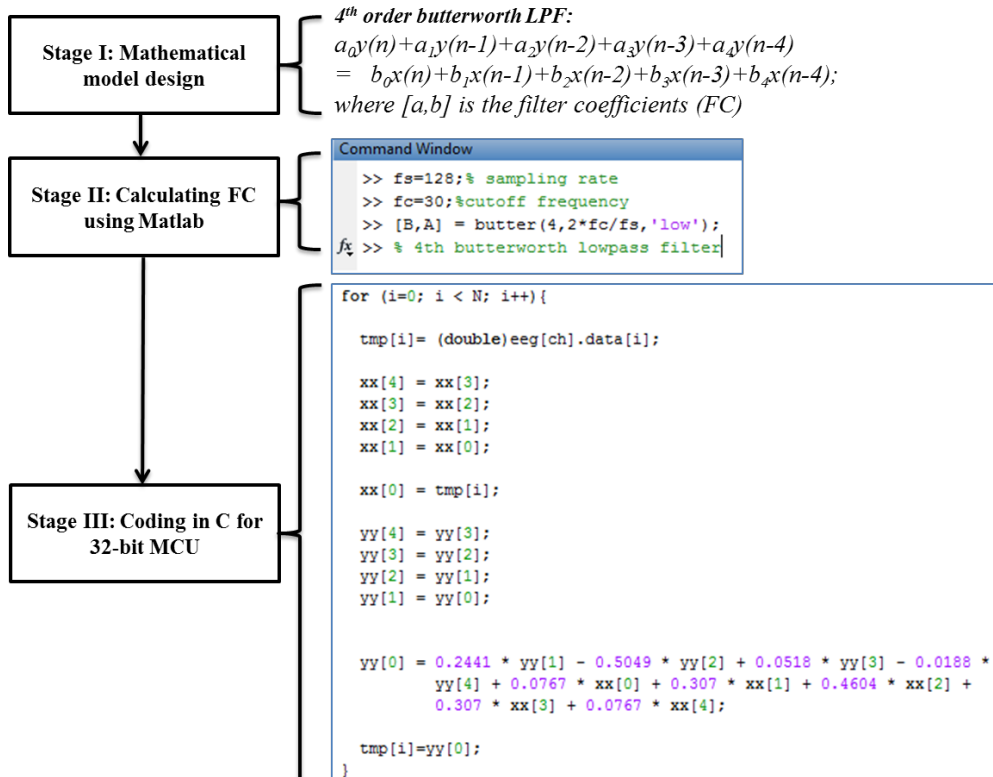


Fig. 4-6 The implementation of on-chip digital LPF

4.2.2 Bluetooth Low Energy

Bluetooth wireless technology is a short-range communication system intended to replace the cable(s) connecting portable and/or fixed electronic devices. In general, there are two forms of Bluetooth wireless technology systems: Bluetooth Basic Rate (BBR) and Bluetooth Low Energy (BLE). The theoretical maximum communication distance is about 100m for

both BBR and BLE, which is long enough for in-vehicle environment based DDD application.

The BBR system supports maximum 2 or 3Mb/s with enhanced data rate alternate media access control and physical layer extensions. With the higher data rate, BBR system was originally designed for continuous, streaming data applications. Given the aforementioned on-chip feature extraction, the BMI headset here transmits data to smartwatch every minute. Therefore, BLE system which was originally designed for applications with lower data rates and lower duty cycles is used in this study.

Figure 4-7 shows the Bluetooth stack for BBR and BLE. The point being, here, that at the bottom, we can see clearly that BLE uses low energy RF. Instead of streaming data like BBR stack, this RF is optimized just for bursting out these small attributes of data and then powering back down again. This is how BLE stays so low energy. And the protocol stack, instead of being this enormous array of protocols, is really focused on the one attribute profile. And on the profiles at the top, instead of all the different profiles, BLE just focuses on the GATT profile. So, actually, BLE stack is a fraction of the size of the BBR stack. And because of the low energy RF, it needs a fraction of the size battery. And BLE devices, of course, are a fraction of the cost and run for a lot longer. To compare more details, Table 4-2 summarizes the comparison of DDD-related technical specification between BBR and BLE including communication distance, data rate, application throughput, power consumption and real-time performance indicators (e.g., latency and minimum total time to send data).

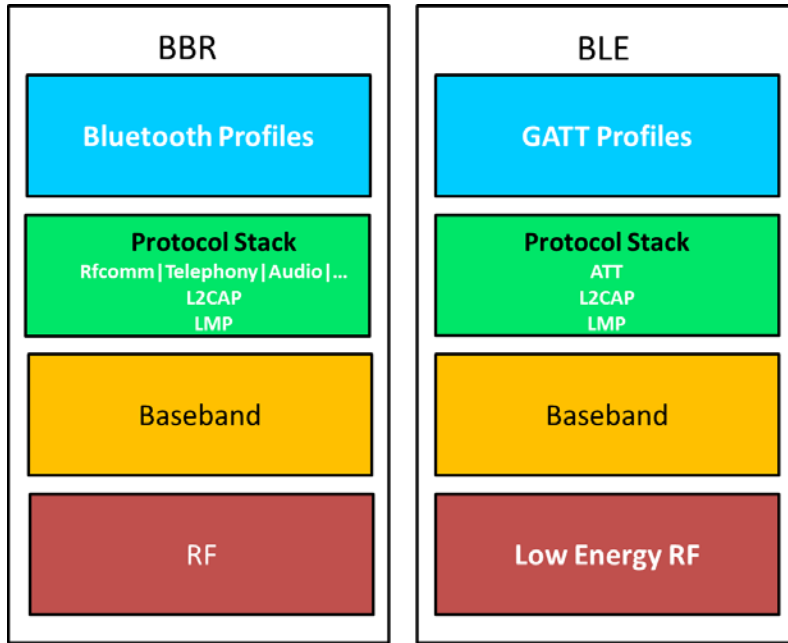


Fig. 4-7. The comparison of Bluetooth stack between BBR and BLE

Table 4-2 Comparison of technical specification between BBR and BLE

Technical Specification	Classic Bluetooth technology	Bluetooth Smart technology
Distance/Range (theoretical max.)	100 m	>100 m
Over the air data rate	1–3 Mbit/s	1 Mbit/s
Application throughput	0.7–2.1 Mbit/s	0.27 Mbit/s
Latency (from a non-connected state)	Typically 100 ms	6 ms
Minimum total time to send data	100 ms	3 ms
Peak current consumption	<30 mA	<15 mA

Figure 4-8 illustrates the BLE data payload packet format in this study. In total, this data payload consists of 34 bytes including 2-byte channel information (1 byte for EEG: 0x00; 1 byte for Gyroscope: 0x01) and 32-byte feature information (3×8 bytes for double-type RBP (θ, α, β) features and 8 bytes for double-type MP feature). For implementation, the BLE mini from redbearlab is used in all experiments.

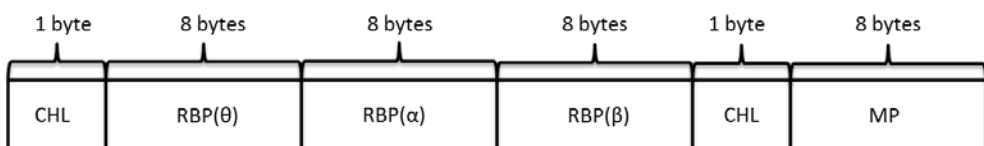


Fig. 4-8. The BLE data payload packet format

4.3 Transcranial Direct Current Stimulation (tDCS)-based Neuromodulation Unit

The tDCS encompasses the induction of a relatively weak constant current flow through the cerebral cortex via scalp electrodes. The technique was established in the 1950s and 1960s primarily in animals [153]. In these early animal studies, researchers found that the tDCS could induce long-lasting after-effects (at least some hours after the end of stimulation) on neuronal excitability [153]. Most of the effects and mechanism of tDCS stimulation seems to be similar or identical to those effects found in humans. Anodal tDCS enhances, while cathodal tDCS reduces cortical excitability. These effects evolve during stimulation and outlast it for hours-long as long as sufficiently long stimulation duration of some minutes is given [153].

For humans, tDCS is originally used to address neurological disorders such as Parkinson's disease, major depressive disorder, stroke

rehabilitation, chronic pain and etc. However, there has been a rapid expansion of research over past decade showing that tDCS is effective in enhancing human performance in everyday life situations, sustained attention in particular [140]. As mentioned in Section 2.4.2.2 and 2.5, tDCS-based neuromodulation technology is the most effective arousing feedback method for drivers. It has long-lasting arousing effect compared to visual, vibrational, auditory feedback and even caffeine.

With regard to the safety of tDCS, currently applied stimulation protocols (typically 1-2mA intensity, electrode size between 25 and 35cm², stimulation for up to 30min per session) should be regarded as safe [153]. Within these limits, no major adverse events had been reported so far for about 2000-3000 subjects in laboratories worldwide. In this section, we will introduce in detail the tDCS-based neuromodulation unit which consists of tDCS electrodes and tDCS circuit.

4.3.1 tDCS Electrodes

Generally, there are two different types of electrodes that can be used with tDCS; self-adhesive and sponge electrodes (as shown in Fig. 4-9).

Self-Adhesive electrodes are inexpensive, and require almost no preparation for use. However, while these types of electrodes are convenient, they can only be used on bare skin areas, with little to no hair. These types of electrodes require a clean surface and secure connection to be most effective. Additionally, self-adhesive electrodes are not recommended for use current ranges above 1.5mA.



Fig. 4-9. Self-adhesive electrodes (the left); Sponge electrodes (the right)

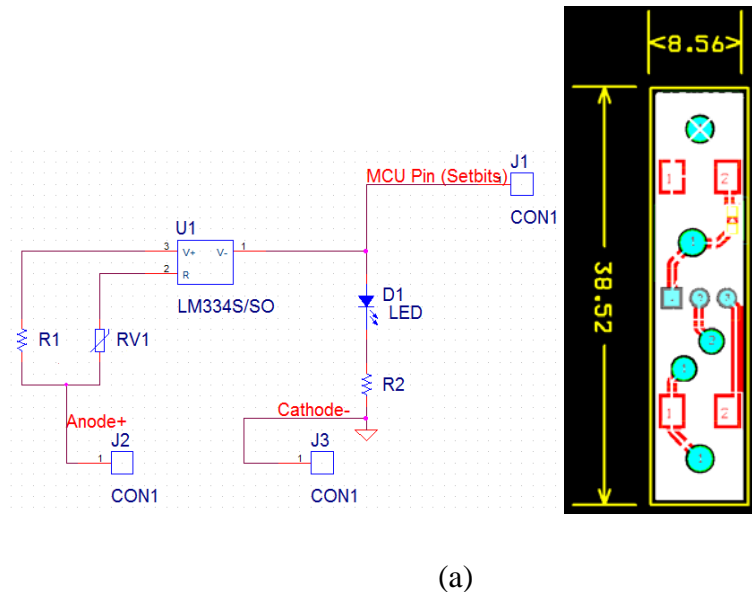
Sponge electrodes are by far the best electrodes for tDCS, however most sponge electrodes on the market are quite expensive. Additionally, sponge electrodes need to be soaked in a saline solution (water + salt), but allow the user to access even thick hair areas with ease. Something such as a headband is usually used to hold sponge electrodes in place during a tDCS session.

In this study, the inexpensive self-adhesive electrodes are used because the electrode placement is non-hairy forehead region (Fp1 and Fp2 as shown in EEG 10-20 International System in Fig. 2-3(b)). It is important to note that the size of the self-adhesive electrodes is $5\text{cm} \times 5\text{cm} = 25\text{cm}^2$ (each), which is three times larger than the EEG dry sensors ($\approx 8\text{cm}^2$ each). The larger size of self-adhesive electrodes here is just for the sake of safety in humans. As we know, the larger the average current density (ACD) under the electrode contacting area is lower. So, a standard 25cm^2 size can obtain

an ACD of $0.06\text{mA}/\text{cm}^2$ if the current is 1.5mA , which can avoid burning skin.

4.3.2 tDCS Circuit

The developed tDCS circuit is based on a chip-level current source (LM334Z, Texas Instruments, USA) that sets and stabilizes the current at a fixed level. LM224Z is a three terminal adjustable current source where the current level was conveniently set with few external resistors, i.e., an analog potentiometer in particular. The developed tDCS circuit is capable of providing a maximum 2mA constant current. The on/off of the current delivering is controlled by the integrated closed-loop DDD algorithm (See Chapter 6) via a MCU's single pin. Fig. 4-10 shows the design of tDCS schematic, PCB layout and implementation.



(a)



(b)

Fig. 4-10. (a) Schematic design (the left), PCB layout design (the right), (b) implementation of the tDCS-based neuromodulation unit.

4.4 Fabricating Headset case using 3D Printer

3D printer has emerged as powerful tool for customized model design. Therefore, in this study, the developed BMI headset circuit is put into a specifically designed headset case which is fabricated by 3D printer (3DISON, Seoul, South Korea), in order to realize a real-life application. The fabricating material is Polylactic Acid (PLA) filament. As shown in Fig. 4-11, applying 3D printer includes three stages – Stage I: Appearance design using Solidwork software; Stage II: 3D printer preparation involving the generation of 3D printer readable G-code from dot stl format of Solidwork; Stage III: Implementation of the fabrication of BMI headset using 3D printer.

Fig. 4-12~14 demonstrates the Stage I-III vividly.

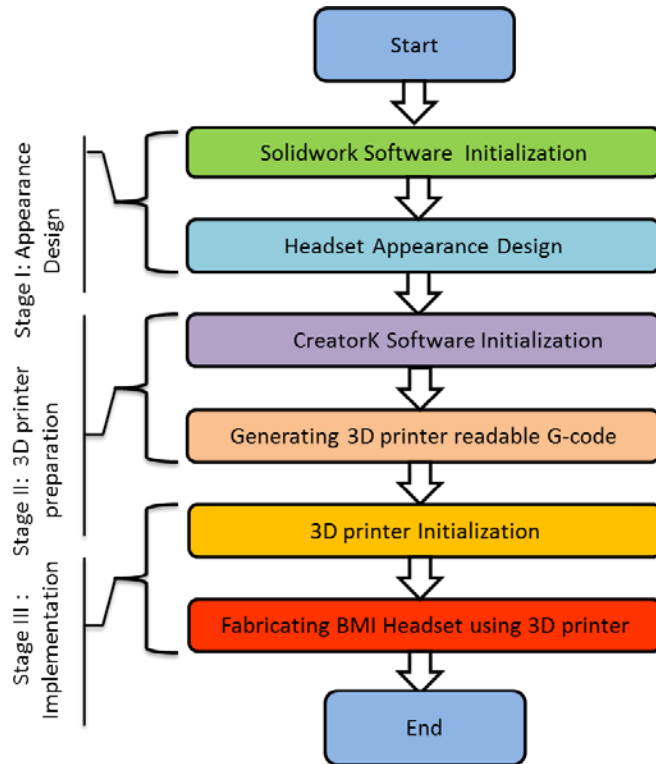
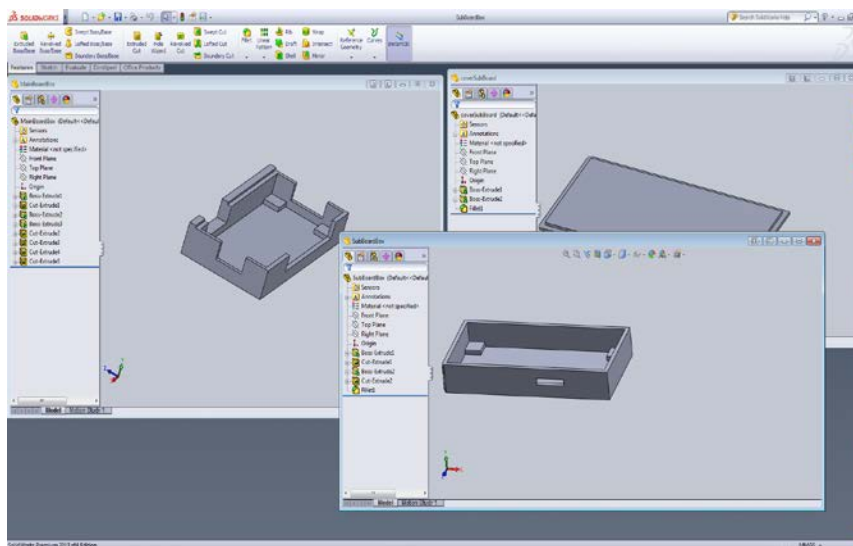
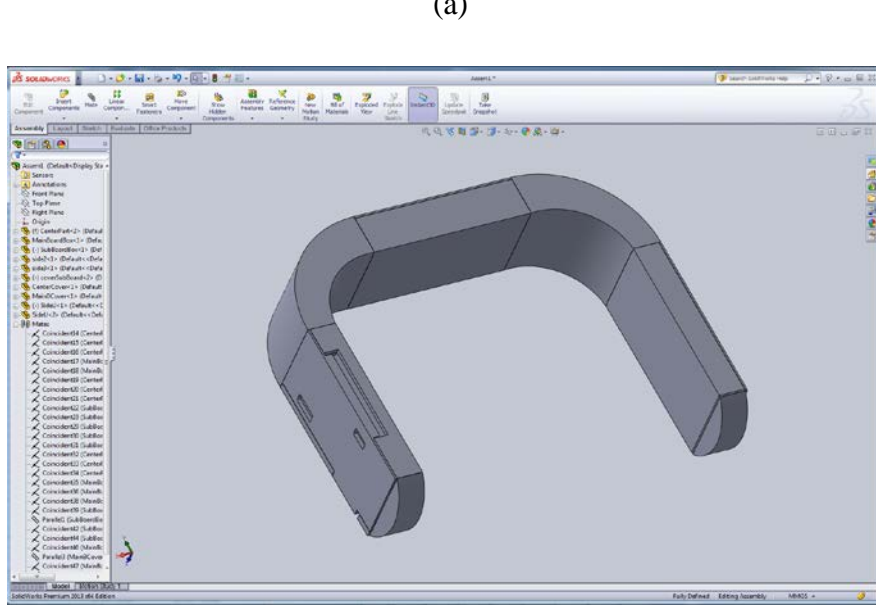


Fig. 4-11 The working flowchart of BMI headset fabrication using 3D printer





(a)

Fig. 4-12 Appearance design including (a) part design and (b) overview design

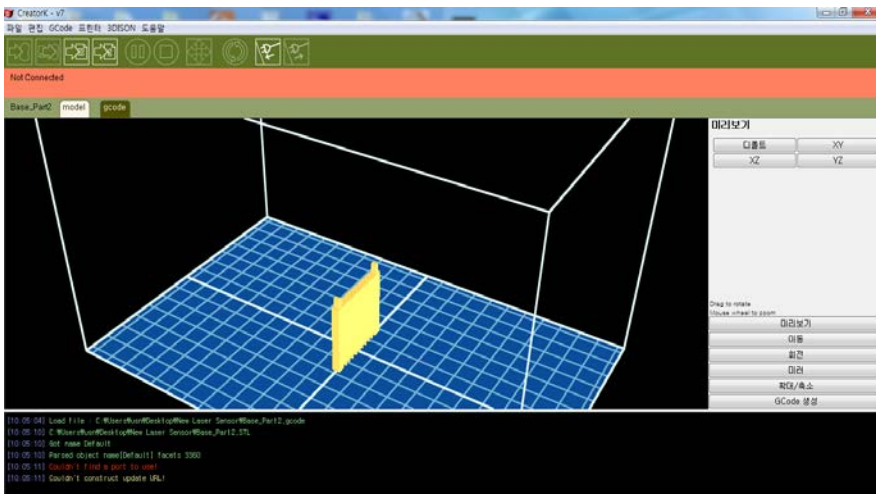


Fig. 4-13 3D printer preparation using Creatork software

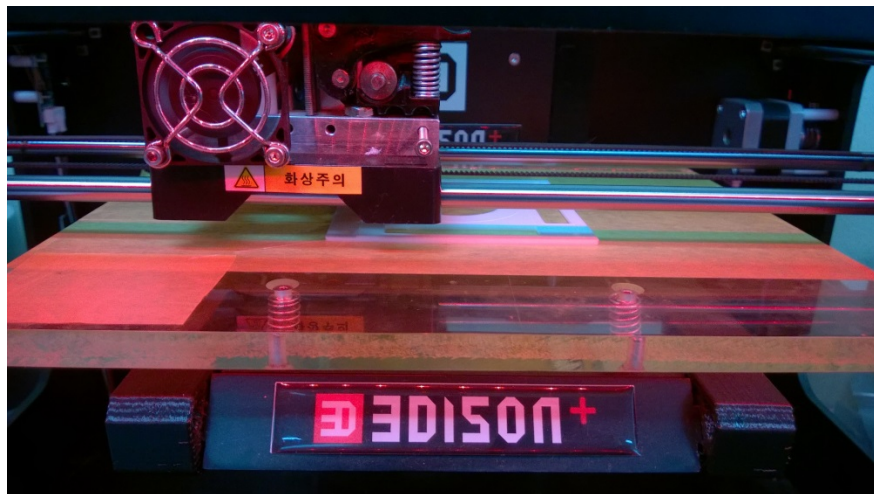


Fig. 4-14 Implementation of fabrication of headset case using 3D printer

4.5 Chapter Summary

This chapter introduced the design and implementation of the brain machine interface headset in detail. The headset is decomposed into several units to reduce the system complexity and increase its flexibility in debugging. The units are: context-aware sensory input unit, context-aware sensory processing unit and transcranial direct current stimulation technology based neuromodulation unit. The principle focus aspect of such design and implementation is the practical utilization of an integrated brain machine interface to carry out multiple tasks for closed-loop driver drowsiness detection.

Chapter 5

5 Design of Android WearTM-based BMI Terminal Device

Wrist-worn smart devices have emerged as miniature but powerful wearable platforms for data acquisition and processing (as shown in Fig. 5-1).

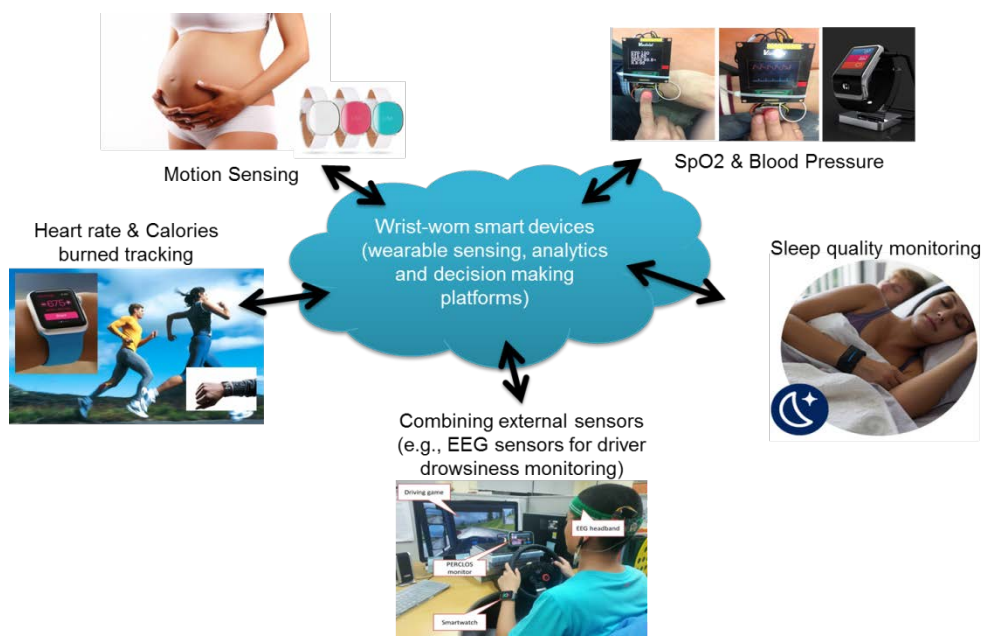


Fig. 5-1 Examples of various wrist-worn device based applications

In general, two operating systems (OS) had been dominating the wrist-worn wearable market: Google Android WearTM OS (first released on March 18, 2014 [172]) and Apple WatchOSTM (first released on April 24, 2015 [173]). Unlike WatchOS's closed source model, Android Wear's source model is open. This means that developers will have the chances to take a closer look into the system to suit their needs. Therefore, there is a

variety of Android WearTM OS based wrist-worn devices in the market including Motorola Moto 360, LG G Watch and Samsung Gear Live. According to Canalys's estimation [154], by the 3rd quarter in 2014, Samsung wrist-worn devices have the largest worldwide market share, accounting for 52%, which is followed by 15% of Motorola and 33% of others.

In this study, an Android WearTM OS based smartwatch, Samsung Gear Live, serves as a wireless and wearable BMI terminal device, which is responsible for continuously collecting the EEG and gyroscope features and estimating drowsiness levels. If the estimated drowsiness level exceeds a particular threshold, the smartwatch will enable tDCS-based neuromodulation to boost driver's alertness, according to the integrated closed-loop DDD algorithm (See Chapter 6). The advantages of using Android WearTM OS based smartwatch as the BMI terminal device are as follows:

- ①. Low-power wireless communication
- ②. Built-in well-designed power-saving mode
- ③. Less distraction from the driving tasks

5.1 What is Android WearTM?

Android WearTM is a version of Android OS. It is specially designed for smartwatches and other wearables. Basically, Android WearTM OS is an UNIX-like OS based on 3.x Linux kernel (Linux kernel is a widely-used open-source kernel for PC and embedded devices since 1991). It can run on many different device types, even ones with square or circular screens. The foremost features provided by Android WearTM OS are as follows:

- ①. **Really simple user interface (UI) that optimized for small screens**
- ②. **Carefully designed power-saving mode** (e.g., Battery saver and deep sleep mode)
- ③. **Low-power wireless communication:** BLE connectivity.
- ④. **Rich integrated sensors:** Compass, accelerometer, gyroscope, vibration sensor and heart rate sensor (hardware dependent).
- ⑤. **Rich healthcare applications:** heart rate monitoring, riding and running tracking, step-counting, calorie expenditure and etc.
- ⑥. **Tactile notification:** The vibration sensor alerts users about important notifications originating from a user-selectable set of applications (e.g., traffic, flights, meeting alerts and etc).
- ⑦. **Hands-free application** (Voice-controlled application): voice-controlled searching engine and etc.
- ⑧. **Efficient communication with smartphones:** Pairing with smartphones running Android version 4.3+ and even iOS 8.2 or later (just since August 31, 2015). For example, Android Wear™ users can reply the incoming text messages by voice.
- ⑨. **Powerful development environment:** Android studio

Although there is no Google official software stack for Android Wear™ OS, based on aforementioned features, we can infer that the most of Google's work on Android Wear™ OS is related to an entirely new interaction model. This results in the fundamental difference between Android Wear™ OS and Android Phone or Tablet OS — the zero or low interaction. Android Wear™ OS focuses on simple interactions, only requiring input by the user when absolutely necessary. Most inputs are based around simple touch swipes and voice, and inputs requiring fine-grained

motor skills are avoided. In this case, the Android Wear™ users not only can have less distraction from the world around them, but also still can get more information about what's happening.

5.2 Android Studio™

The Android Wear™ applications are written in JAVA language based on the APIs provided by the Android Wear™ Software Development Kit (SDK). In this section, we will briefly introduce the recommended SDK for Android Wear™ application — Android Studio™ [174].



Fig. 5-2 The history of Android development tools: From Eclipse ADT to
Android Studio™ v1.0+

Android Studio is an integrated development environment (IDE) for the Android platform including phone platform, tablet platform and wearable platform. Android Studio was first released in May 2013, and then entered beta stage which was released in June 2014. The first stable version was released in December 2014, starting from version 1.0. Since the launch of stable version, the majority of users of Eclipse Android Development Tools

(ADT) have made the transition over to Android Studio (as demonstrated by Fig. 5-2).

Eclipse ADT is a plugin for the Eclipse IDE (a multi-language software development environment which is developed by Eclipse open-source community). Once the ADT is installed on the Eclipse IDE, it allows Eclipse to create Android application, start up the Android virtual device and offer debugging tools for extensive debugging the developed application. Table 5-1 shows the reasons why Android Studio outperforms Eclipse ADT, the last statement in bold and italic in particular.

Table 5-1 Comparison of Eclipse ADT and Android Studio

Eclipse ADT	Android Studio
Mature and very stable	New and powerful, relatively stable (v1.0+)
Heavy	Lightweight
Slow	Flexible build management system
Building is a pain	Improved visual editor for UI design
Poor UI design preview	Fast and accurate code completion and refactoring
Untimely crashes	Advanced lint checker options
Lint checker is basic	Built-in support for Google cloud platform
Mainly for JAVA	ProGuard and app-signing capabilities
<i>Services will be suspended by Google at the end of 2015.</i>	<i>Continuously updated by Google</i>

5.2.1 Android Studio Interface

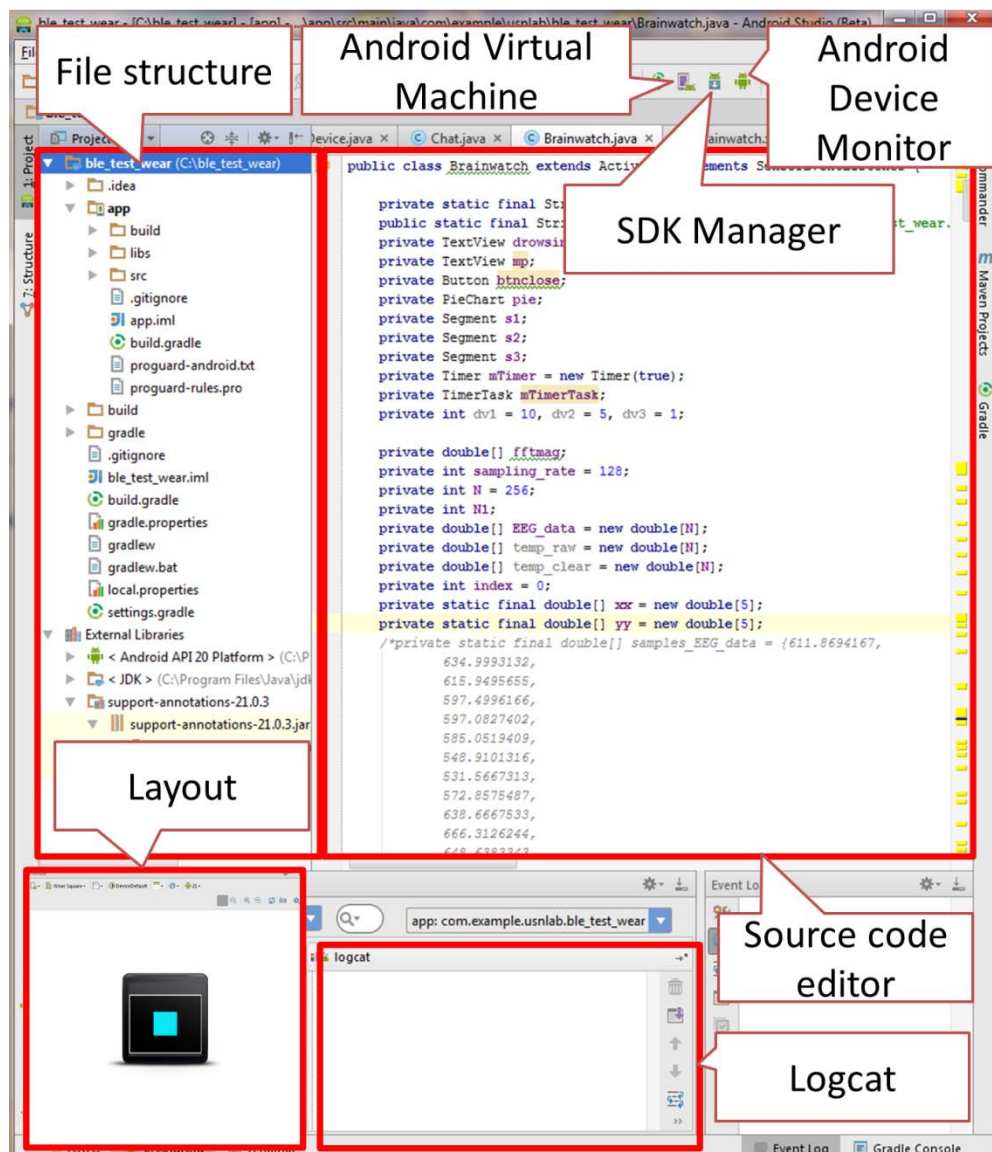


Fig. 5-3 Android Studio interface for Android Wear™ project

Fig. 5-3 shows the interface of Android Studio™ for a new Android Wear™ project which mainly consists of Android Studio™ SDK Manager, file structure, source codes editor, layout, Android Virtual Device (AVD), Android Device Monitor (ADM) and Logcat.

5.2.2 Android Studio™ SDK Manager

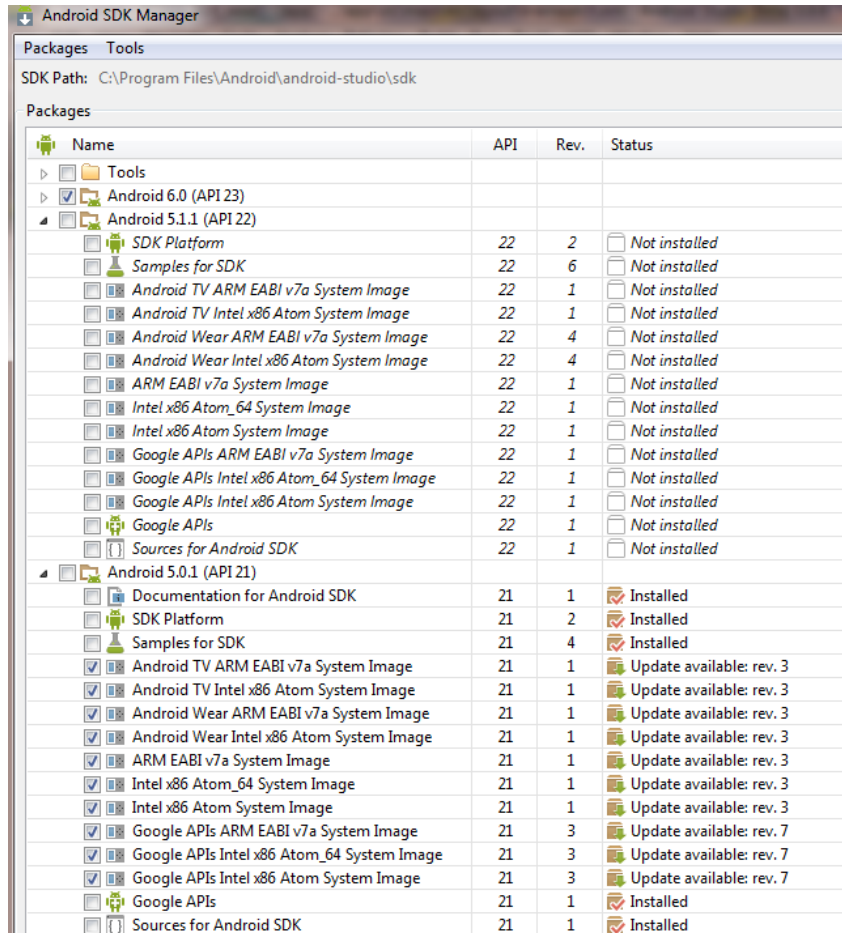


Fig. 5-4 An example of the interface of Android SDK Manager

SDK Manager is mainly used to update the necessary API libraries. As can be seen in Fig. 5-4, the SDK Manager informs the user that the current Android Studio have installed Android 5.0.1 API libraries, but not included Android 5.1.1 API libraries yet. Thus, if the user would like to develop an Android 5.1.1-based application, the API libraries need to be

updated. The SDK Manager is able to download the needed libraries and install them automatically once the download is completed.

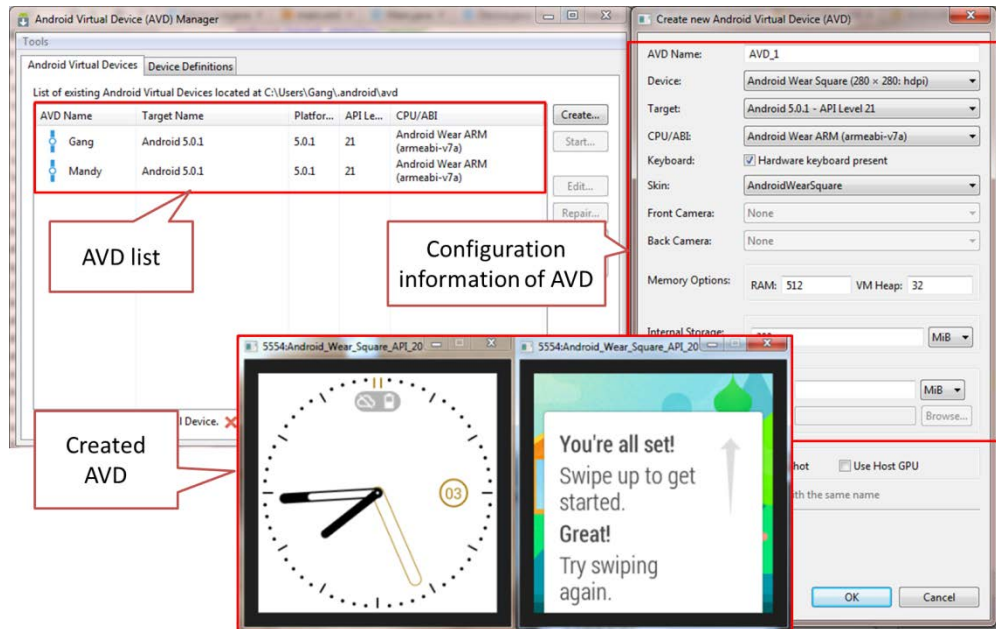


Fig. 5-5 An example of creating an Android WearTM OS based virtual smartwatch

5.2.3 Android Virtual Device

Android Virtual Device (AVD) is a simulated android device that runs on the computer. It allows the development and testing of the Android applications on the computer without a physical device. Fig. 5-5 demonstrates that creating AVD in Android Studio needs three steps. Step1: configuring AVD, including the AVD name, device type (e.g., phone, tablet and watch), target API level, CPU type (e.g, ARM-based or Intel-based) and

etc. Step 2: Press the “create” button in the AVD list interface. Step 3: Waiting the launch of AVD.

5.2.4 Android Device Monitor

Android Device Monitor (ADM) is mainly used to explore the Android file system and capture the device screen (as shown in Fig. 5-6). In this study, the well-trained DDD prediction model is just imported by the function of file system exploring of ADM. More specifically, we pushed the well-trained DDD prediction model (.txt format) onto the Secure Digital (SD) card memory of the smartwatch device via the interface of File explorer of the ADM.

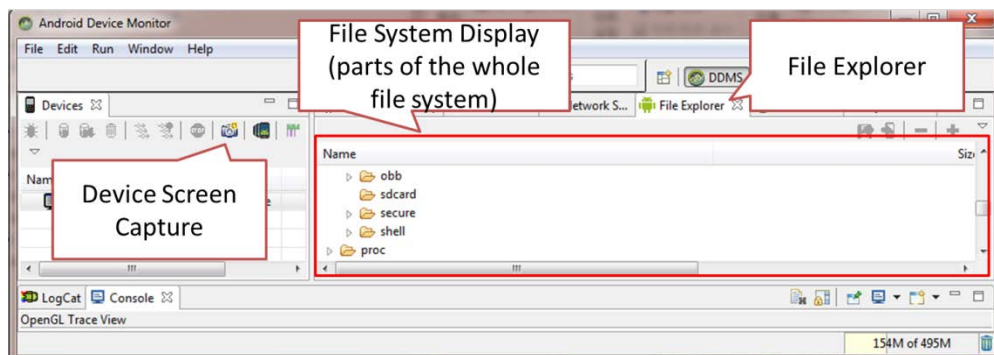


Fig. 5-6 An example of the interface of ADM

5.2.5 Logcat

Logcat is a very important debugging tool in Android Studio. To some extent, Logcat plays the role of “printf” in MCU development environment. It not only supports real-time debugging by instant information “printing”, but also supports off-line debugging by information-saving

function. It is also important to note that Logcat not only automatically points out the fatal errors that lead to application crash, but also points out the developers' logic errors by customized “TAG” function (as shown in Fig. 5-7). According to our experience, developers were able to solve all programming problems by the combination of real-time/off-line debugging and automatic/“TAG” debugging.

Automatically pointed-out fatal errors

```

09-02 23:15:18.864 1059-1059/com.example.usnlab.ble_test_wear E/AndroidRuntime: FATAL EXCEPTION: main
Process: com.example.usnlab.ble_test_wear, PID: 1059
java.lang.RuntimeException: Unable to instantiate application android.app.Application: java.lang.IllegalStateException: 
    at android.app.LoadedApk.makeApplication(LoadedApk.java:563)
    at android.app.ActivityThread.handleBindApplication(ActivityThread.java:4491)
    at android.app.ActivityThread.access$1500(ActivityThread.java:144)
    at android.app.ActivityThreadH.handleMessage(ActivityThread.java:1339)
    at android.os.Handler.dispatchMessage(Handler.java:102)
    at android.os.Looper.loop(Looper.java:135)
    at android.app.ActivityThread.main(ActivityThread.java:5221) <2 internal calls>
    at java.lang.reflect.Method.invoke(Native Method)
    at android.os.ZygoteInit$MethodAndArgsCaller.run(ZygoteInit.java:899)
    at android.os.ZygoteInit.main(ZygoteInit.java:694)
eException: Unable to get package info for com.example.usnlab.ble_test_wear; is package
initializeJavaContextClassLoader(LoadedApk.java:409)
makeApplication(LoadedApk.java:555)

```

Customized information

```

09-02 23:15:40.979 1128-1128/com.example.usnlab.ble_test_wear W/ContextImpl: Implicit intents with startService are not
09-02 23:15:40.991 1128-1128/com.example.usnlab.ble_test_wear I/River: BMI terminal device is successfully initialized.
09-02 23:15:41.011 1128-1128/com.example.usnlab.ble_test_wear I/Choreographer: Skipped 33 frames! The application may b
09-02 23:15:41.080 434-1058/? I/ActivityManager: Delay finish: com.google.android.gms/.config.ConfigFetchSe

```

Fig. 5-7 An example of the automatic/“TAG” debugging using Logcat

5.3 Smartwatch-based BMI Application

This application has a very fashionable name - “BrainWatch”. Its complete working flow chart is given by Fig. 5-8, where we can see clearly that it has following four distinct features:

- ①. Wirelessly control the start-up and stop of the whole BMI system;

- ②. Estimate driver drowsiness level using SVM-based DM model and EEG and gyroscope features;
- ③. Display the driver drowsiness level and EEG and gyroscope features when absolutely necessary (e.g., when drowsy driving is detected), in order to achieve the purpose of low-level interactions.
- ④. Enable tDCS-based neuromodulation by integrated closed-loop DDD algorithm;

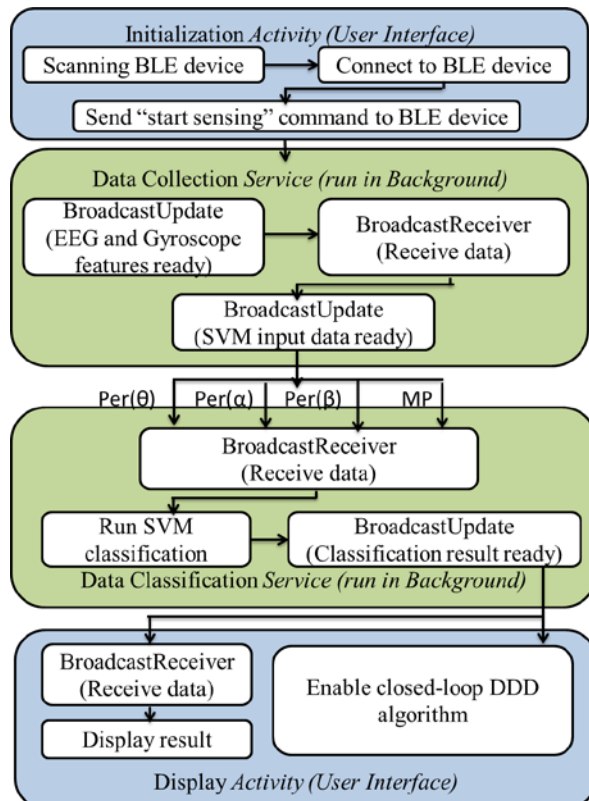


Fig. 5-8 The working flowchart of smartwatch application

The following subsections demonstrate the major components of this wearable application in detail (except for closed-loop DDD algorithm).

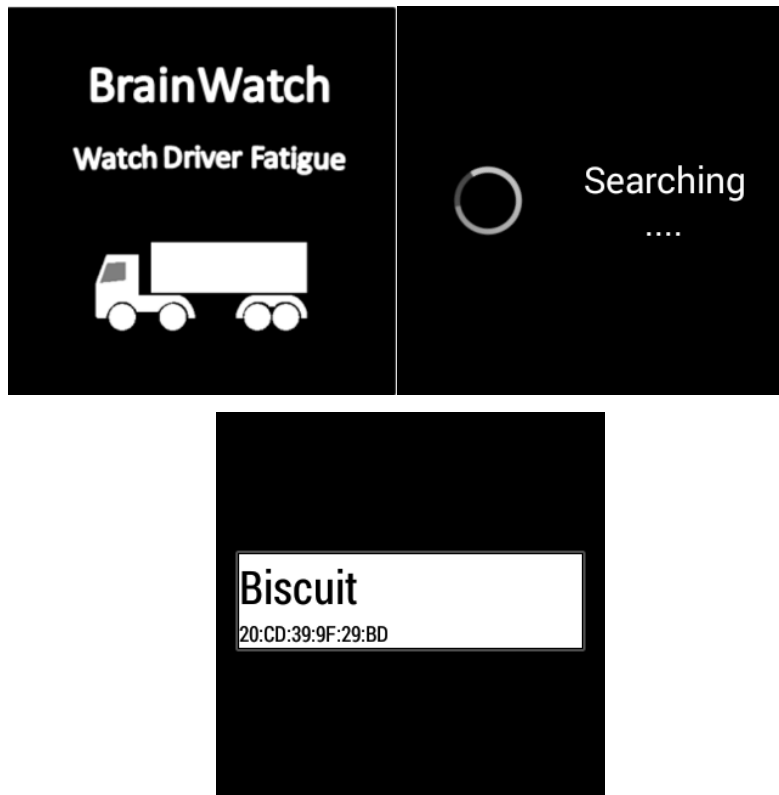


Fig. 5-9 The screenshot of the initialization procedure of the proposed wearable application, including start-up display (the top left), scanning BLE device (the top right) and pop-up window of the BLE device list (the bottom)

5.3.1 Application Initialization

Fig. 5-8 shows that the initialization of this wearable application mainly includes the initialization of BLE. As can be seen, the smartwatch is a Bluetooth master which scans and connects to Bluetooth slave (EEG headband). Then, the smartwatch wirelessly sends command to start-up BMI headset. The initialization procedure is manually triggered, which is the only

one absolutely necessary procedure involving manual operation indicating the characteristics of low-level interaction. Fig. 5-9 demonstrates the implementation of this initialization procedure.

5.3.2 Feature Collection

The BLE-based feature collection mainly involves two Android API components: *BroadcastUpdate* and *BroadcastReceiver*. By using the two components, the smartwatch just needs to burst out the collected EEG and gyroscope features when they are ready and then powering back down again. This is how BLE stays so low energy. In contrast, the classic Bluetooth needs to use a polling-loop to stream data, which consumes lots of power. More simply, the *BroadcastUpdate* and *BroadcastReceiver* components in BLE are just like the interrupt mechanism in MCU which is designed for replacing polling-loop to response external or internal events. This not only can reduce power consumption, but also can release the workload of core processor.

In addition, we implement the feature collection using a *Service* not an *Activity*, in order to further reduce the power consumption. In Android OS, each *Activity* corresponds to each user interface. Each user interface has a short life time due to the power save mode of smartwatch screen. So, the simplest and *Activity*-based way to collect features continuously is to keep the screen always ON by using the *WindowManager* component; while *Service* is independent of *Activity* and specifically designed to run the repeating task in background. So, in this study, we employed *Service* to collect features continuously in background instead of keeping screen ON. In this case, much power can be saved.

5.3.3 Support Vector Machine-based Drowsiness Classification

To test the classification performance with the collected features, a multi-category SVM classifier is used. As shown in Fig. 5-10, applying SVM includes three stages – Stage I: Data collection, Stage II: Validation and Stage III: Optimization. Stage I involves the input of EEG and gyroscope features and the one-hour simulated driving experiment (See Chapter 7). Stage II and Stage III involve the leave-one-subject-out (LOSO) cross-validation and its optimization respectively. The following subsections briefly introduce the SVM theory and introduce in detail the Stage II and Stage III, as well as the implementation strategy of SVM-based drowsiness estimation.

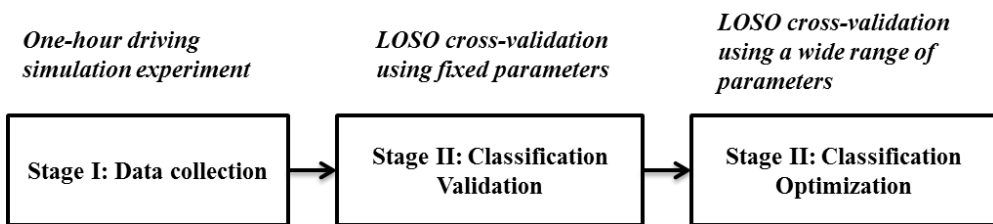


Fig. 5-10 The classification model building chain containing three different tasks: data collection, classification validation and classification optimization

5.3.3.1 Multi-Category SVM Classifier

In recent years, support vector machine (SVM) has emerged as a powerful technique for data classification [155-157]. The primary advantage of SVM is its ability to minimize both structural and empirical risk [158],

thereby leading to better generalizations for new data classifications, even with limited training datasets. With the success of LibSVM library, SVM is already coding and packaged in Java, C and MATLAB language. Therefore, SVM can be easily implemented on multiple platforms, such as wearable and mobile device (e.g., Android WearTM device), microprocessor-based device and PC. For these reasons, the SVM classification model is used to automatically recognize drowsy events in this study.

SVM is originally designed for binary classification. A binary SVM-based DDD systems can successfully classify driving status into two classes, for example drowsy driving and alert (safe) driving class. However, one limitation is that these systems are not capable of estimating the drowsiness level. As a result, they are unable to address driver drowsiness at its early stage, when feedback might be the most effective. One focus of this study is to detect driver drowsiness at its early stage. Therefore, multi-category SVM classifier, which is suitable for estimating drowsiness level, is adopted instead of the binary SVM classifier. The multi-category SVM classifier is actually constructed based on a group of binary SVM classifiers. Thus, to begin, the theoretical principle of binary SVM classifier will be introduced, which is followed by that of multi-category SVM classifier.

The aim of binary SVM is to find a decision surface that splits the dataset into two parts. All data lying on one side of the decision surface will be classified as members of one class and all data lying on the other side of the decision surface will be classified as members of another class. However, this kind of decision surface is not unique (see Fig. 5-11). It follows the fundamental difference between SVM and other classifiers: SVM is able to find the unique (optimal) decision surface which has a maximum distance or margin between the two datasets.

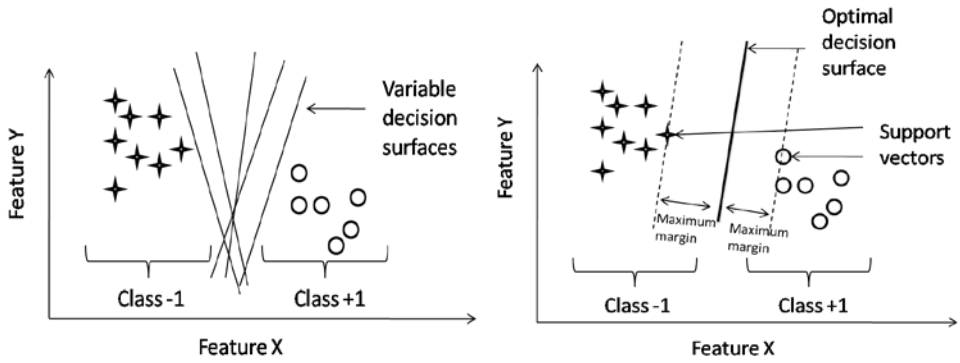


Fig. 5-11. An example of the two-class (+1 & -1) classification problem with optimal decision surface. The circles and stars represent samples of class +1 and -1, respectively. (a) multiple decision surfaces (b) optimal decision surface.

In brief, the mathematic theory of binary SVM is as follows: Assume that the input dataset is represented by N n-dimensional data points $\vec{x}_1, \vec{x}_2, \dots, \vec{x}_N \in \Re^n$ and corresponding labels $y_1, y_2, \dots, y_N \in \{-1, +1\}$, SVM maps each point \vec{x}_i from the input space \Re^n to the feature space \mathbf{H} by means of the mapping function $\Phi(\vec{x}_i)$ and finds a linear decision surface to classify the negative data points and the positive ones in the feature space. The linear decision surface is defined as Equation 15 with constraint function 16:

$$\vec{w} \cdot \Phi(\vec{x}) + b = 0 \quad (15)$$

$$y_i(\vec{w} \cdot \Phi(\vec{x}_i) + b) \geq 1 \quad \forall i \quad (16)$$

Where the \vec{w} is a vector perpendicular to the decision surface and b is a scalar (decision surface bias). In order to maximize the margin of

separation between the classes ($\frac{2}{\|\vec{w}\|}$ or equivalent to minimize $\frac{1}{2}\|\vec{w}\|^2$), SVM constructs a unique decision surface by applying Lagrange multiplier and transforming into the following dual problem:

$$\min_{\lambda} \left(\frac{1}{2} \sum_{j,k=1}^N \lambda_j \lambda_k y_j y_k K(\vec{x}_j, \vec{x}_k) - \sum_{j=1}^N \lambda_j \right) \quad (17)$$

$$\text{subject to } \sum_{i=1}^N \lambda_i y_i = 0 \text{ and } 0 \leq \lambda_i \leq C \quad \forall i \quad (18)$$

Where $\lambda = (\lambda_1, \dots, \lambda_N)$ is the Lagrange multiplier, C is a constant parameter which determines the tradeoff between the maximum margin and minimum classification error. In general, C has to be selected for the input dataset at hand by the user. $K(\cdot, \cdot)$ is denoted as $K(\vec{x}_j, \vec{x}_k) = \Phi(\vec{x}_j) \cdot \Phi(\vec{x}_k)$, which is so-called kernel function. By using kernel function (e.g., radial basis function (RBF)), SVM does not need to know explicitly the mapping function $\Phi(\vec{x}) : \Re^n \rightarrow \mathbf{H}$; it is sufficient only to know the dot product between mappings of two data points. Having determined the optimum Lagrange multiplier, the optimum solution for the vector \vec{w} is given by

$$\vec{w} = \sum_{j=1}^N \lambda_j y_j \Phi(\vec{x}_j) \quad (19)$$

Then SVM is able to classify any input \vec{x} using the function given by

$$f(\vec{x}) = \text{sign}(\vec{w} \cdot \Phi(\vec{x}) + b) = \text{sign}(\sum_{j=1}^N \lambda_j y_j K(\vec{x}_j, \vec{x}) + b) \quad (20)$$

The linear kernel and RBF kernel are defined by following equations:

①. Linear kernel

$$K(\vec{x}, \vec{x}_j) = \vec{x} \cdot \vec{x}_j \quad (21)$$

②. RBF kernel

$$K(\vec{x}, \vec{x}_j) = \exp\left(-\frac{\|\vec{x} - \vec{x}_j\|^2}{2g^2}\right) \quad (22)$$

Where, parameter g , supplied by the user, acts as the scaling factor or radius of RBF kernel. Small value of g produces smooth decision boundaries, preventing overfitting of the model to the data samples; while high value of g generates complex decision boundaries which has the possibility to be too specific to the data samples, resulting overfitting of the model.

In LibSVM library, multi-category classification is implemented by “one-against-one” approach [159]. Assuming that there are k classes that we want to classify; “one-against-one” approach will firstly construct a group of binary SVM classifiers to classify each pair of classes: class 1 against class 2, class 1 against class 3, … , class $k-1$ against class k . Thus, in total $\binom{k}{2} = k(k-1)/2$ binary SVM classifiers will be constructed. Then, each binary classification is considered to be a voting. Finally, a new input \vec{x} will be classified to the class that has the majority of votes. If two classes have identical votes, the input \vec{x} will be classified based on the classification provided by the furthest hyperplane.

One-against-rest approach [160], methods by Crammer and Singer, and methods by Weston and Watkins are other strategies for multi-category SVM. However, the down-side of one-against-rest approach is computationally expensive [160]. Also, methods by Crammer and Singer and by Weston and Watkins usually do not outperform one-against-rest or one-against-one SVM classifiers in biomedical datasets [160].

These facts indicate the advantages and robustness using one-against-one-based LibSVM for the implementation of multi-category SVM classifier.

5.3.3.2 LOSO Cross-validation and Optimization

The procedure of LOSO cross-validation and optimization is depicted in Fig.5-12. For evaluating classification performance, the classification accuracy which is based on LOSO cross-validation for all participants was calculated. The specific steps are as follows: (1) Omit one subject from all available feature sets; (2) Train the classifier; (3) Test the omitted feature sets; (4) Repeat the steps that are listed above until each subject has been omitted and tested once; (5) Calculate the average classification accuracy (e.g., based on the N Rounds).

In this study, the EEG features (e.g., Per (θ), Per(α) and Per (β)) and gyroscope features (e.g., MP) were used as input features to the SVM. The SVM outputs 5-level driving types (Level 0: Alert, Level 1: Slightly drowsy, Level 2: Moderately drowsy, Level 3: Significantly drowsy and Level 4: Extremely drowsy). Both of linear and non-linear kernel (e.g., RBF) were studied in order to obtain the highest level of classification accuracy. Also, the parameter C and RBF parameter g are optimized using a simple search procedure with $C, g = \{0.01 \sim 10\}$ in steps of 0.01 and each searching step corresponds to each cycle of Round 1 to N.

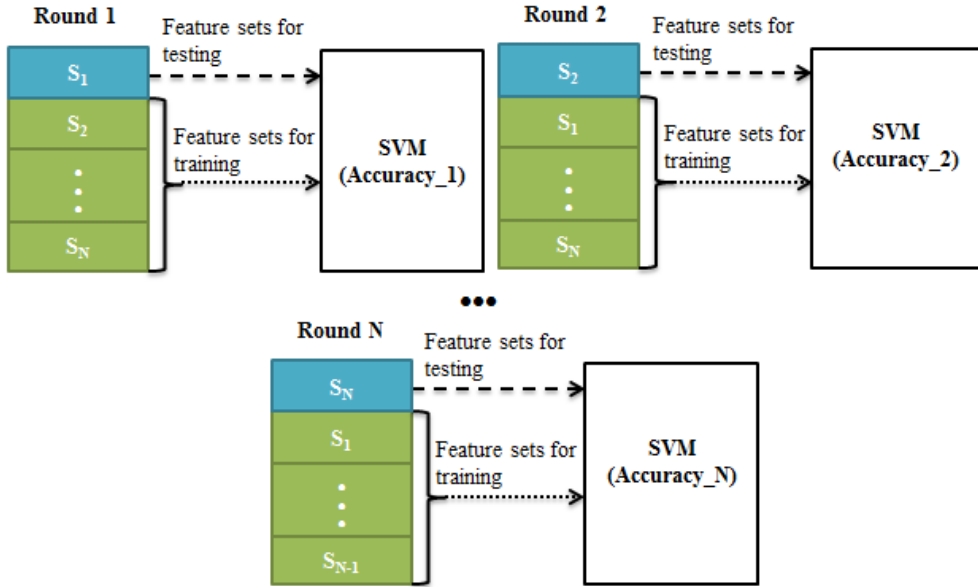


Fig. 5-12 The procedure of LOSO cross-validation and optimization, where S_i means the i^{th} subject and Accuracy_i means the classification accuracy for i^{th} Round.

5.3.3.3 Implementation

Fig. 5-13 shows the complete procedure for smatwatch-based SVM classification. Each step in Fig. 5-13 is demonstrated in detail by Fig. 5-14~15. It is important to note that the number symbols ②-⑦ in Fig. 5-14~15 have a one-to-one corresponding relationship with that in Fig. 5-13. First, the multi-category SVM model was well trained on a PC using LOSO cross-validation tests with different kernels (e.g., linear and non-linear RBF kernels). Then, the parameters of the well-trained SVM model were hardcoded in text-file format and stored on the SD card memory of the smartwatch by using ADM tool (as shown in Fig. 5-14). Meanwhile, the highly successful LibSVM library (a 51KB JAR file version 3.17) was

embedded into the smartwatch by file structure tool (as shown in Fig. 5-15). Finally, the smartwatch was able to instruct library functions, such as `svm.svm_load_model` and `svm.svm_predict`, to test the SVM model in a real-time manner (as shown in Fig. 5-15). The highly successful LibSVM implementation for the SVM [159] was used in all experiments. It is also important to note that similar to feature collection *Service* we designed classification *Service* for low-power application.

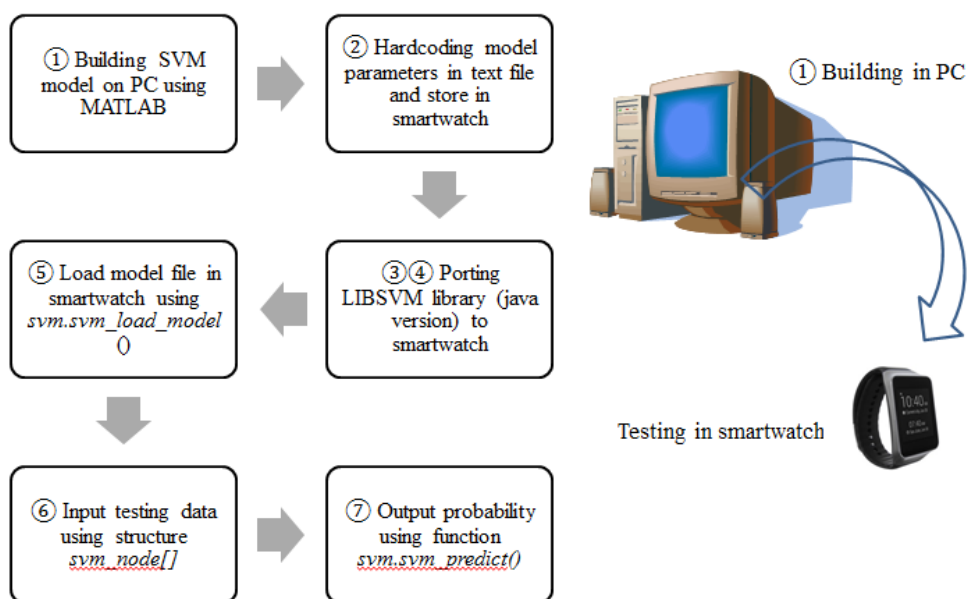


Fig. 5-13 The implementation procedure of smartwatch-based SVM classification

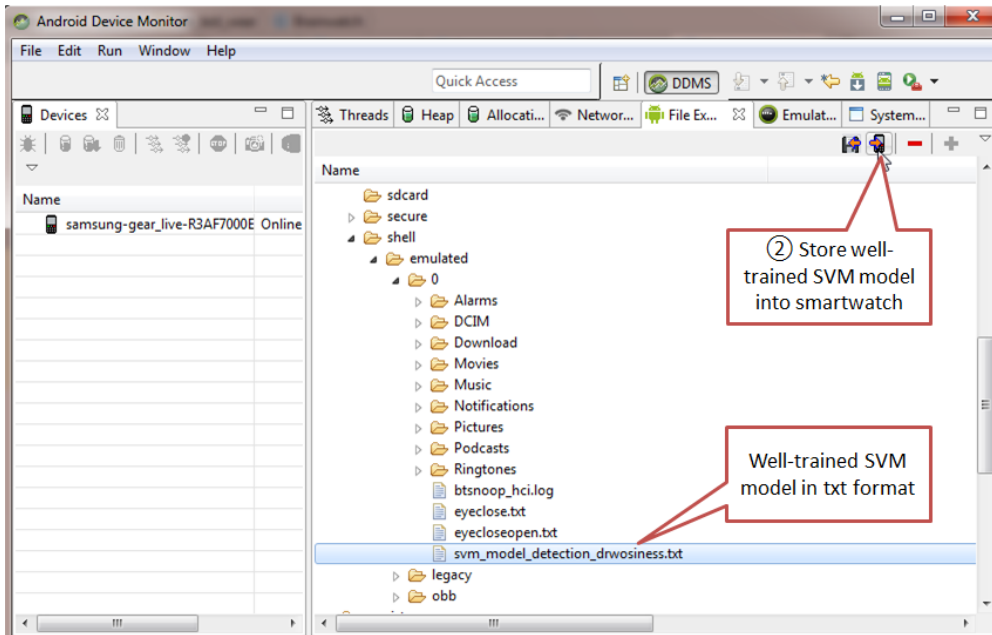


Fig. 5-14 Pushing well-trained SVM model onto the smartwatch by using ADV tool

The screenshot shows the Android Studio interface with the following details:

- Project Structure:** The project is named "ble_test_wear". It contains an ".idea" folder, an "app" module with a "build" folder, a "libs" folder containing "androidplot-core-0.6.0.jar" and "libsvm.jar" (marked with a red circle ③), and a "src" folder with a "main" package.
- Code Editor:** The file "bleservice.java" is open. The code imports various Java and LibSVM classes. A red box highlights the LibSVM import statements:


```
import libsvm.svm;
import libsvm.svm_model;
import libsvm.svm_node;
import libsvm.svm_parameter;
import libsvm.svm_problem;
```
- RunSVM Function:** The "runSVM" function contains several numbered steps:
 - ⑤

```
svm_model model = svm.svm_load_model("/storage/emulated/0/svm_model_detection_drowsiness.txt");
```
 - ⑥

```
x[0] = new svm_node();
```
 - ⑦

```
x[0].index = 1;
```
 - ⑧

```
x[0].value = alpha_power_percentage;
```
 - ⑨

```
estimated_label=svm.svm_predict(model, x);
```

Fig. 5-15 Porting LibSVM to smartwatch and implement SVM functions in smartwatch

5.3.4 Warning Signal

The warning signal is generated by the built-in vibration sensor of the smartwatch as illustrated in Fig. 5-16. The warning vibration will last 10 seconds and then the neurostimulation will be enabled according to the closed-loop DDD algorithm (See Chapter 6).

```
Vibrator v = (Vibrator) this.getSystemService(Context.VIBRATOR_SERVICE);  
v.vibrate(10000);
```

Fig. 5-16 The use of built-in vibration sensor of the smartwatch

5.3.5 User Interface

Wearables provide a brand new set of design opportunities and challenges, graphic user interface (GUI) design in particular. Compared to other devices like phones or tablets, smartwatch has a tiny screen. Thus, the design principle for smartwatch GUI is that the GUI not only should be as simple as possible, but also should be effective enough to provide the maximum information. So as a designer the opportunity here is not to think about how to shrink a smart phone GUI down to a tiny screen. Instead, we should think about the fundamental problems our design solves.

Fortunately, Google has already made a really simple GUI structure for Android Wear™ based developers. More specifically, the core of the Android Wear™ GUI is a stream of cards and each card can have multiple pages. The user navigates through cards with vertical swipes; while each page is accessed with horizontal swipes from right to left. A card can be dismissed with a left-to-right swipe. Cards can be stacked and can be accompanied by a notification sound and/or vibration.

In this study, we managed to make the smartwatch GUI as simple as possible and make the content optimized for the tiny screen, so that most users who have little professional training can use it easily. To achieve this goal, a single “all-inclusive” card is used as the smartwatch GUI. Fig. 5-17 shows that this GUI uses a simple traffic light principle to indicate driver drowsiness level. Green light (left side) indicates Level 0. Yellow light

(middle) indicates Level 1. Red light (right side) indicates Level 2 plus. The pie chart shows the EEG RBP features. The icon in the center of the pie chart stands for gyroscope. The number overlapped with this icon is the gyroscope MP feature. If drivers no longer want any help from this DDD application, an “Exit” button placed at the bottom can be pressed.

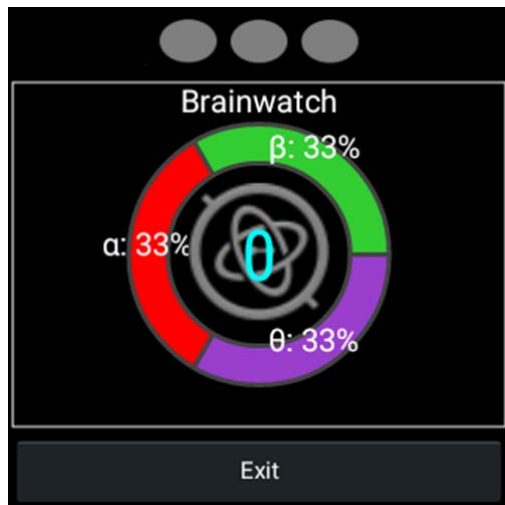


Fig. 5-17. Smartwatch screen showing the designed GUI for this wearable application termed “Brainwatch”. Green, Yellow and Red lights are placed at left side to right side.

5.4 Chapter Summary

This chapter focused on the design and implementation of DDD application in Android Wear™ OS based wearable BMI terminal device. First of all, the Google Android Wear™ is introduced including its distinct features and its fundamental difference with Android phone and tablet OS. Then, the recommended SDK for Android Wear™ application, Android

Studio, is introduced including its brief development history, the comparison with traditional Eclipse ADT and the interface of Android Studio, as well as the powerful tools integrated in Android Studio, such as SDK Manager, AVD, ADM and Logcat. Next, the major components of the proposed wearable DDD application are introduced in detail, including the initialization, feature collection, SVM-based DDD and UI design. Conclusively, the proposed wearable application shifts the EEG-based BMI system from portable to on-body, which is low-power, less distracting and thus more suitable for real-life DDD application.

Chapter 6

6 Design of Closed-Loop DDD Algorithm

The proposed closed-loop DDD algorithm consists of three states: 1) SVM-based DDD; (2) smartwatch-based drowsy warning and 3) tDCS-based drowsiness management. Fig. 6-1 shows the diagram of the proposed algorithm.

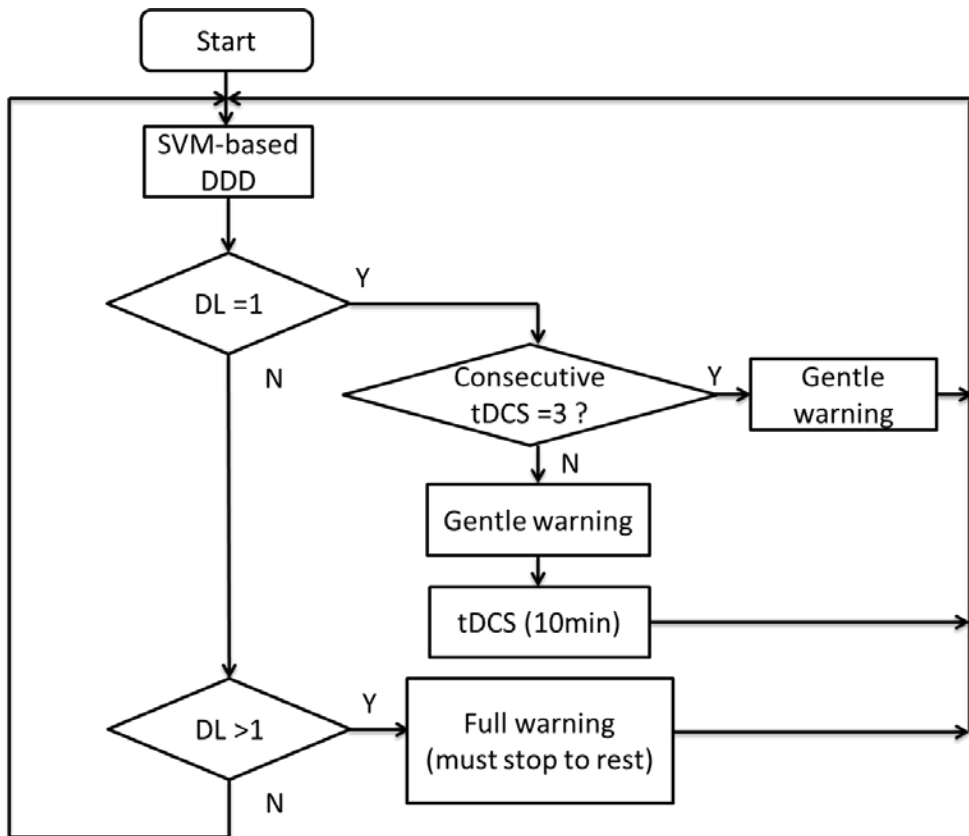


Fig. 6-1 Flowchart of proposed closed-loop DDD algorithm

At the beginning, the algorithm enters the SVM-based DDD state. In this state, the algorithm monitors the subject's drowsiness level by feeding

EEG RBP features and gyroscope MP features to a SVM-based multi-category classifier. Once the drowsiness level is Level 1 (slightly drowsy), the algorithm will deliver a gentle warning by “turning on” the yellow “light” of the virtual traffic light in the smartwatch UI. In the meantime, the algorithm will enable 10-min tDCS by wirelessly sending command to headset. After that, the algorithm enters to SVM-based DDD state again to assess the effectiveness of the tDCS. If the drowsiness level is still at Level 1, another 10-min tDCS session will be enabled until maximum consecutive 3 tDCS session is finished. After that, if the drowsiness level is still at Level 1, the algorithm will disable tDCS and deliver gentle warning only. If drowsiness level is Level 2+ (moderately drowsy ~ extremely drowsy), the algorithm will deliver a full warning by “turning on” the red “light” of the virtual traffic light in the smartwatch UI. In the meantime, the 10-sec vibration will be activated by using the built-in vibration sensor of the smartwatch.

The design principles behind this closed-loop DDD algorithm are as follows:

- ①. **Low-level interaction:** Driving needs sustained attention, so this algorithm is designed to interrupt drivers when absolutely necessary, for example, the gentle warning delivered at Level 1 is actually transparent to drivers if they do not see smartwatch; while vibration warning will be activated when estimated drowsiness level is Level 2+. It is also important to note that a 10-min tDCS session will be enabled silently and invisibly at the same time with gentle warning
- ②. **Effectiveness:** As a closed-loop DDD system, the more effective it is, the longer period of alert driving it should maintain. To

achieve this goal, this algorithm is designed to combat drowsiness at its early stage by enabling tDCS at Level 1. For the drivers whose drowsiness level is Level 2+, this algorithm directly warns them to stop driving and have a good rest rather than using this assistive technology.

- ③. **Safety:** As mentioned in Section 4.3, consecutive tDCS within 30 minutes is regarded as safe. Therefore, the 10-min tDCS session is limited to maximum 3 times in this algorithm.

Chapter 7

7 Experiments and Results

In order to evaluate the system performance for DDD, a set of experiments was designed and conducted.

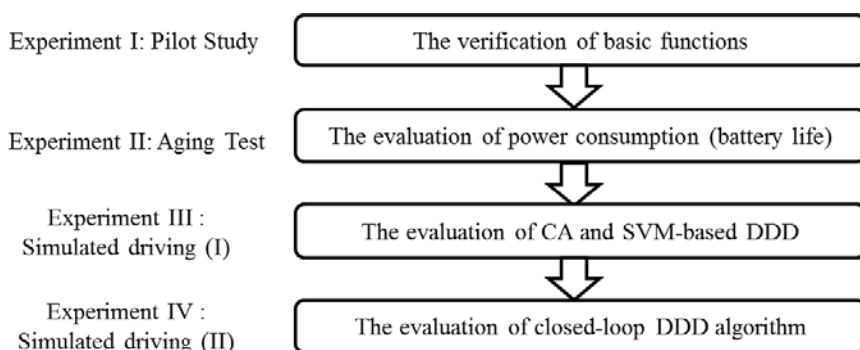


Fig. 7-1 A comprehensive experiment paradigm containing four different tasks.

Fig. 7-1 shows that the feasibility of the proposed DDD system was tested in four aspects. First, a pilot test was conducted to verify several basic functions of the proposed system including sampling rate, real-time FFT and SVM performance, the EEG signal quality from the dry electrodes, as well as the arousing feedback of tDCS. Also, the performance of a commercial EEG headset that is made by pure hard material was compared with that of the proposed headset that combines hard material and elastic headband. Then, the battery life of the whole system was investigated by aging test with an attempt to determine whether the proposed system is suitable for DDD application that features with long-term monitoring. Next, a one-hour driving

simulation experiment was conducted to collect, analyze and compare EEG and gyroscope features with each drowsiness level. Meanwhile, the SVM-based driver drowsiness classification model was built and detection accuracy of the proposed system was evaluated. Also, the closed-loop DDD algorithm was designed at this stage. Finally, a two-hour driving experiment was conducted to evaluate the closed-loop DDD algorithm in real-time way.

The comprehensive experimental results show the feasibility of the proposed system for DDD application. The following sections introduce the major components of the experiments in detail.

7.1 Verification of Basic BMI Functions

7.1.1 Sampling rate

We employed a *Timer* in the 32-bit MCU and let this *Timer* count the number of the converted EEG samples every second. Totally, we run this *Timer* one hundred times. The averaged number is 128.13 ± 0.11 , which could verify the sampling rate is 128Hz indeed.

7.1.2 Real-time FFT performance

The 256-point FFT was implemented by the 32-bit MCU and a commercialized software Complexity ver 2.82 from LAXTHA, Inc (Daejeon, Korea) under eye-closed (EC) conditions. The correlation coefficient between the two FFT spectrum series is 0.999 as shown in Fig .7-2. For the real-time performance, we programed the MCU to print out the system time before and after running FFT via a serial port terminal. We found that the time difference is negligible at the millisecond level (as shown in Fig. 7-3).

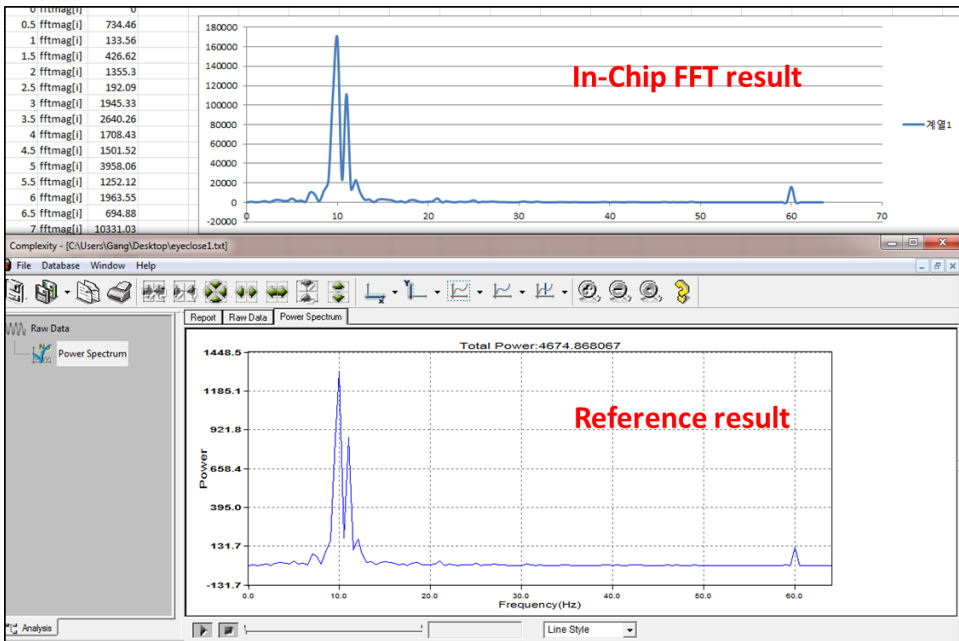


Fig. 7-2 The comparison of FFT series between on-chip calculation and PC-based calculation

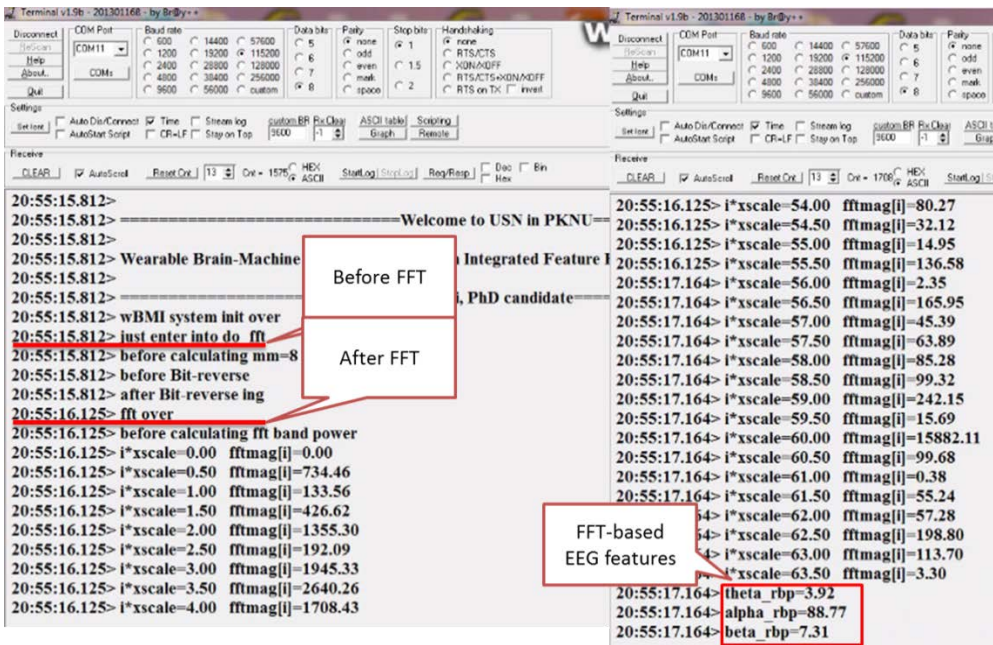


Fig. 7-3 The evaluation of the real-time performance of on-chip FFT

7.1.3 Real-time SVM performance

The classification accuracy by smartwatch and PC (MATLAB) based on the same 3-category dataset (<https://www.csie.ntu.edu.tw/~cjlin/libsvmtools/datasets/multiclass.html#iris>) were compared. The values are exactly the same. For the real-time performance, we used the debugging tool *Logcat* and let *Logcat* print out the system time before and after running the SVM. A 4-ms time delay is found.

7.1.4 EEG Signal Quality

The testing of the EEG signal quality can be divided into two phases, off-line and on-line testing. Both phases were based on the same SIU and SPU. For the first phase, the EEG signals from dry electrodes were compared with that from conventional wet Ag/AgCl electrodes. We recorded the EEG signals using the two types of electrodes in the same positions (O1 & O2), but in separate sessions (dry electrodes were tested first) when one subject was instructed to close his eyes for five seconds. What we expected to be common between these two sessions was the appearance of obvious α rhythmicity in the time domain and the largest power percentage for the α band in frequency domain. The observed results are consistent with this expectation, as shown in Fig. 7-4. Then, in order to evaluate the sensing resolution of the dry electrodes, the subject was required to remain as still as possible and instructed to do eyelid movements as follows: full open (FO), slight closure (SC), half closure (HC), almost closure (AC) and full closure (FC). What we expected is the linearly growing α power percentage. The observed results are consistent with this expectation, as shown in Fig. 7-5. For the second phase, we developed a Visual Basic Dot Net GUI to wirelessly receive the EEG signals under the simulated driving environment, and plot them on the display screen. What we expected was the obvious α

rhythmicity when subjects close their eyes due to real drowsiness instead of instructed eye closure. The observed results are consistent with this expectation, as shown in Fig. 7-6.

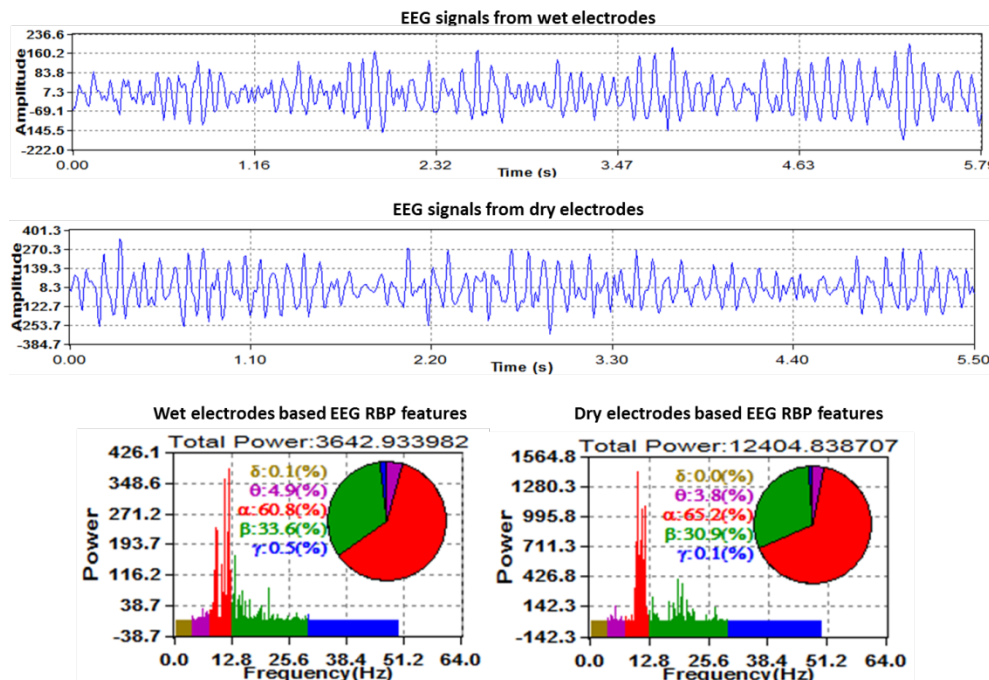
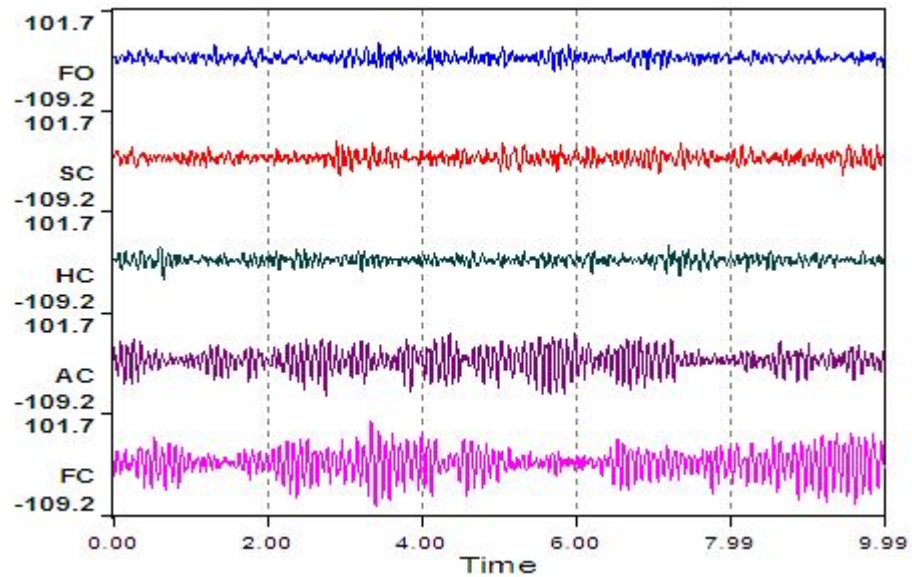
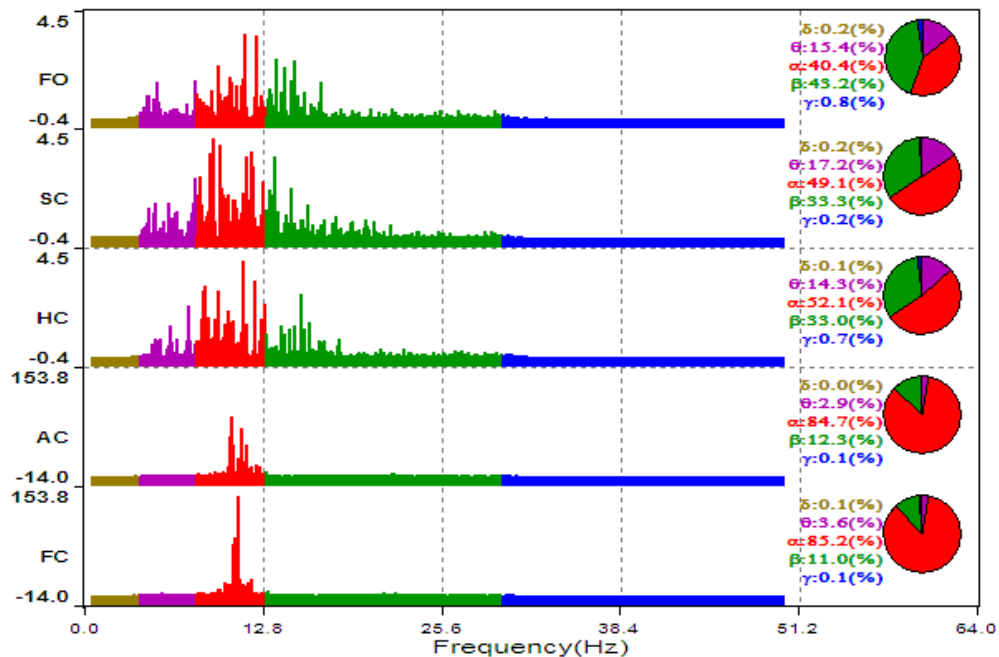


Fig. 7-4 EEG signals (line chart) and EEG band power (pie chart) comparison between wet electrodes (the top) and dry electrodes (the bottom).

For the line chart, the x-axis indicates the time in seconds. The y-axis indicates the amplitude of the digitalized EEG samples which are already filtered by the digital LPF in SPU. For the pie chart, the x-axis indicates the frequency range from 0 to 64Hz (the half of the sampling rate 128Hz). The y-axis indicates the magnitude of FFT power.



(a)



(b)

Fig 7-5. (a) A group of EEG signals and (b) its FFT results with the reduction of eye closure degree

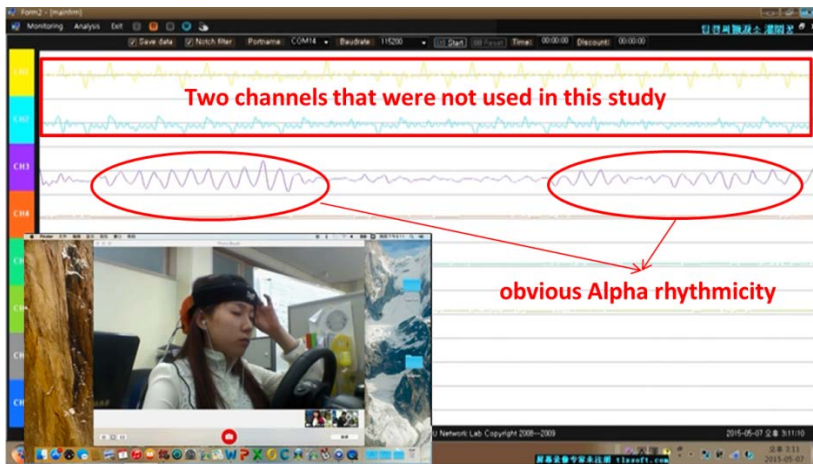


Fig 7-6. EEG signals under simulated driving environment. The female subject shown in the left bottom was too drowsy to keep her eyes open. At that moment, the EEG signals from the developed headset show obvious alpha rhythmicity, as marked by the two red circles. The two channel plots in yellow and blue were not EEG signals and not used in this study.

A commercial wireless EEG device named Emotiv EPOC from Emotiv, Inc (Eveleigh, Australia) was used to compare the output EEG data with our device under the same conditions: 1) collecting 10-sec eye-open (EO) and EC data under sitting quietly (SQ) condition; 2) collecting data under 1-min simulated driving (SD) condition. The purpose to collect data under SD condition is to check whether the slight head movements (HM) that are caused by watching car's rear view mirrors could lead to a distorted baseline or not. According to our previous experiences about wired EEG device, the HM usually results in distorted baseline and an increased θ power (low frequency component). So, before formal driving simulation experiment, we must check this point, in order to get effective EEG features.

Emotiv is a 14-channel unipolar EEG device (as shown in Fig. 7-7). Its data is also sampled at 128Hz but with 16-bit resolution. To compare with our bipolar single-channel device, we employed independent component analysis (ICA) to extract clear O1 and O2 data from Emotive and then based on the basic theory of differential amplifier, the difference of O1 and O2 (denoted by X_{O1} and X_{O2}) was used as the bipolar signal for comparison. Finally, the calculated θ , α and β power percentages were compared with that obtained from our device. The ICA was implemented by using EEGLAB Toolbox (Ver. 7.1.3.13b) which is developed by Swartz Center for Computational Neuroscience, (University of California San Diego) [35].



Fig. 7-7 A commercial wireless EEG headset (Emotiv, Inc)

Ten subjects participated in this comparison test and completed all testing procedures. Fig. 7-8 shows the extracted 14 ICA components from Emotiv EEG. Fig. 7-9 shows the time series from 14 Emotiv channels.

Analysis result shows that O1 and O2 are little impacted by eye blinks artifacts since the power of eye blinks is gradually decayed from frontal scalp to occipital scalp. This result is also confirmed by W.Z. Kong *et al*'s study [161].

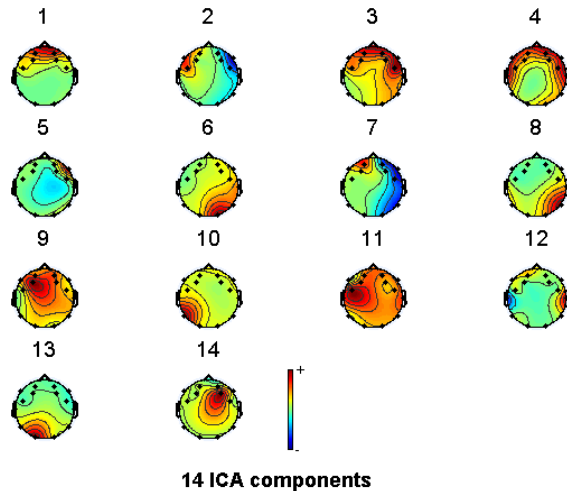


Fig. 7-8. The extracted 14 ICA components from Emotiv EEG.

Component#1 is the typical components of eye blinks.

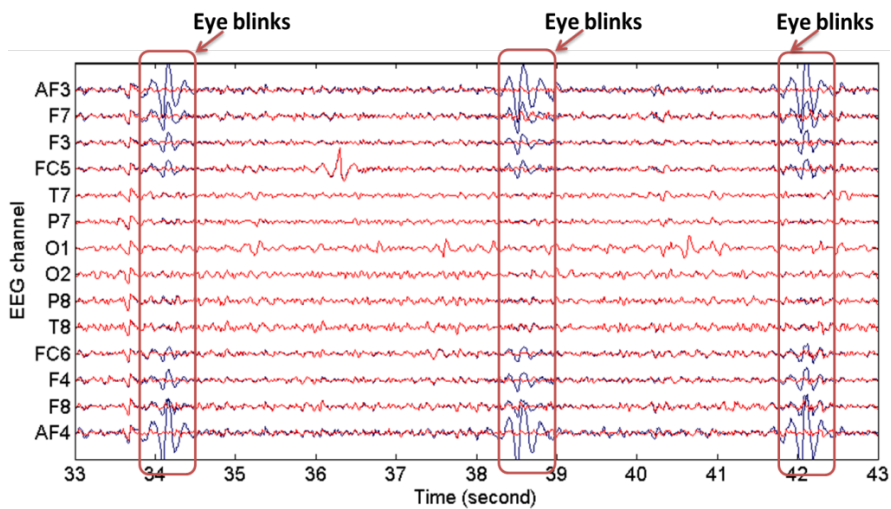


Fig. 7-9. The time series of 14-channel Emotiv EEG. Blue series are original EEG data. Red series are eye-blinks-removed EEG data.

Fig. 7-10 and 7-11 show a representative subject's data under EO and EC conditions. Analysis result shows that the power percentage difference between the commercialized device and our device at θ , α and β bands are very small. They are 0.1%, 0% and 0.8% for EO condition and 0.4%, 4.7% and 4.9% for EC condition. Table II shows the complete comparison results comprising all EEG features which are obtained via different devices and during different conditions.

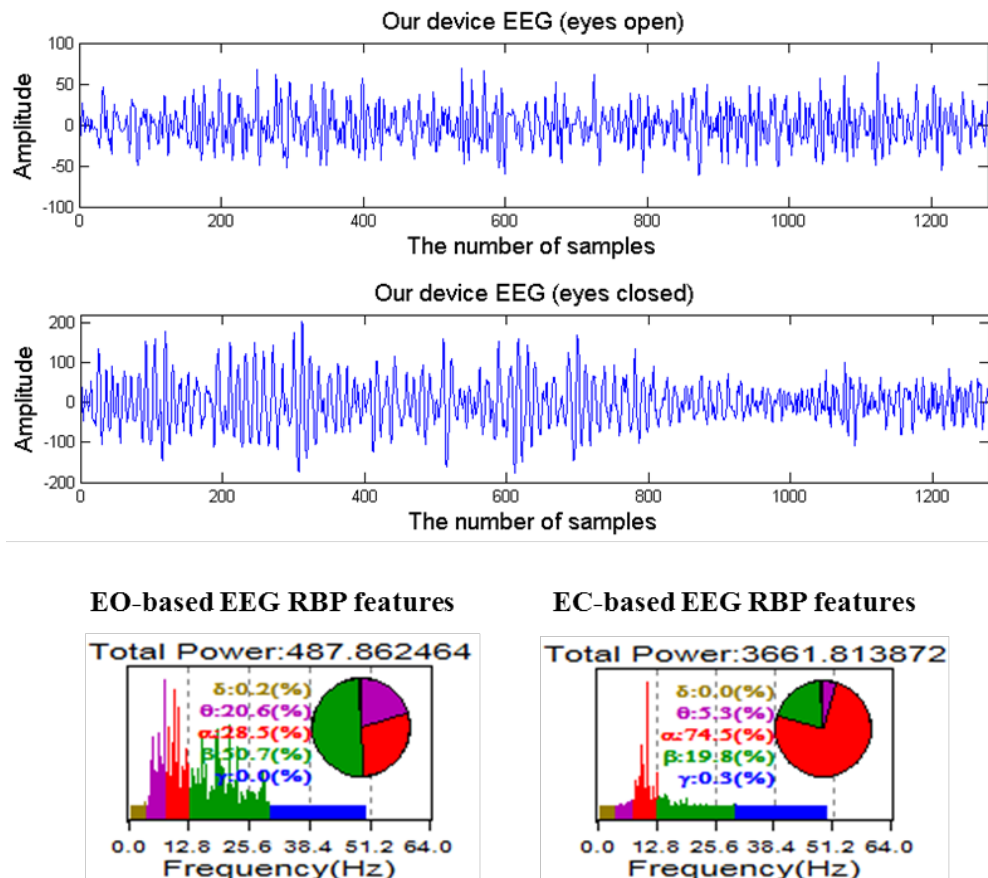


Fig. 7-10 Comparison of EEG signals (line chart) and EEG band power (pie chart) under EO and EC condition for our device. For the line chart, the x-axis indicates the number of EEG samples. The y-axis indicates the amplitude of the digitalized EEG samples which are already filtered by the

digital LPF in SPU. For the pie chart, the x-axis indicates the frequency range from 0 to 64Hz (the half of the sampling rate 128Hz). The y-axis indicates the magnitude of FFT power. The EEG signal here is collected by our device from a representative subject.

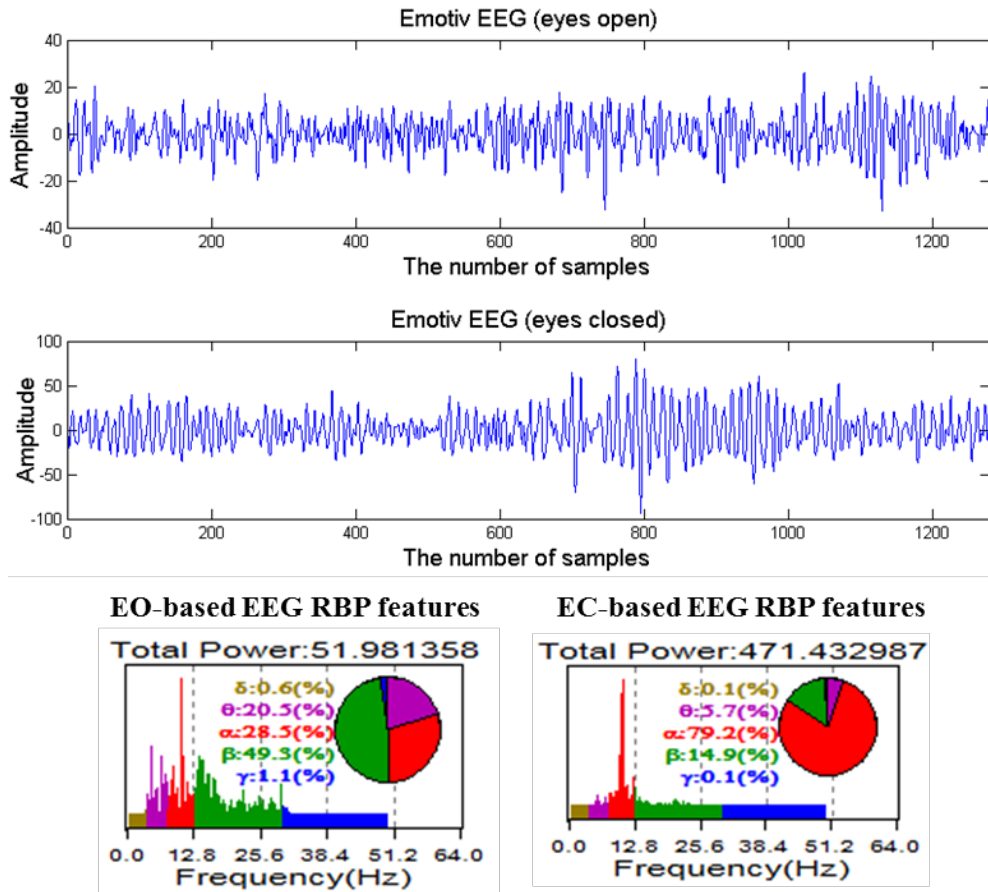


Fig. 7-11 Comparison of EEG signals (line chart) and EEG band power (pie chart) under EO and EC condition for a commercial EEG device. For the line chart, the x-axis indicates the number of EEG samples. The y-axis indicates the amplitude of the digitalized EEG samples which are already filtered by the digital LPF in SPU. For the pie chart, the x-axis indicates the frequency

range from 0 to 64Hz (the half of the sampling rate 128Hz). The y-axis indicates the magnitude of FFT power. The EEG signal here is collected by a commercial device from a representative subject.

Table 7-1 The means and standard deviations of EEG features obtained from commercialized device and our device

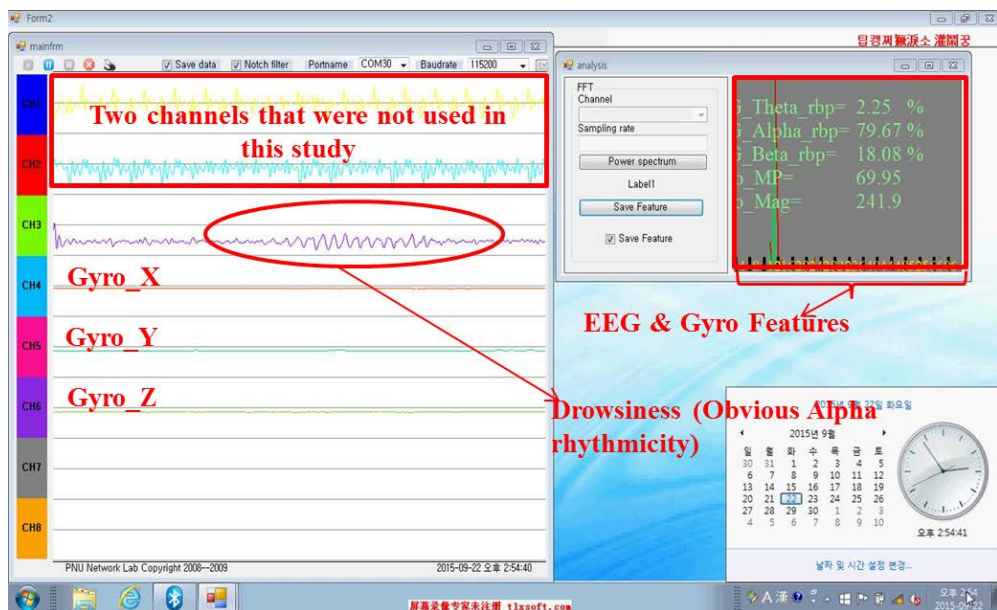
EEG feature	Condition		Emotiv	Our device
Per(θ)	SQ	EO	23.52 ± 7.12	14.7 ± 6.48
		EC	15.63 ± 6.18	5.68 ± 1.95
	SD	Normal	24.6 ± 6.37	11.32 ± 3.76
		HM	45.4 ± 16.95	14.18 ± 7.32
Per(α)	SQ	EO	28.75 ± 5.52	39.85 ± 6.58
		EC	63.38 ± 11.54	63.38 ± 7.18
	SD	Normal	21.17 ± 6.55	35.13 ± 7.91
		HM	25.78 ± 10.01	46.41 ± 3.87
Per(β)	SQ	EO	45.38 ± 6.58	39.75 ± 9.38
		EC	20.68 ± 7.06	29.26 ± 5.75
	SD	Normal	50.44 ± 9.07	48.5 ± 17.47
		HM	25.32 ± 8.92	33.15 ± 5.87

As expected, the mean α power is obviously increased for both devices for EC condition, compared to the EO condition (as shaded in grey). Coincidentally, the mean α power obtained from the two devices are the same for EC condition, up to 63.38%. The mean θ power is greatly increased for Emotiv device under HM condition (24.6% vs 45.4%; one-way ANOVA $P < .001$, $\alpha = .05$), compared to normal driving condition; while there is no significant power change in our device (11.32% vs 14.38%; $P = .07$, $\alpha = .05$) (as shaded in blue). This is what we expected because our device is using an elastic headband which could make the EEG electrodes and scalp very tight and thus reduces the friction noise between electrodes and scalp. In contrast, Emotiv is using a hard headset which cannot ensure a good electrode contact

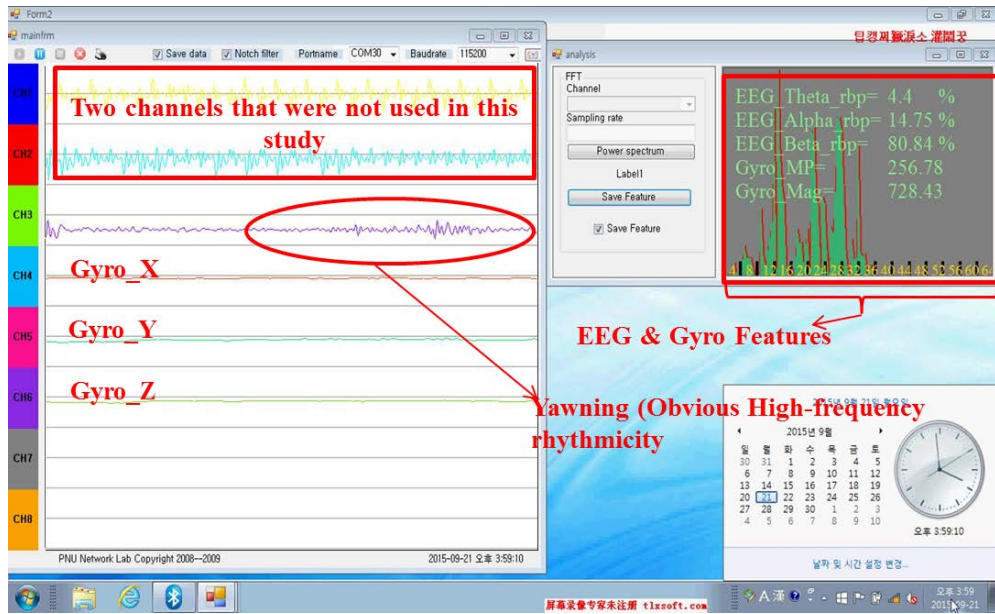
if the head is swaying. Another obvious power change is in β band for normal driving condition if compared to EO condition. Emotive device increased about 5%, while our device increased about 10% (as shaded in green). The physiological reasoning behind this should be that subjects are more alert when driving if compared to pure EO condition. This reasoning is based on a previous conclusion that the β wave is associated with alertness and concentration [69]. There is a power increase in β wave if the driver's alertness and concentration is increased [69].

7.1.5 Gyroscope Signal Quality

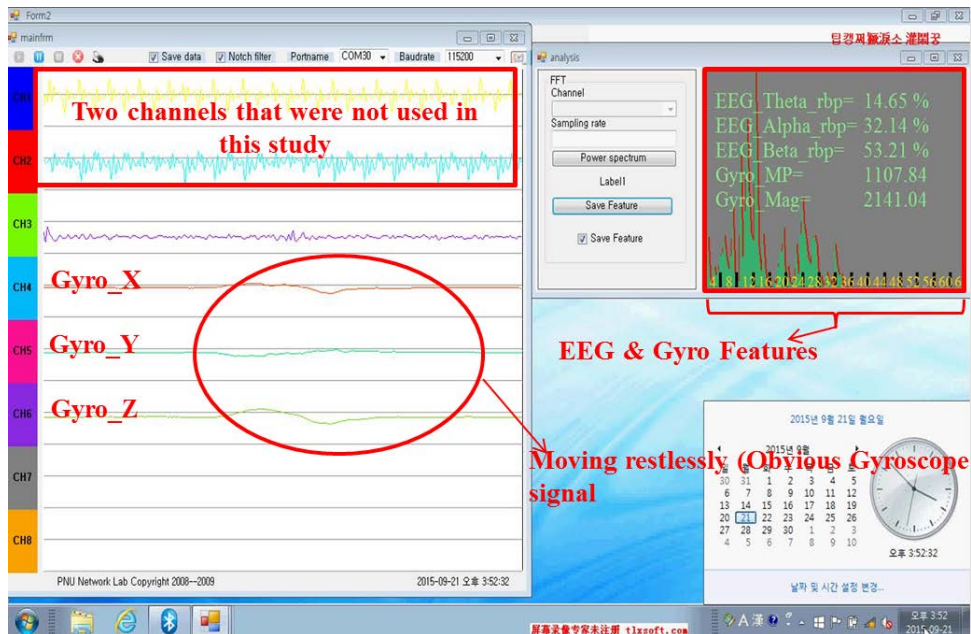
We developed a Visual Basic Dot Net GUI to wirelessly receive the gyroscope signal and test its quality under the simulated driving environment. Fig. 7-12 shows that this test consists of three steps: Step I: normal drowsiness situation; Step II: slightly drowsy situation including two typical slightly drowsy behaviors (yawning and moving restlessly).



(a)



(b)



(c)

Fig. 7-12 Gyroscope signal quality test including (a) normal drowsy situation; (b) yawning; (c) moving restlessly on chair

What we expected was the small signal amplitude for normal drowsy situation, the obvious signal fluctuations for yawning and moving restlessly on chair situations. The observed results are consistent with this expectation, as shown in Fig. 7-12, where we can see clearly that there was a significant increase in MP for yawning ($MP=256.78$) and moving restlessly on chair situations ($MP=1107.84$) if compared to normal drowsy situation ($MP=69.95$).

7.1.6 Proof-of-Concept Study on tDCS

Before applying tDCS to simulated driving experiment, a pilot study was conducted to verify its arousing effect, as well as the safety of tDCS on the non-hairy forehead area. Totally, eight subjects participated in this pilot study. On the day of experiment, they were not allowed to drink tea or anything containing caffeine. The subjects sat comfortably on a chair in a laboratory environment. Two self-adhesive tDCS electrodes, as mentioned in Section 4.1.3, were placed on the non-hairy forehead area (Fp1 and Fp2 respectively, according to the EEG International 10-20 System). For each subject, the individual current intensity (ICI) was used in this pilot study. It is important to note that the use of ICI is not only for the consideration of safety, but also for the consideration of avoiding intra-personal effect or auto-suggestive effect. The ICI was defined as following steps:

- ①. Enable tDCS session with 1.5mA;
- ②. Reduce the current intensity in steps of 0.1mA;
- ③. Until each subject reported that there was no tingling sensation at the source of the bipolar self-adhesive electrodes after 30-sec tDCS session;
- ④. Before each step of reducing current intensity, each subject was

instructed to have a rest until they reported that there was no pain at the source of the bipolar self-adhesive electrodes

7.1.6.1 Arousing effect

The arousing effect was verified by the comparison of EEG RBP features between before, during and after 10-min tDCS sessions (as shown in Fig. 7-13). The experimental results for a representative subject are shown in Fig. 7- 14. The experimental results for all subjects including the ICI and EEG RBP features are summarized in Table 7-2. It is important to note that before finally settling with 10-min-long session duration, 5-min-long session duration was tested. For 5-min-long session, tDCS could enhance subject's alertness indeed (6 out of 8 subjects), however the after-effect is poor (3 out of 8 subjects) and the duration of after-effect is only 1min~5min.

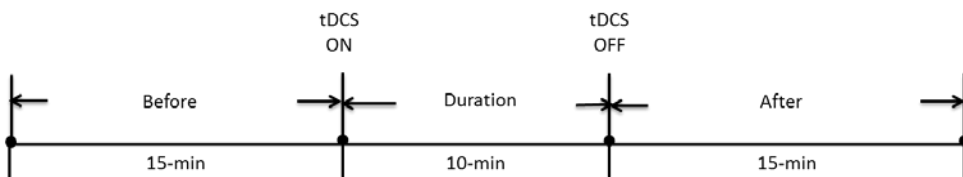


Fig. 7-13 The paradigm of the proof-of-concept study on the arousing effect of tDCS

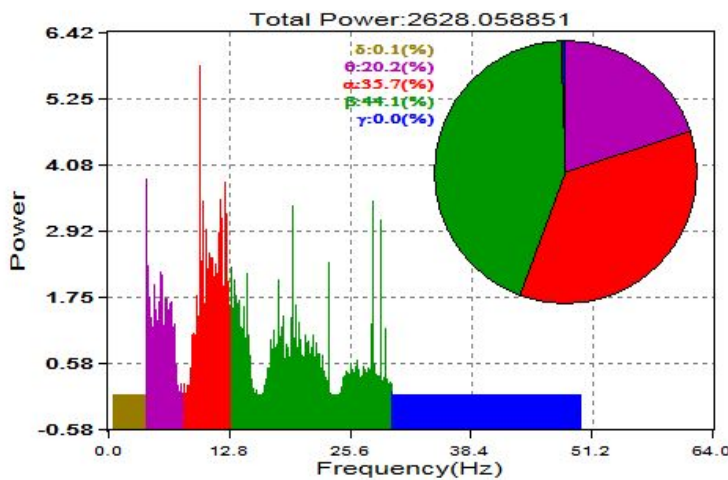
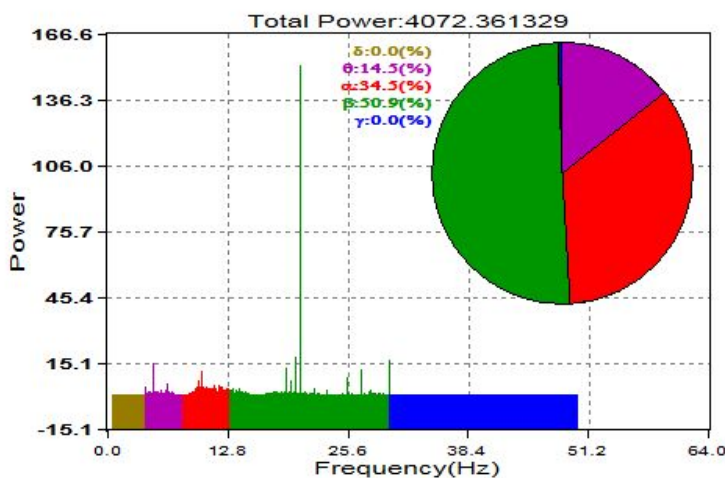
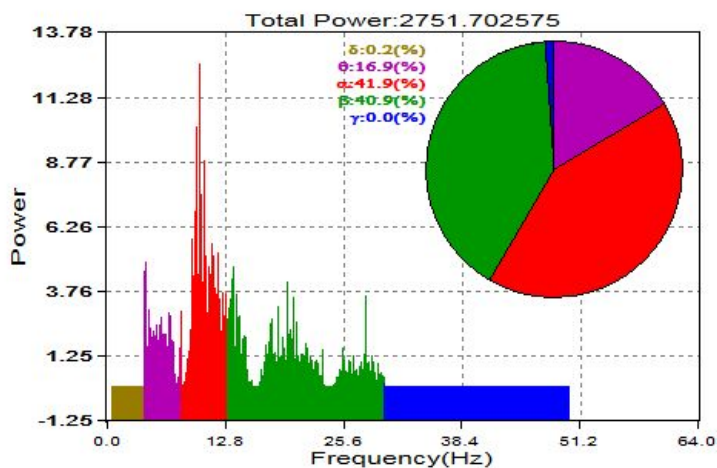


Fig. 7-14 A representative experimental results of the proof-of-concept study on the arousing effect of tDCS. The EEG RBP features of before, during and after the tDCS are shown in the top, the middle and the bottom, respectively.

Table 7-2 Experimental results of the proof-of-concept study on the arousing effect of 10-min tDCS

Subject No.	ICI (mA)	RBP(α)			RBP(β)		
		Before	During	After	Before	During	After
1	1.0	46	40.6	43.4	39.6	45.6	41.5
2	1.2	53	47.2	49.5	33	41.1	34.5
3	1.2	41.9	34.5	35.7	40.9	50.9	44.1
4	1.0	58.1	57.7	55.6	28	30.5	28.3
5	1.0	59	58.4	58.6	32.5	37.1	34.5
6	1.0	37.3	32.5	32.1	52.7	56	55.3
7	0.8	46.3	45.7	51.5	37	43.3	47.8
8	1.0	30.8	27.7	22	52.8	53.5	65.5
Overall	1.0	46.6	43.0	43.6	39.6	44.8	43.9

As can be seen in Table 7-2, the averaged ICI is 1mA. The averaged RBP(α) of before tDCS was 46.6, which was decreased to 43.0 during tDCS session; while the averaged RBP(β) of before tDCS was 39.6, which was increased to 44.8 during tDCS session. Regarding the averaged RBP features of after tDCS, there was still 3% decrease in RBP(α) and 4.3% increase in RBP(β) indicating the feasibility of arousing drivers using non-hairy forehead-based tDCS. It is important to note that the long-lasting after-effect (15-min versus auditory 40 sec) was confirmed in this pilot study.

It is also important that the proof-of-concept experimental results were perfect. The arousing effect during tDCS and after tDCS was found for all eight subjects. The physiological reasoning behind this might be that

tDCS is more effective to modulate awake brains. More specifically, during the whole experiment procedure, the subjects sat comfortably on a chair in a laboratory environment and were basically in awake status. So, the brain is easy to be modulated or stimulated by external factors, such as electrical current. Further studies considering a simulated driving environment needs to be conducted aimed at boosting driver's alertness in real-time way through the integrated closed-loop DDD algorithm (See Section 7.4).

7.1.6.2 Safety

To evaluate the safety, all subjects who participated in this pilot study were invited to our laboratory again 48 hours later. They were required to fill out a questionnaire comprising survey questions such as "Did you experience headache?" and "Did you experience insomnia?" None of them reported obvious negative feeling if compared to that of before participating in this pilot study.

7.2 Aging Test

7.2.1 Power consumption and battery life

The proposed system is powered by batteries. So, an aging test was conducted to investigate power consumption and the battery life. The system power consumption and battery life for remote feature extraction (where both the EEG and gyroscope feature extraction are performed remotely by the smartwatch) is compared to that with locally processing (where both the EEG and gyroscope feature extraction is performed directly on the MCU chip inside the headset). As can be seen in Table 7-3, the battery life is 9 hours for the whole system using the on-chip feature extraction approach, which is 6 hours longer than using remote feature extraction. This battery life

is acceptable for real-life applications where the recommended maximum continuous driving period is 2 hours, according to worldwide driver's handbooks [115-117].

Table 7-3 Comparison of power consumption and battery life of the headset and smartwatch under remote and local feature extraction conditions

Device	H/W Components	Power consumption (mA)/ Battery life (Hours)	
		Remote	On-chip
Headband	SIU	1 mA	
	SPU	49 mA	
	Bluetooth	10 mA	6 mA
	Overall	60 mA	56 mA
Smartwatch	-	3 Hours	9 Hours

7.2.2 Battery Life Comparison with Prior Work

To compare the battery life with that found in prior work, three studies that use the same wireless protocol (Bluetooth) and main signal source (EEG) are carefully chosen from the existing literature. In the previous studies, Table 7-4 shows that the maximum battery life of 45 hours was obtained by using a relatively high-capacity battery (16000 mAh). This is compared to 23 and 33 hours by using 750 and 1100 mAh batteries, respectively. A major limitation of these reported long battery lives is that they only relate to the EEG acquisition device. They do not include the end device, which is indispensable to the DDD system. Considering the practical utility (e.g., the requirement for low-cost and ease-of-use), we combined the DDD application-specific EEG acquisition device and the mass consumer electronics (e.g. wearable smartwatch). Therefore, we carefully evaluated the

battery life of the smartwatch, which serves as the DDD terminal device in this study, and a 9-hour battery life was obtained from its built-in 300 mAh battery.

Table 7-4 Comparison of Battery life of Bluetooth-enabled and EEG-based DDD systems

Ref No.	EEG acquisition part				DDD end device	Battery life
	Signal Source	ADC	Sampling rate (Hz)	Wireless module		
[61]	1-ch EEG	12 bit	512	Bluetooth v2.0+ EDR	×	33 hours (by 1100mAh battery)
[95]	4-ch EEG	24 bit	256		×	23 hours (by 750mAh battery)
[5]	4-ch EEG	8 bit	295	Bluetooth and RF dual modules	×	45 hours (by 16000mAh battery)
Proposed method	1-ch EEG+ 3-ch Gyroscope signals	12 bit	128	BLE	√ (Smartwatch)	46 hours for EEG headset (by 2600mAh battery)
						9 hours for Smartwatch (by 300mAh battery)

7.3 Simulated Driving I: Evaluating CA and SVM-based DDD

A simulated driving experiment was conducted to evaluate the CA and SVM-based DDD. Although driving simulation cannot completely replace the real field testing, the advantage is that we could recruit more participants and collected more data. In addition, there may be several ethical difficulties to perform in real driving condition and thus the driving

simulator is possibly the next best choice. For example, PC-based driving simulators are not uncommon in DDD studies [26, 66, 96, 103]. In our study, the PC-based driving simulator is Euro Truck Simulator 2 in which participants play the role of commercial truck drivers. One important reason we used Euro Truck Simulator 2 is that U.S National Highway Traffic Safety Administration ever selected commercial truck drivers as the DDD research targets for real field testing [18].

7.3.1 Experiment Paradigm Design

7.3.1.1 Participants and Driving Task

According to our previous work [19, 20], one-hour monotonous driving after lunch (typically around 1:00-2:30 pm) results in drowsiness in a majority of subjects. Therefore, to evaluate the proposed system, seventeen subjects, in possession of valid driver's licenses, participated in a one-hour monotonous driving simulation experiment. Experimental data (EEG RBP features and gyroscope MP features) from twelve subjects was used for training the SVM-based drowsiness detection model. The final testing phase was performed for the remaining subjects.

During the monotonous driving experiment, the participants drove with a few road simulators on a highway and experienced various realistic cognitive loads, just like a real driving with a multitask nature, such as keeping or changing lanes to avoid collisions, turning on the windshield wipers when driving in rainy conditions, and early deceleration before red lights.

On the day of the experiment, subjects were prohibited from caffeinated beverages. Moreover, the consumption of soporific medicines, such as standard cold medications, was prohibited. Prior to the monotonous driving experiment, each subject was given ten minutes to familiarize himself/herself with the operation of the driving simulator.

7.3.1.2 Ground Truth

For labeling true alert and drowsy events, the Wierwille scale was used [104]. Wierwille scale is a widely-used and video-based DDD ground truth. The well-trained observers can manually classify the driving status into pre-defined five levels based on 1-min video clips (Level 0: Alert, Level 1: Slightly drowsy, Level 2: Moderately drowsy, Level 3: Significantly drowsy and Level 4: Extremely drowsy). In particular, Wierwille scale classifies slightly drowsy driving according to following indicators: 1) increase in the duration of eye blinks; 2) possible increase in the rate of eye blinks; 3) increase in the duration and frequency of sideway glances; 4) appearance of a “glazed-eye” look; 5) appearance of abrupt irregular movements – rubbing face/eyes, moving restlessly on the chair; 6) abnormally large body movements following drowsiness episodes; and 7) occasional yawning. We can see clearly that the indicators 5) ~7) can directly cause head-movements and can be easily captured by the gyroscope.

Two undergraduate students were recruited and paid to participate in scoring this study in addition to a postgraduate student, all from the Pukyong Natioanl University, Busan. The three observers rated the video segments of 1-min duration and assigned a corresponding drowsiness level according to the scoring criteria defined by Wierwille scale. In order to form a convincing class label for each subject’s data segments, a majority voting process was used. In such a process, each segment is assigned the label that most of the

observers agreed on. The convincing label was then used as the final class label for building SVM model.

7.3.2 Experiment Environment Setup

Fig. 7-15 shows that the driving simulation environment consisted of a commercial truck driving simulator (Euro Truck Simulator 2), a Logitech® steering wheel, and acceleration and brake pedals. The participants were wearing the proposed smart BMI sensing headset and the smartwatch-based terminal device. In addition, a built-in video camera of the Macbook air was used to record participants' facial expressions and driving behaviors. The recorded video was used for off-line drowsiness scoring according to Wierwille scale. The synchronization of recorded video and BMI-extracted features was done by time stamps.

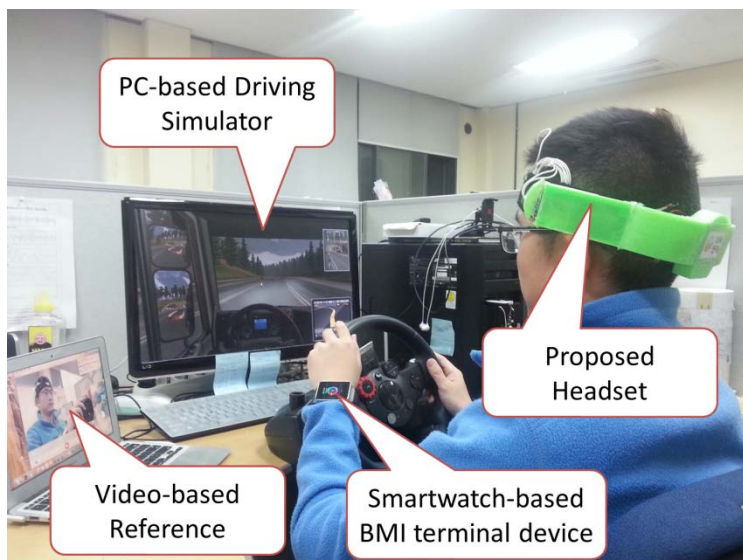


Fig. 7-15 Example of experimental setup for evaluating drowsiness detection

7.3.3 Experiment Analysis

Fig. 7-16 shows that all collected features were analyzed by descriptive statistics method firstly, in order to examine the effectiveness of the features in a quick way. Here, Box-Whiskers plots were used, which is just a quick way of examining one or more sets of data visually. Also, Box-Whiskers plots are particularly useful for comparing distributions between several groups of data. For these facts, it was used to compare the collected 5-level features first. The implementation of Box-Whiskers plots was based on IBM SPSS Statistics software (IBM, Armonk, NY, USA), where the boxes have three lines to present the values for first quartile (the bottom), median, and third quartile (the top) for column data. The length between the first quartile (Q1) and the third quartile (Q3) is called the interquartile range (IQR). Two addition lines at both ends of the whisker indicate the $Q1 - 1.5 \times IQR$ and $Q3 + 1.5 \times IQR$ value of a column data. Any data not included between the whiskers is plotted as outliers represented by “o” for mild outliers and “*” for extreme outliers. The number next to the outlier is the number of the data in that column, called the case number.

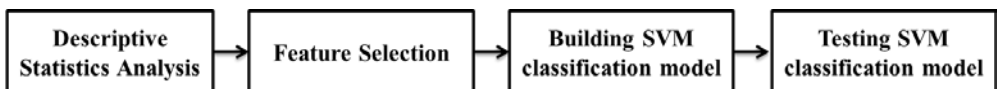


Fig. 7-16 Experiment analysis chain

Secondly, to select the best features for SVM classification, the extracted EEG and gyroscope features were compared by using ROC_{area} . ROC_{area} is the area under the receiver operating characteristic (ROC) curve, which is an effective measure of the class-discrimination capability of a

specific feature [19, 162]. Its value can be any value from 0.5 to 1. A value of 0.50 implies that the features are completely overlapped and thus non-separable; while a value of 1 implies that the features are completely separable. The ROC analysis was implemented on IBM SPSS Statistics software, where the features need to be analyzed (“Test variable” in SPSS) are $\text{Per}(\theta)$, $\text{Per}(\beta)$, $\text{Per}(\alpha)$ and MP. The “State variable” is observer-scored Wierwille scale (5-level driver drowsiness).

Thirdly, the best features from twelve participants were used to build 5-level category SVM classifier according to LOSO across-validation principle. Finally the well-trained classifier was tested by the features from the remaining five participants.

7.3.4 Experiment Results

7.3.4.1 Feature Analysis Results

In total, 1017 labeled feature sets containing 255 alert feature sets (Level 0), 477 slightly drowsy feature sets (Level 1), 167 moderate drowsy feature sets (Level 2), 98 significant drowsy feature sets (Level 3) and 20 extremely drowsy feature sets (Level 4) were collected through this simulated driving experiment. Each feature set consists of four features: RBP (θ), RBP (α), RBP (β) and MP. The Box-Whiskers plots (Fig. 7-17) show that the median values of EEG features RBP (θ), RBP (α), RBP (β) and the gyroscope feature MP are 16.5, 38.6, 43.2 and 57.8%, respectively for the alert group (Level 0), and 14.8, 34.7, 48.0 and 147.8% for the slightly drowsy group (Level 1). This trend in EEG features is in accordance with previous associated conclusions [29], that is, when a driver passes from the alert to the drowsy stage, β power decreases, and α power increases to

becomes abundant. However, Table I shows that the EEG features are not clearly separable with $ROC_{area} = 0.615$, 0.581, and 0.558 for RBP (θ), RBP (α) and RBP (β), respectively; while the gyroscope feature MP shows an outstanding class-discrimination capability with $ROC_{area} = 0.992$. To explain this further, the EEG and MP features of one representative subject that were extracted from three typical slightly drowsy symptoms (rubbing of eyes, moving restlessly and yawning) are shown in Fig.7-18. We can see clearly that the MP increased significantly when this subject passed from the alert to the slightly drowsy stage, while his α power decreased and β power increased during this period. This is contrary to previous conclusions. However, this phenomenon is expected since the intermittent head-movements caused by slightly drowsy symptoms lead to poor contact between the dry electrodes and the scalp [163]. This results in artifacts and friction noise for the EEG signals, but it is useful contextual information for DDD that can be easily captured by the gyroscope sensor.

Table 7-5 Comparison of ROC_{area} of EEG features and gyroscope features under one-to-one drowsiness level condition

DL*	ROC_{area}			
	RBP(θ)	RBP(α)	RBP(β)	MP
0 vs 1	0.615	0.581	0.558	0.992
0 vs 2	0.789	0.998	0.830	0.693
0 vs 3	0.754	1.000	0.925	0.780
0 vs 4	0.854	1.000	0.949	0.713
1 vs 2	0.691	0.996	0.805	0.778
1 vs 3	0.669	1.000	0.891	0.713
1 vs 4	0.770	1.000	0.948	0.875
2 vs 3	0.501	0.998	0.678	0.580
2 vs 4	0.583	1.000	0.869	0.535
3 vs 4	0.581	0.983	0.837	0.629
Overall	0.681	0.956	0.829	0.729

*DL=Drowsiness Level

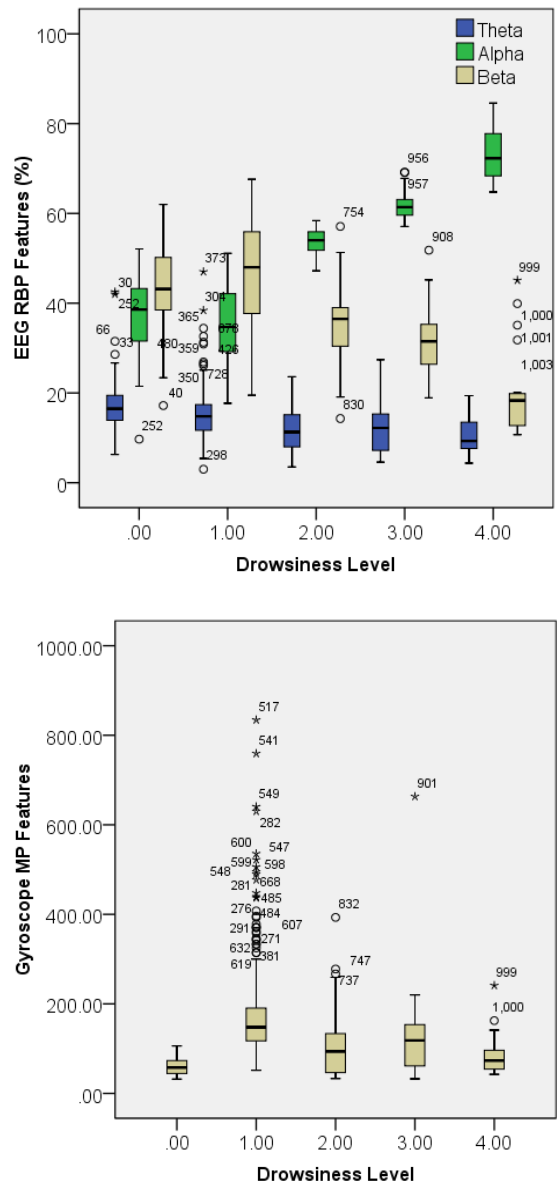
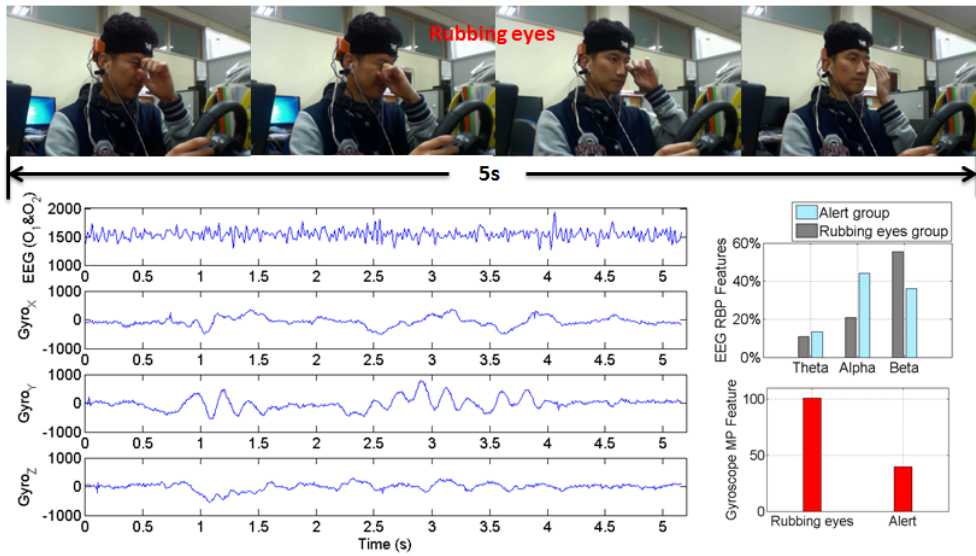
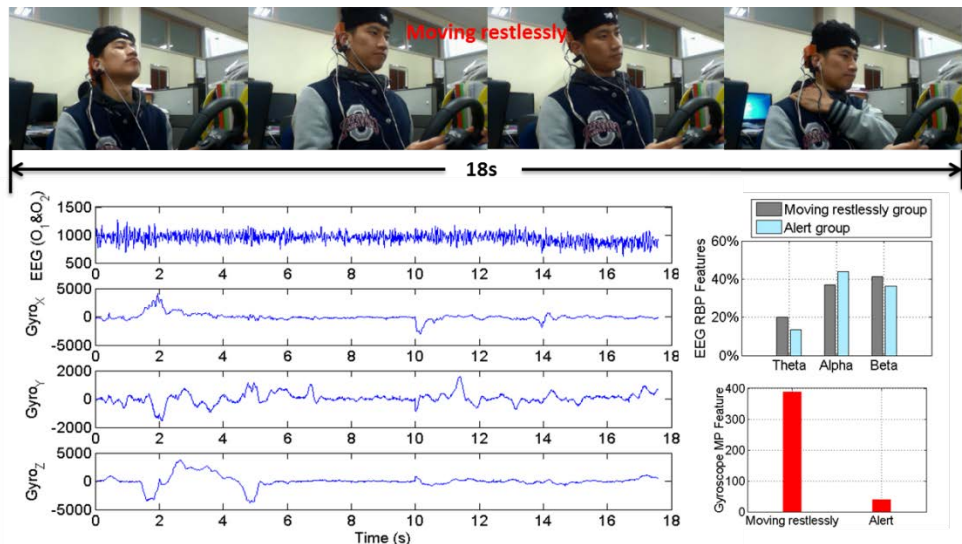


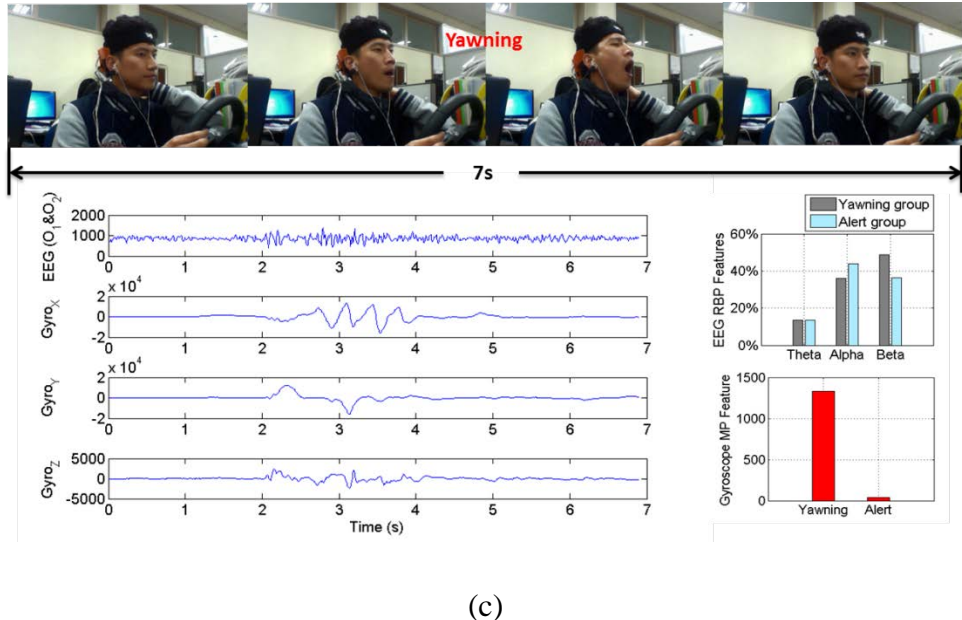
Fig. 7-17 Box-Whiskers plots of (the top) EEG and (the bottom) Gyroscope features extracted from labeled alert and drowsy datasets



(a)



(b)



(c)

Fig 7-18. The typical three slightly drowsy symptoms captured by video as well as EEG and gyroscope from a representative subject. (a) Rubbing eyes (b) Moving restlessly on chair (c) Yawning. The blue line charts for each figure represent EEG raw signals, X-axis, Y-axis and Z-axis signal of gyroscope respectively. The two bars on the right side of the line charts represent the EEG RBP features (the top) and the gyroscope MP features (the bottom).

The remaining labeled drowsy events are: moderately drowsy events (Level 2), significantly drowsy events (Level 3), and extremely drowsy events (Level 4). As can be seen in Fig. 7-17, the RBP (α) and RBP (β) show an obvious increasing and decreasing trend, respectively. This is predominantly due to the reduction in the degree of eye closure and the extended duration of eye closure events defined by the Wierwille scale ground truth. This clear trend has been verified by our previous study [105],

in which a positive linear relationship between the degree of eye closure and the RBP (α) was found ($r^2=0.93$). Table 7-5 shows that with the $ROC_{area} = 0.983-1.000$, the class-discrimination capability of $RBP(\alpha)$ for Level 2 to 4 is far superior to that of $RBP(\theta)$ and $RBP(\beta)$, where $ROC_{area} = 0.501-0.869$. For the MP feature, the boxplot does not show a clear trend. It has the second highest median value for Level 3 due to the abrupt large body movements defined by the Wierwille scale. The lowest median value of MP in the drowsy groups is obtained by Level 4, which is almost as low as that of Level 0. This is due to the longer duration of drowsy episodes with no body movement, which is also defined by the Wierwille scale. Table 7-4 further shows that the class-discrimination capability of MP for Level 2 to Level 4 is poor, with $ROC_{area} = 0.535-0.629$.

Based on the ROC analysis above, we find that the gyroscope feature is quite successful at classifying the alert and slightly drowsy groups. However, with the increase in drowsiness level, EEG features, particularly RBP (α) start to outperform gyroscope feature MP. Therefore, from the perspective of early detection of driver drowsiness, MP is the single best feature; while from the perspective of comprehensive detection task (e.g., 5-level classification), the combination of MP and RBP (α) is the best feature set.

7.3.4.2 Classification Results

In the model training stage, SVM was used to classify the EEG, MP and hybrid features of EEG and MP that were extracted from 12 of the 17 subjects. The results are summarized in Table 7-6, where each accuracy value has been optimized by adjusting the SVM parameters. In this study, the performance of the Linear-SVM was the best. As expected, the overall accuracy of 93.87% was obtained using the hybrid features, compared to the

64.15 and 71.17% obtained using the EEG and MP features, respectively, in isolation. The results of the final test using the remaining five subjects are summarized in Table 7-7. The overall accuracies of the EEG and MP features alone were 66.33 and 67.33%, respectively. Using the hybrid features, the accuracy increased to 93.67%, indicating the robustness of the proposed approach.

Table 7-6 Results of the LOSO cross-validation experiments using EEG feature, gyroscope feature and the combined feature

DL	Number of feature sets	Detection accuracy (%)		
		RBP(α)	MP	Combined features
0	183	22.95	96.72	94.54
1	341	81.82	97.95	94.72
2	101	96.04	0	92.08
3	75	96	0	97.33
4	17	64.71	0	64.71
Overall	718	64.15	71.17	93.87

Table 7-7 Results of the final test using EEG feature, gyroscope feature and the combined feature

DL	Number of feature sets	Detection accuracy (%)		
		RBP(α)	MP	Combined features
0	73	5.48	97.26	97.26
1	135	84.44	97.04	95.56
2	66	90.91	0	89.39
3	23	86.96	0	91.30
4	3	33.33	0	33.33
Overall	300	66.33	67.33	93.67

It is important to note that using the EEG feature alone obtained a significantly low accuracy in recognizing Level 0 (22.95% in the model building stage and 5.45% in the testing stage). The MP feature obtained a detection accuracy of 96.72 and 97.26% for Level 0, and 97.95 and 97.04%

for Level 1, at the model building and testing stages, respectively. However, it is unable to recognize Level 2 to Level 4, with a detection accuracy of 0% at both stages. It is further important to note that although the EEG feature obtained a better detection accuracy for classifying Level 2 to Level 3, the detection accuracy for classifying Level 4 is considered to be low (64.71 and 33.33% for the model building and testing stage, respectively). More specifically, a total of 12 of the available 20 Level 4 events at both stages were misclassified as Level 3. We found that these misclassifications occur due to the overlapping stages of Level 3 and Level 4. This is expected as subjects had to continue driving, and prior to finally entering into Level 4, subjects returned to Level 3 several times within the 1-min video clip.

The possibility of developing a DDD system limited to an early-warning function is also investigated when the problem is converted to a binary classification task (Level 0 vs Level 1 only). The accuracies were 94.65% for the model training stage and 96.15% for the testing stage using the combined features, compared to 60.11 and 56.73%, respectively using the EEG feature alone. This indicates the advantage of the proposed combined approach.

7.3.5 Discussion

We apply a gyroscope to driver drowsiness detection in order to recognize a drowsy driver's early features, when warning feedback might be the most effective. As expected, the experimental results show that our proposed method is quite successful for early detection of driver drowsiness with a detection accuracy of 96.15% between the alert and slightly drowsy group. In addition, the proposed method is implemented and evaluated on a

fully wearable BMI system, which highlights the important practical utility of the system.

7.3.5.1 Principle Results

A new approach for the classification of the drowsiness level is proposed in this study. We use a gyroscope combined with an EEG signal to measure the intensity of head movement and to detect driver drowsiness. The gyroscope features are used and compared with FFT-based EEG features. It is clear that the FFT-based features are effective in detecting driver drowsiness from the EEG, particularly in mid or late-stage drowsiness. However, for classification of early drowsiness, the information provided by EEG alone is proved to be insufficient. The information presented in the head movements (early drowsy symptoms) is lost. Taking the gyroscope into consideration, it provides richer contextual information, which is highly useful in detecting early-stage drowsiness. This additional information is the reason for the better results obtained using a combination of the gyroscope and EEG features in this study.

To explain this further, we explored the relationship between the EEG and gyroscope features extracted from all 17 subjects' head movements during the alert status and the three typical slightly drowsy symptoms, as shown in Table 7-8 and Table 7-9. Compared to the alert status, the movement of rubbing eyes increases the value of RBP (α) (37.5 vs 43.97%, $ROC_{area}=0.733$) and decreases the value of RBP (β) (44.56 vs 39.10%, $ROC_{area}=0.711$), while, in contrast, the movements of moving restlessly on the chair and yawning both decrease the value of RBP (α) and increase the value of RBP (β). In particular, the movement of moving restlessly on the chair causes a greater increase in RBP (β) (44.56 vs 56.82%, $ROC_{area}=0.894$). As mentioned previously, ROC_{area} is an effective measure of the class-

discrimination capability of a specific feature. Thus, the larger the ROC_{area} difference between the EEG and gyroscope features, the more information is lost. Table 7-9 indicates that the information presented in yawning movements is more lost by FFT-based EEG features (averaged ROC_{area}=0.593) but more enriched by gyroscope features (ROC_{area}=1.000) if compared to rubbing eyes movements and moving restlessly movements. We further observed that yawning movements were the most frequent slightly drowsy symptom during the driving experiment, which indicates that the combination of the gyroscope and EEG has a strong practical utility to recognize early driver drowsiness.

Table 7-8 Comparison of means of EEG features and gyroscope features under different head movements conditions

Head movements	Feature value			
	RBP (θ)	RBP (α)	RBP (β)	MP
Alert	16.63 \pm 0.30	37.50 \pm 0.43	44.56 \pm 0.49	59.57 \pm 1.07
Rubbing eyes	13.83 \pm 0.50	43.97 \pm 0.87	39.10 \pm 0.67	172.91 \pm 14.47
Moving restlessly on chair	11.03 \pm 0.95	30.17 \pm 0.98	56.82 \pm 1.27	405.43 \pm 47.94
Yawning	14.82 \pm 0.68	34.80 \pm 1.23	47.01 \pm 1.44	238.65 \pm 17.41

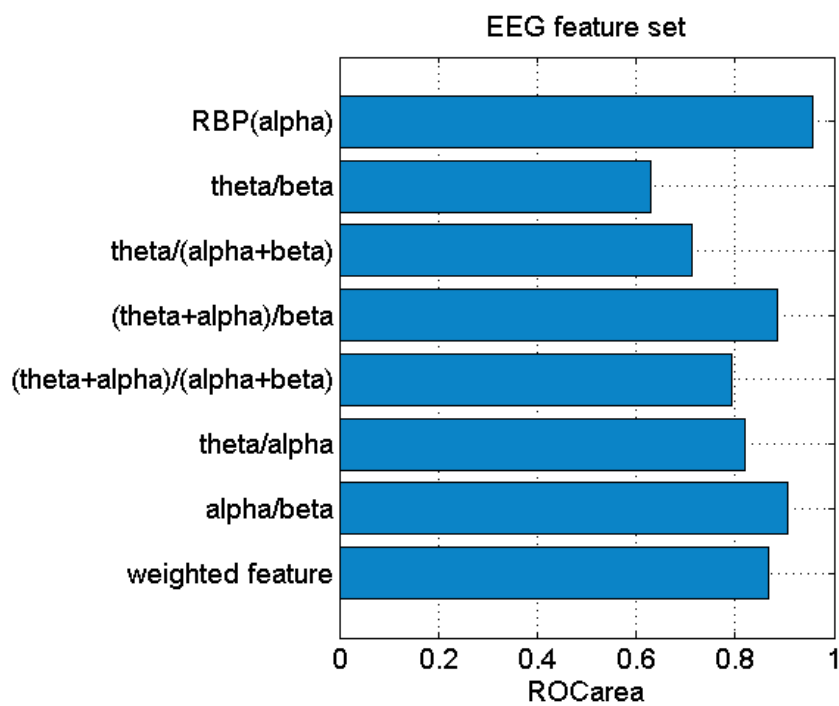
Table 7-9 Comparison of ROC_{area} of EEG features and gyroscope features under different head movements conditions

Condition	ROC _{area}			
	RBP (θ)	RBP (α)	RBP (β)	MP
Alert vs Rubbing eyes	0.718	0.733	0.711	0.999
Alert vs Moving restlessly	0.822	0.813	0.894	1.000
Alert vs Yawning	0.603	0.602	0.576	1.000

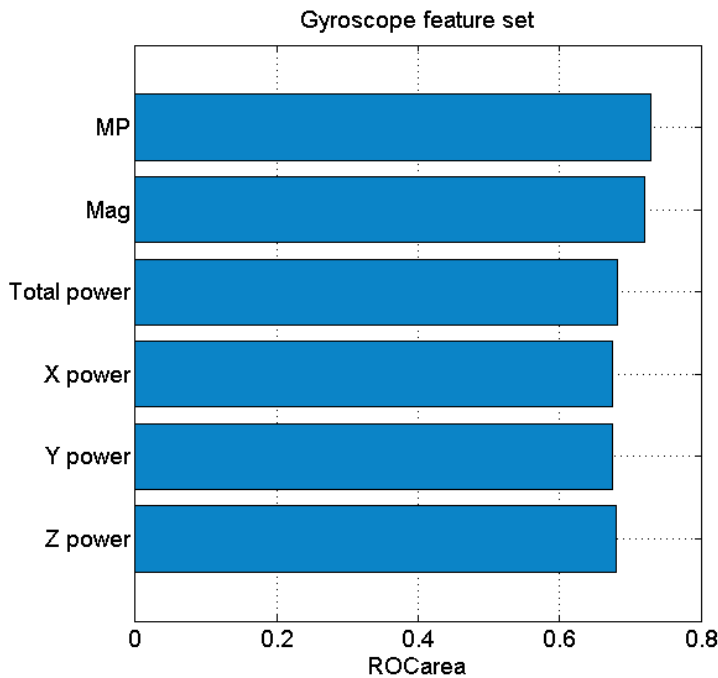
7.3.5.2 Feature Extraction

In this study, we employed the EEG feature RBP(α) and gyroscope feature MP, and obtained a 93.67% overall accuracy. In order to determine

whether the accuracy can be increased further, other commonly-used EEG and gyroscope features were compared using ROC_{area} , as shown in Fig. 7-19. Comparison of the results shows that RBP(α) and MP are the best feature for the EEG feature group (e.g., the equations in Table 2-5) and gyroscope feature group (e.g., total power [144, 145], X-axis power, Y-axis power and Z-axis power), respectively.



(a)



(b)

Fig. 7-19. The comparison of ROC_{area} of extracted features in this work and features proposed by previous works. (a) and (b) show the comparative results of the EEG and gyroscope feature groups, respectively.

It is important to note that one possible limitation of the MP feature is that left and right motions from one may cancel motions in another and so no motion looks like if the cancelling effect really happened. However, a reasonable explanation behind its success at this time should be that the head-movements caused by driver drowsiness were random and asymmetric. So, the cancelling effect was not significant. For example, the movement of rubbing eyes is a typical movement involving right and left motions. The experimental results (see red bar chart as shown in Fig. 7-14) show that the

MP value during rubbing eyes has a twofold increase if compared to that during alert events indicating the feasibility of MP-based DDD.

7.3.5.3 Comparison of Detection Accuracy with Prior Work

To compare the detection accuracy with prior work, three EEG-based DDD studies that use the same ground truth - Wierewille scale and also combine contextual information are carefully found from the numeric DDD studies. One of them recorded contextual information using motion sensor; while the remaining two studies recorded contextual information using physiological signals. Specifically, S. Prtchett et al. [68] also proposed an EEG-based context-aware solution for DDD. The main difference between the current system and that presented in [68] is that they recorded contextual information from the driver's seat where a piezoelectric film sensor is attached rather than from the headset directly. In addition, unlike the SVM model used in our study, they used linear regression model to estimate the drowsiness level (dependent variable), in which a wide range of α burst parameters and body movement parameters were used as features (independent variables). Experimental results show that hybrid features ($R^2=0.308$) outperform EEG features ($R^2=0.272$), where R^2 is the squared correlation coefficient, a commonly-used methods of estimating the performance of the proposed regression model [80]. If R^2 is high (maximum value is 1), it can be claimed that the driver drowsiness level and the extracted features have a strong linear relationship and that the performance of the regression model is superior if compared to a low R^2 . Clearly, the performance of the regression model above is poor. This is expected because regression models are good for estimating a continuous variable not the discrete labels here (5-level driver drowsiness). R. N Khushaba et al. [26] extracted features using normalized logarithmic energy of the wavelet-packet

coefficients from 5-channel physiological signals: 3-ch EEG, 1-ch ECG and 1-ch EOG. Then, a mutual information (FMI)-based method was used to select features. Finally, the kernel spectral regression (KSR)-based linear discrimination analysis (LDA) model and fuzzy classifier obtained an outstanding detection accuracy of 97% for all five levels. However, they did not mention the detection accuracy between Level 0 and Level 1, which indicates the capability of early detection of driver drowsiness. Also, R. N Khushaba et al. [88] extracted time domain autoregressive (TDAR) features from the aforementioned 5-ch signals and then used uncorrelated fuzzy neighborhood preserving analysis (UFNPA) to select features. All five Levels were detected with 89% accuracy, and Level 0 and Level 1 with 94% accuracy using a RBF–SVM classifier. These pattern recognition techniques mentioned above are more complicated than that used in the proposed method. Not surprisingly, these complicated feature extraction and selection methods are able to obtain higher overall detection accuracy (97% vs 93.67% in this study). However, they do not outperform our proposed method to detect drowsy driver's early symptoms (94% vs 96.15%). This result shows that the selection of signal source remains the most important part of designing the best detection models or systems. In addition, compared with the two studies, this study has several advantages. Firstly, we used dry electrodes instead of conventional wet electrodes, which show a more realistic detection accuracy. Secondly, we used 4-ch signals (1-ch EEG + 3-ch gyroscope) instead of 5-ch physiological signals (3-ch EEG + 1-ch ECG + 1-ch EOG), which is a less intrusive method. Thirdly, our proposed approach is evaluated on miniaturized and source-limited devices instead of laboratory-oriented devices, which shows strong practical utility.

7.3.5.4 Pilot study of SVM-based probabilistic DDD model

As mentioned in Section 2.4.1.3, probabilistic models can transform the drowsiness level to any value of 0~1 instead of discrete labels. However, since there is no ground truth which outputs non-discrete labels (See Table 2-6), the direct validation of probabilistic models to another technique are currently impossible. In this pilot study, we propose to apply SVM-based posterior probabilistic model (SVMPPM) for automated drowsiness detection and estimation of the severity of drowsy driving based on dry EEG sensor signals obtained from a simulated driving experiment. Then, the Bland-Altman plot and the proposed smartwatch-based BMI system were used to validate the estimated probability values in off-line way and real-time way respectively.

Compared with previous studies, this study has several advantages. First, this study uses probabilistic model which can estimate the probability of drowsy driving with a value range from 0 to 1 and thus can effectively increase the detection resolution. Second, an early-warning threshold probability was developed to detect drowsiness at its early stage. Third, the ground truth of percentage of eyelid closure over pupil over time (PERCLOS) was used in all the experiments. Unlike other ground truth mentioned above, PERCLOS technique is real-time ground truth and has been commercialized and intensively tested for more than ten years by U. S. NHTSA for field application (actual truck drivers driving commercial trucks) [16-18]. Therefore, it can ensure more convincing experimental results.

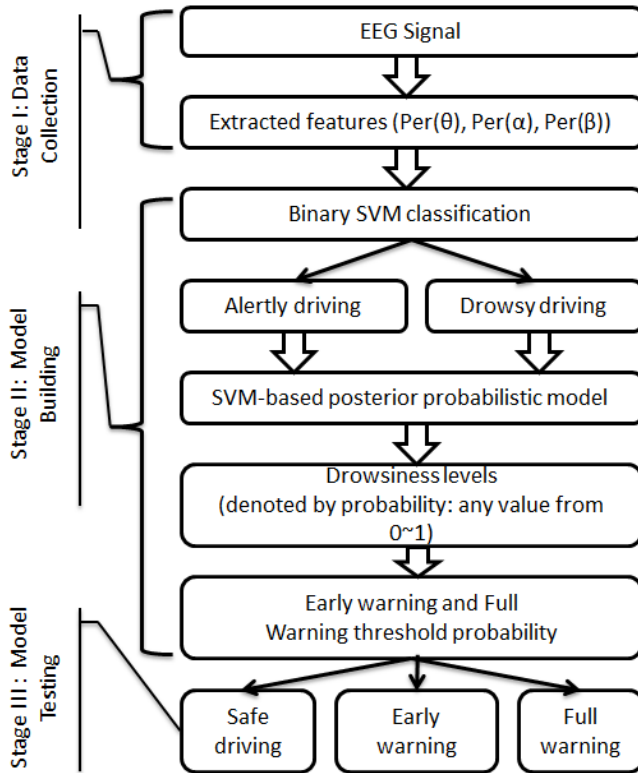


Fig. 7-20 Flowchart of estimation of driver drowsiness using SVM-based posterior probabilistic model.

As shown in Fig. 7-20, applying SVMPPM includes three stages - Stage I: Data collection, Stage II: Model building and Stage III: Model testing. The Stage I and Stage III involve one-hour simulated driving experiment (see Section III), during which both EEG signals and features were recorded. The Stage II was implemented on MATLAB in PC in off-line way, which aims to build an optimized model and develop the threshold probabilities for recognizing early drowsy warning group and full drowsy warning group. The well-trained model was then transferred to smartwatch

for real-time final testing. The following paragraphs introduce in detail the major components of proposed approach.

A conventional binary SVM classifier outputs a class label (e.g., +1: drowsy driving or -1: alert driving) for each input dataset \vec{x} comprising several features (e.g., Per (θ), Per (α) and Per (β) in this study), according to the sign function $f(\vec{x}) = \text{sign}(\vec{w} \cdot \Phi(\vec{x}) + b)$, where the \vec{w} is a vector perpendicular to the decision surface and b is a scalar (decision surface bias). $\Phi(\vec{x})$ is the mapping function which is used to map each input dataset \vec{x} from the linearly non-separable input space \Re^n to linearly separable feature space \mathbf{H} . By using kernel functions (e.g., radial basis function (RBF), polynomial kernel function (Poly)), sigmoid kernel function (Sig) and regulation parameter C, SVM is able to do this mapping work and accomplish classification without the need to know explicitly what the mapping function is.

In addition to classifying the labels into the categories of “drowsy” or “alert,” the posterior class probabilities, i.e., $P(\text{class}=+1|\vec{x})$ can be calculated based on the outputs of binary SVM classification model using the method initially described by Platt [164]. Briefly, its main idea is given by Equation 23, where, $\vec{w} \cdot \Phi(\vec{x}) + b$ is just the SVM output for input dataset \vec{x} . A and B are parameters that are determined by an improved Platt algorithm [165].

$$P(\text{class} = +1 | \vec{x}) = \frac{1}{1 + \exp(A(\vec{w} \cdot \Phi(\vec{x}) + b) + B)} \quad (23)$$

Therefore, compared to previous multi-class classification based models, the SVMPPM can further increase the resolution of detected drowsiness level (any value from 0 to 1). For example, the probability “0” indicates a full alert state, whereas a value close to “1” indicates a severely

drowsy driving state. In addition, through the combination of true labels and estimated posterior probabilities, a threshold probability could be found to provide early warning before drivers actually become severely drowsy.

Twenty subjects possessing valid driver's licenses participated in the one-hour monotonous driving experiment. Experimental data from fifteen subjects (subjects No.1-15) was used for building drowsiness detection model. Final testing phase was performed for the remaining subjects (subjects No.16-20). The experimental setup is the same with driving simulation I (except a smartphone which was placed behind the steering wheel for implementing PERCLOS ground truth). The true alert and drowsy data are labeled based on the combination of percentage of eyelid closure over pupil over time (PERCLOS) and the number of adjustment (NOA) on steering wheel. PERCLOS is a video based real-time driver drowsiness monitoring technology. It assesses drowsiness by measuring slow eyelid closure and estimating the proportion of time for which the eyes are closed over 1-min interval (high sensitivity) or 3-min interval (medium sensitivity) or 5-min interval (low sensitivity) [166]. The approach of NOA on steering wheel is developed by our group by using the built-in accelerometer and gyroscope of smartwatch [167]. The basic assumption of this approach is that alert drivers who are driving on a highway (not city driving or countryside driving) would have more NOA on steering wheel if compared to drowsy drivers. We found that some drivers' faces are occasionally outside of the camera field of view while their NOA data can remain stable. Thus, in order to provide a robust ground truth, we combined the two methods together in this study. According to [166] and [167], $\text{PERCLOS} \geq 12\%$ and $\text{NOA} \leq 9$ was chosen as the threshold to identify the presence of true drowsy driving and $\text{PERCLOS} < 8\%$ and $\text{NOA} > 26$ for true alert driving. PERCLOS measures between 8% and 12% and NOA measures between 9 and 26 can be

used as the early-warning reference. In our previous study [19, 105], we already developed a smartphone application to measure PERCLOS. Thus, in this study, the measures of PERCLOS were automatically implemented on the smartphone which was placed in front of the steering wheel.

The LOSO binary classification result is summarized in Table 7-10, where the parameter “C”, RBF parameter “g” and Poly parameter “d” are optimized using a simple search procedure with C, g={0.01~10} in steps of 0.01 and d={1, 2} in steps of 1. As expected, the best accuracy was found to be 93.59% (in RBF kernel of g=2 and C=5) when single Per(α) were used as the SVM inputs.

Table 7-10 Leave-one-subject-out Classification Accuracy of SVM Classifier with Different input feature sets and Different Kernels

Kernel	Feature sets						
	θ	α	β	θ, α	θ, β	α, β	θ, α, β
Accuracy %							
Linear <i>C</i>	76.66 0.03	93.14 0.02	83.75 1.56	92.9 0.09	92.91 0.3	92.91 0.01	92.91 0.12
	77.57 2 3	93.59 5 2	84.67 0.03 0.01	92.9 1 0.29 0.02	93.16 1.57 0.01	93.14 1.45 0.05	93.14 0.62 0.01
RBF <i>C</i> <i>g</i>	76.66 0.03 1	93.14 0.02 1	83.75 1.56 1	92.9 1 0.17 1	92.91 0.59 1	92.91 0.02 1	92.91 0.16 1
Poly <i>C</i> <i>d</i>	76.66 0.03 1	93.14 0.02 1	83.75 1.56 1	92.9 1 0.17 1	92.91 0.59 1	92.91 0.02 1	92.91 0.16 1

In addition to classifying all datasets into the categories of “drowsy” or “alert,” the posterior probability of being drowsy driving was then calculated by using the best feature Per(α) and RBF kernel. The histogram of estimated posterior probability (Fig.7-21) shows that there is a clear separation between the two groups. Most of alert datasets were classified into the bins of 0~0.1; while most of drowsy datasets were classified into the bins of 0.9~1. It is also important to note that unlike the informative class labels, the

probabilities in the same group are varied, from about 0.55 to 0.95 for drowsy group, and 0.05 to 0.4 for alert group. This result confirmed the feasibility of estimating the relative severity of drowsiness by using SVMPPM.

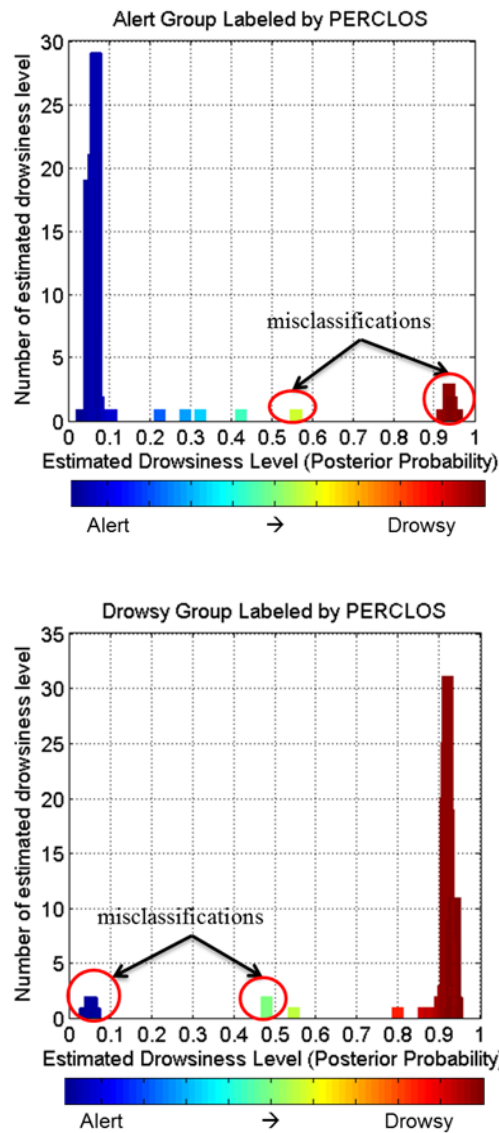


Fig. 7-21 The histogram of estimated posterior probability for each subject (#1~#15) in training phase for alert group (the top) and drowsy group (the

bottom). The X-axis indicates the drowsiness level (0~1). The Y-axis indicates the number of dataset that falls into the corresponding bins of estimated drowsiness levels.

The Bland-Altman plot [168] is the preferred method for assessing the agreement between an established measurement (e.g., the PERCLOS measurement) and a new measurement technique (e.g., the SVMMP measurement). Thus, a Bland-Altman plot (Fig. 7-21) for the 15 subjects was generated so that the relationship between PERCLOS and SVMMP measurement could be examined. For comparability among the two measures, the PERCLOS measures were normalized to the range of 0~1 by simply removing the unit %. For example, PERCLOS value of 1% is equal to value 0.01.

As can be seen in Fig. 7-22, all data is within the 1.96SD limits of agreement. However, there is a bias of -0.432 (95% CI -0.467 to -0.397) indicating that systematically the SVM-based measures have higher magnitudes than PERCLOS measures. This is mainly caused by the big differences in measures for drowsy driving (cluster_2) between the two methods. Specifically, most of SVM-based probabilities for drowsy driving are around 0.9; while the range of most of PERCLOS measures for drowsy driving is from 0.12 to 0.20. Few of them can reach to 0.30 and very few of them can reach to 0.90. In contrast, the measures representing alert driving (cluster_1) show better agreement because there is no big difference (near the bias of zero). Specifically, most of SVM-based probabilities for alert dataset are around 0.05. This corresponds to the range of PERCLOS measures for alert dataset (min=0 and max=0.07).

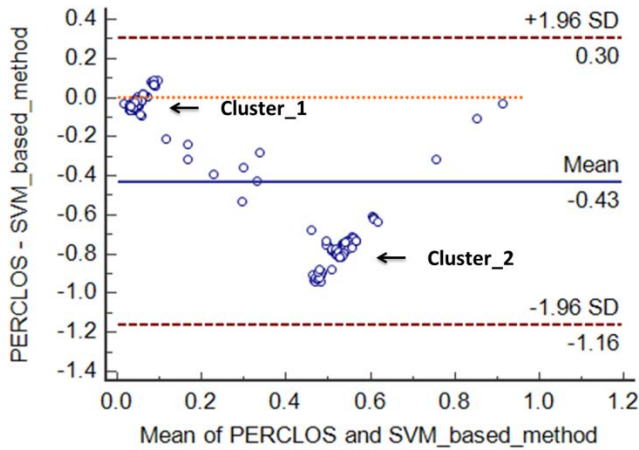


Fig. 7-22. Bland-Altman plot for the relationship of the difference between the observed PERCLOS vs. the estimated probability vs. their average values. Mean bias, $+1.96\text{SD}$, and -1.96SD lines are shown. SD = standard deviation.

Besides the Bland-Altman plot, the threshold probabilities for each subject were summarized in Fig. 7-23 and two overall threshold probabilities which indicate early warning threshold ($TH_1: P=0.424$) and fully warning threshold ($TH_2: P=0.545$) were developed to validate the calculated probabilities in real-life application. The rules for this validation are summarized in Table 7-11.

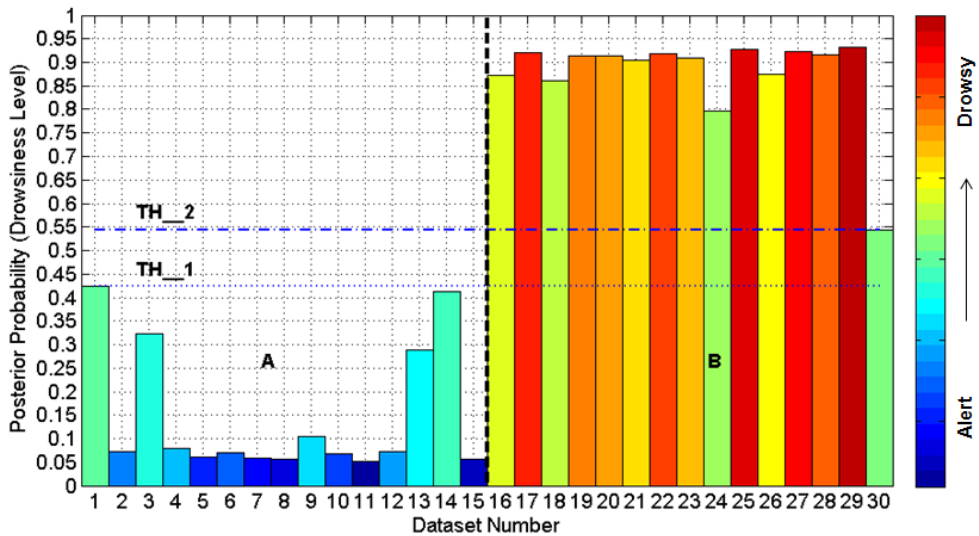


Fig. 7-23. The threshold probabilities for each subject in training phase for (panel A) alert group with X-axis 1~15 and (panel B) drowsy group with X-axis 16~30. The threshold probabilities for each subject refer to the maximum probability in alert group and minimum probability in drowsy group.

Table 7-11 Rules (Thresholds for DDD)

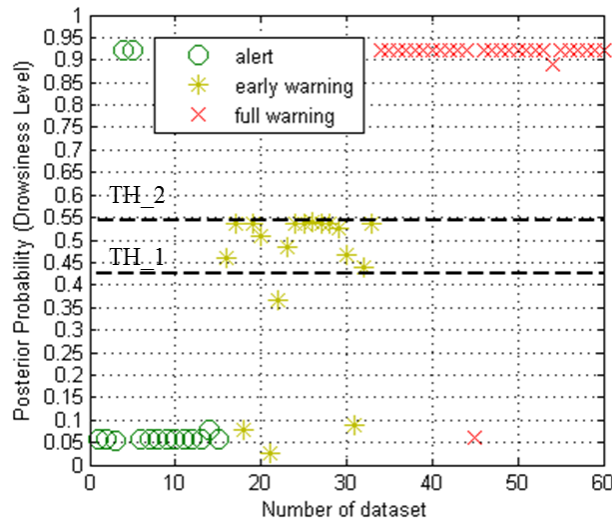
Rules	Ground truth	Decision
$0.424 \leq P < 0.545$	$8\% \leq \text{PERCLOS} < 12\%$	Early warning
	$9 < \text{NOA} \leq 26$	
$P \geq 0.545$	$\text{PERCLOS} \geq 12\%$	Full drowsy warning
	$\text{NOA} \leq 9$	

Based on the detection rules in Table 7-11, five subjects that were not used in the model building phase were used in this final test. The test results are summarized in Table 7-12. The overall classification results were 91.25% accuracy for alert group, 83.78% accuracy for early-warning group and 91.92% accuracy for full warning group. The calculated posterior

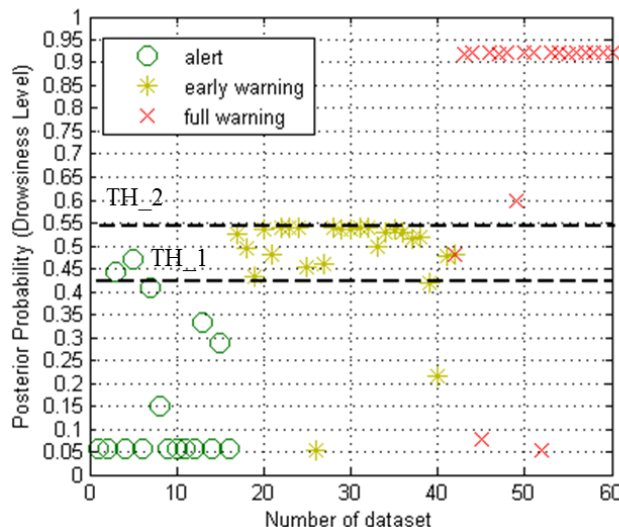
probabilities and classification results for subject No. 16 and 18 are shown in Fig. 7-24.

Table 7-12 Results of final test using proposed wearable BMI system

Subject No	Number of 1-min labeled epochs			Number of detected epochs by probabilistic thresholds			Accuracy (%)		
	Alert	Early- warning	Drowsy	Alert	Early- warning	Drowsy	Alert	Early- warning	Drowsy
16	15	18	27	13	14	26	93.33	77.78	96.30
17	11	26	13	11	22	10	100	84.62	76.92
18	16	26	18	13	23	16	81.25	88.46	88.89
19	26	13	21	24	11	20	92.31	84.62	95.24
20	12	28	20	12	26	19	100	92.86	95.00
Overall	80	111	99	73	93	91	91.25	83.78	91.92



(a)



(b)

Fig.7-24. Posterior probability estimate $P(y=+1|f(x))$ calculated for each class for (a) subject #16 and (b) subject #18.

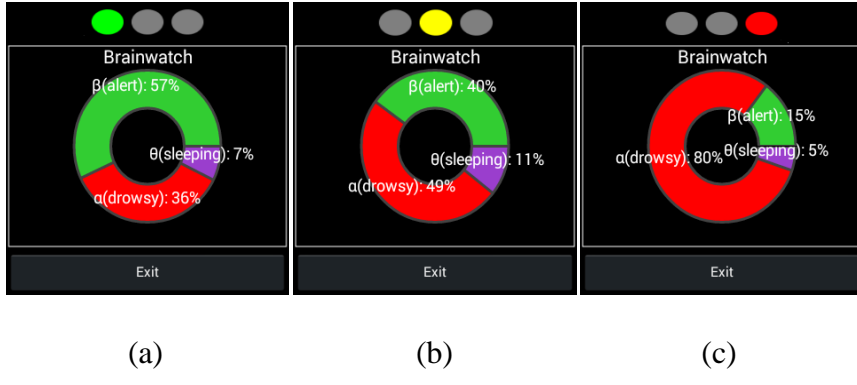


Fig.7-25. Screenshots of the smartwatch that show the estimated driving status by real-time EEG power percentage features and a virtual traffic light.
a) green: safe driving; b) yellow: early warning; c) red: fully warning).

To compare the prediction model in current work with prior studies, three DDD-related studies that also involve EEG signals and probabilistic models are carefully found from the existing literatures (as shown in Table IV).

For example, in 2010, G. S. Yang *et al.* [108] proposed a Dynamic Bayesian Network (DBN) based posterior probabilistic model to detect driver drowsiness. They employed Independent Component Analysis (ICA) to preprocess EEG signals and FFT to extract EEG features. Then, thirty sleep-deprived subjects who participated in a simulated driving experiment were used to validate the proposed model. However, the EEG channel location and the ground truth used in this study are not clear and the detection accuracy using EEG alone was not reported. In addition, the length of the time window was 6 minutes, which might be a major drawback for practical application. The other possible practical hurdles include: 1) The

usage of ICA. The ICA is a complex algorithm that is not suitable for real-time application [169]. 2) The usage of wet electrodes.

In 2011 and 2014, A. Murata. *et al* [74, 75] proposed a Basic Bayesian Estimation (BBE) based posterior probabilistic model. They used shorter time window, 1 minute, to extract FFT-based EEG features and also conducted a simulated driving experiment to validate the proposed model. However, the ground truth used was subjective (subject self-assessment-based) and wet electrodes were also used. Also, the detection accuracy using EEG alone was not reported. Besides the practical hurdles and technical drawbacks mentioned above, building Bayesian-based probabilistic model needs many empirical work including the construction of prior probability, the conditional probabilities and transitional probability (if DBN is used) [108]. However, the primary advantage of SVM is its ability to minimize both structural and empirical risk [158]. In this study, we apply SVM-based probabilistic model to detect driver drowsiness. There are presently no ‘gold-standard’ methods for assessing the estimated probabilities thus direct validation of the calculated posterior probability values to another technique is not currently possible. However, based on PERCLOS measurements, the Bland-Altman plot and a smartwatch-based wearable EEG system were used to validate the estimated probability values in off-line way and real-time way respectively.

7.4 Simulated Driving II: Evaluating Closed-Loop DDD Algorithm

7.4.1 Experiment Paradigm Design

Similar to simulated driving I, simulated driving II was also conducted after lunch time under long-distance monotonous highway driving

environment. The difference is that the experimental duration was extended from one hour to two hours, in order to investigate the tDCS-based long-lasting arousing effect. Totally, ten subjects, in possession of valid driver's licenses, participated in this two-hour driving experiment. For the purpose of comparison, two experimental conditions were employed: 1) monotonous driving with proposed closed-loop DDD algorithm (See Chapter 6); 2) monotonous driving with sham closed-loop DDD algorithm. For condition 1, five participants were randomly assigned in. tDCS anodal and cathodal electrodes were placed at Fp2 and Fp1 respectively, according to the EEG 10-20 International System. tDCS was applied with a current intensity of 1mA. For condition 2, although the number of participants, electrode placement and current intensity were identical to those in condition 1, the tDCS session was shortened from 10min to 30s (as shown in Fig. 7-26).

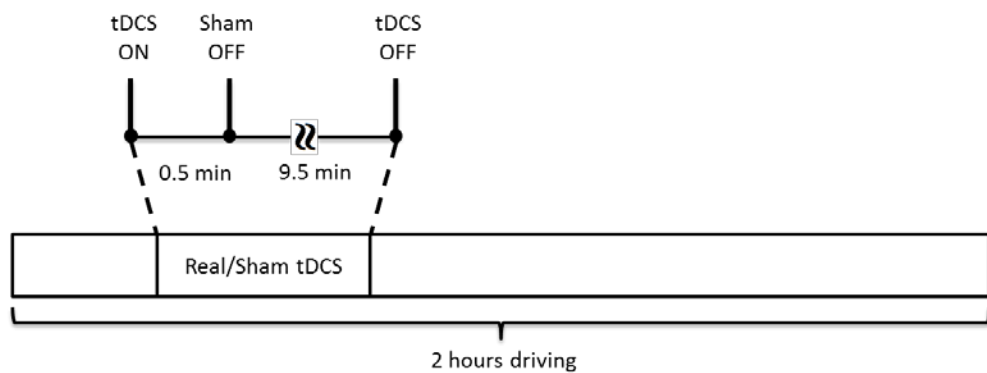


Fig. 7-26 An example of real and sham tDCS procedure during 2-hour driving experiment

7.4.2 Experimental Environment Setup

The experimental environment setup of simulated driving II is the same as that of simulated driving I.

7.4.3 Experiment Analysis

The experiment was analyzed in two aspects. First, the numbers of traffic accidents (including car collision and guard rail collision) under condition 1 were compared with that under condition 2 by using bar charts, in order to evaluate the effectiveness of the proposed closed-loop DDD algorithm. Secondly, for condition 1, the EEG RBP features of before, during and after tDCS were compared on a 15-min time window, in order to give a physiological background behind this experiment. The 15-min time window was used because we assumed that the beginning 15-min driving is alert driving so that each 15-min RBP features after tDCS were used to compare with that of the beginning 15min.

7.4.4 Experiment Results

Fig. 7-27 shows that the average number of traffic accidents under condition 1 has a significant decrease if compared to that under condition 2, which indicates the effectiveness of the proposed closed-loop DDD algorithm.

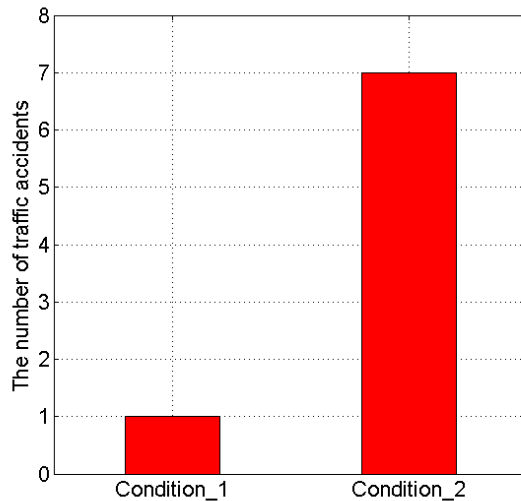


Fig. 7-27 The comparison of the number of traffic accidents between condition 1 (closed-loop DDD) and condition 2 (open-loop DDD)

Fig. 7-28 shows several arousing effect by using non-hairy forehead tDCS for monotonous-induced driver drowsiness, where we can see that the duration of after-effect varies from 15min to 45 min. Fig. 7-29 shows that the arousing effect by using non-hairy forehead tDCS decreases as time goes by, which indicates that tDCS could improve the driver's alertness but could not stop the drowsiness progress. Fig. 7-30 shows that the MP has a decrease trend after tDCS indicating tDCS could improve drivers alertness and make drivers sit still to drive without abnormal movements.

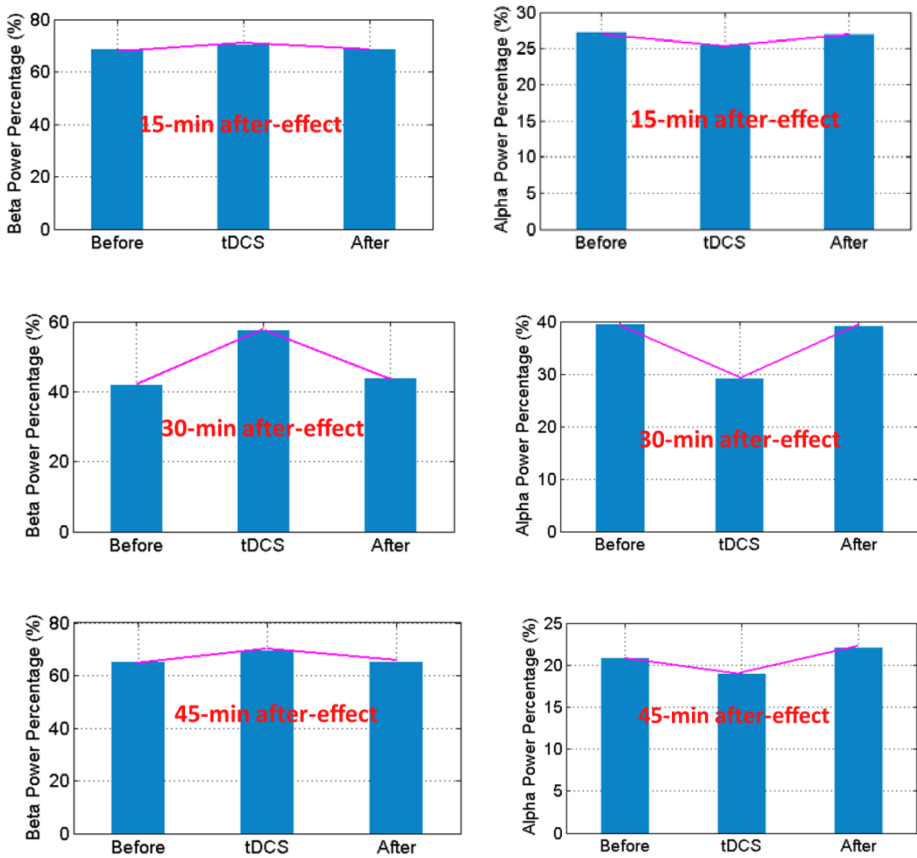


Fig. 7-28 The duration of after-effect and EEG RBP features under condition 1. The left column and right column show RBP (β) and RBP(α) respectively.

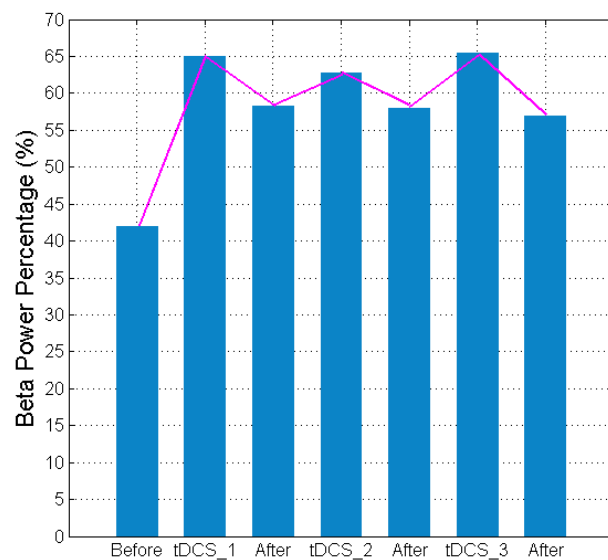
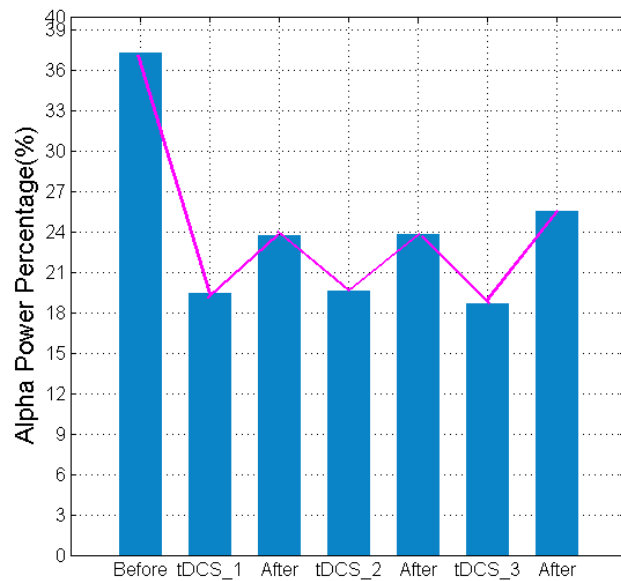


Fig. 7-29 The comparison of EEG RBP features between each tDCS sessions for the whole 2-hour driving simulation from a representative subject.

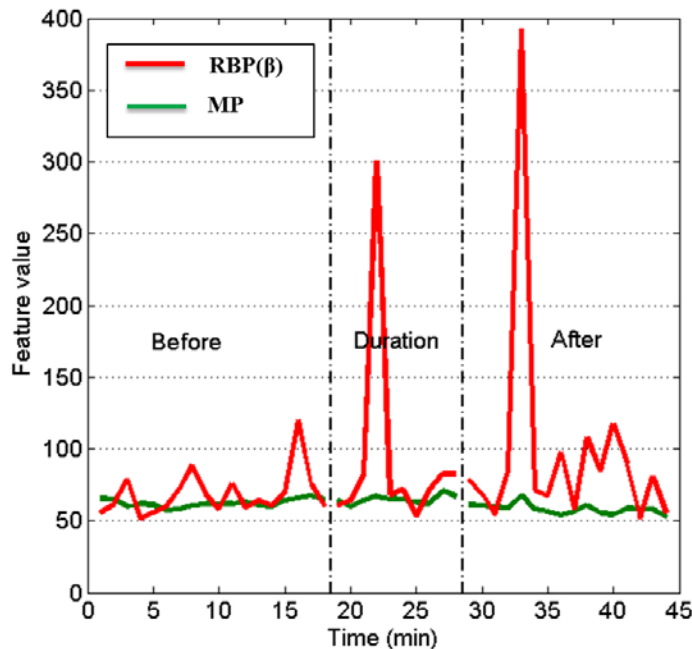


Fig. 7-30 The comparison of EEG RBP features and gyroscope MP features between before, during and after tDCS session. The X-axis indicates the time in min. The Y-axis indicates the feature values. For example, 50% for RBP features and absolute value 50 for MP.

7.4.5 Discussion

7.4.5.1 Principle Results

A new approach for the closed-loop DDD is proposed in this dissertation. We use EEG sensors combined with non-hairy forehead based tDCS neuromodulation module to estimate the driver drowsiness level and boost driver's alertness in real-time way. Experimental results show that the boosts in alertness could last 15~45 minutes amongst the five subjects, which

is more beneficial than tens-of-seconds-long auditory feedback-based closed-loop algorithm

7.4.5.2 How long after-effect do we need in real-life application?

As mentioned in Section 2.4.2.2, the arousing effect of tDCS could reach 6 hours on hairy forehead area by using wet saline-soaked sponge electrodes. In this study, the arousing effect of non-hairy forehead tDCS could reach maximum 45 minutes by using self-adhesive electrodes. To further explain the practical utility of the after-effect of non-hairy forehead tDCS, we take the highway driving environment as an example.

For real-life application, the best solution for drowsiness is rest. So, the acceptable duration of after-effect must allow the drivers have enough time driving to the nearest parking area (PA) or service area (SA) (as shown in Fig. 7-31).



(a)



(b)

Fig. 7-31 Examples of the (a) conventional parking area in the highway worldwide and (b) a novel drowsiness shelter in the highway in South Korea

According to data from Korean Ministry of Land, Infrastructure and Transport [170], the standard space of each PA is 8~10km, 10-12km, 15km and 16km in Germany, France, Korea, Japan and U.S. So, assuming averaged car speed is 80km/hour, the acceptable after-effect is 6~12min. Our experimental results show that the tDCS-based closed-loop DDD algorithm could achieve maximum three times longer than the acceptable after-effect indicating the advantage and robustness of the proposed closed-loop DDD solution.

7.4.5.3 Pilot Study on Non-contact Neuromodulation Technologies

As mentioned before (see Section 2.4.2.2), although there is a long-lasting arousing effect, the success of tDCS-based neuromodulation might be limited because of several practical hurdles. Therefore, a pilot study on the

non-contact neuromodulation technologies was conducted in this study with attempt to achieve a more easy-to-use closed-loop solution. Nevertheless, these efforts were proved to be failed.

Firstly, steady status visual evoked potential (SSVEP) technology based arousing effect was investigated. Flashing a light steadily into the eyes will stimulate the brain and cause the brain waves (EEG) to show the same frequency as the flashing light. That is, the FFT power of the EEG at the same frequency as the flashing light will increase. The increased brain waves are just called SSVEP. Based on this fact, in theory (see Section 2.4.1.2), setting the flashing frequency to around β band (12-30Hz) is likely to boost driver's alertness.

To conduct this pilot study, a smartphone was placed behind the steering wheel (as shown in Fig. 7-32). The screen of a smartphone was programmed to flash at the frequency of 20Hz and serves the flashing light source of SSVEP for 10 minutes (the same duration with tDCS). Totally, five subjects participated in this experiment.

Experimental results show that when the participant was in alert status, the SSVEP was very obvious. A clear peak frequency could be found in β band in every subject's EEG power spectral (as shown in Fig. 7-33). However, when the subject was in drowsy status (even though in slightly drowsy status), the peak was no longer prominent. Also, the SSVEP is more evenly spread over the spectral, which has no significant difference before using SSVEP (one-way ANOVA $p>0.05$).

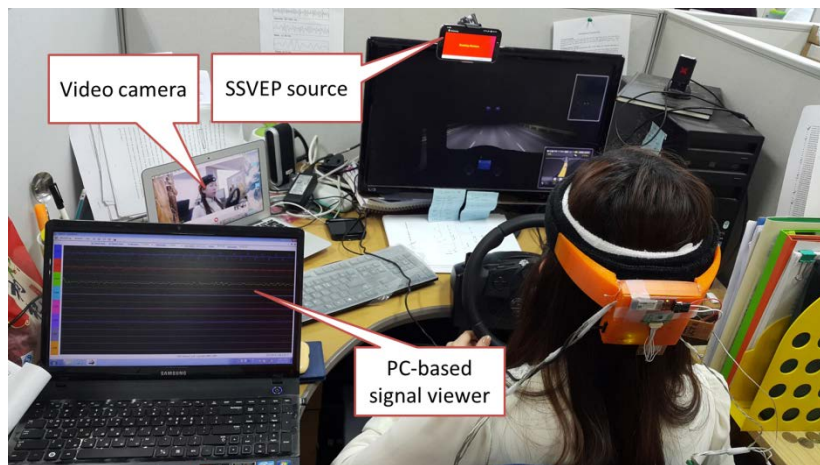
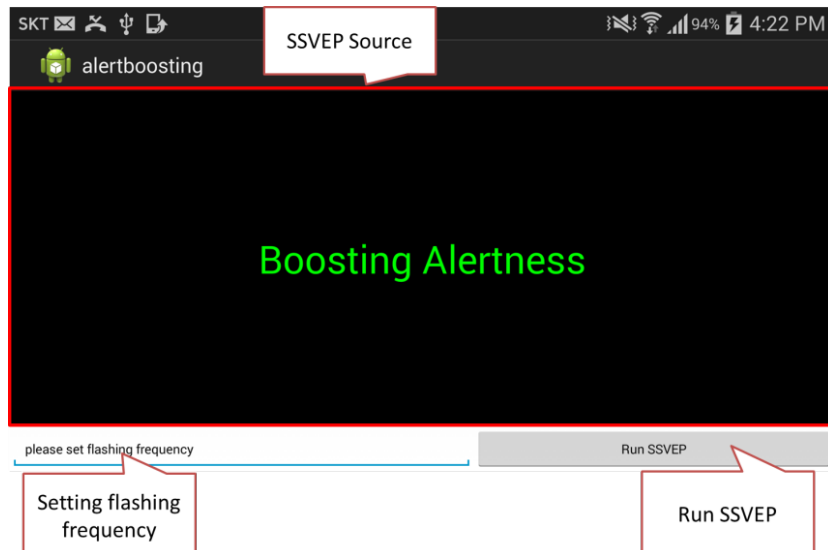
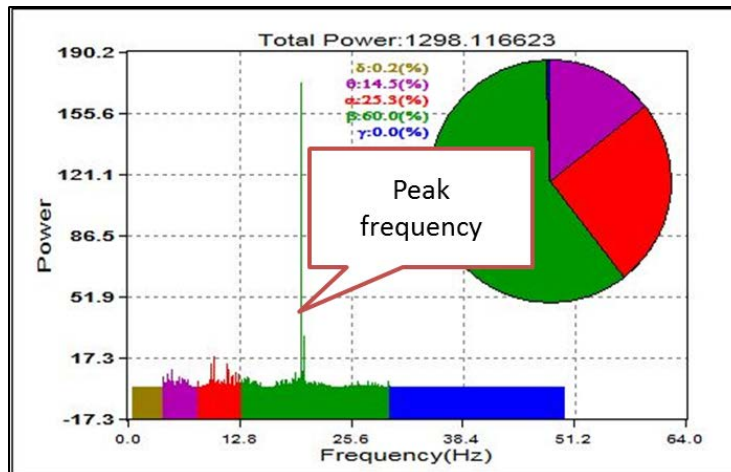
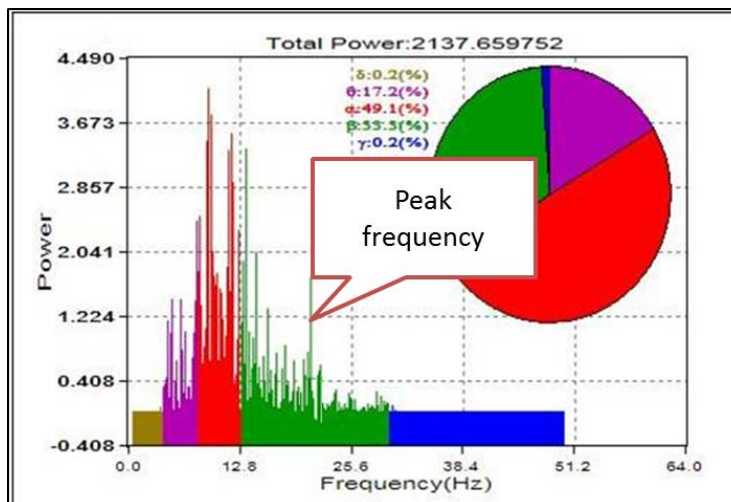


Fig. 7-32 The screenshot of a self-developed smartphone-based SSVEP source (the top) and the experiment setup of pilot study on SSVEP-based arousing effect for driver drowsiness (the bottom)



(a)



(b)

Fig. 7-33 Comparison of SSVEP power spectral between alert and drowsy status (The data is from a representative participant)

Our original idea about the usage of SSVEP is to stimulate a drowsy driver's brain wave with an aim to boost his/her alertness. However,

according to this pilot study, this idea is proved to be failed. A reasonable explanation for this might be:

- ①. SSVEP belongs to visual arousing feedback which is less sensitive to drivers since they needed to pay attention to road conditions and dashboard as we mentioned in Section. 2.4.2.2.
- ②. The tired (drowsy) brain is hard to be stimulated. We say this because even if we placed the SSVEP source in front of the driver's eyes the effect was still not good.

Similarly, audio-based neuromodulation was also investigated. When we listen to music with a fast beat, our brain waves tend to speed up. When we listen to music with a slow beat, our brain waves slow down. Therefore, in theory, playing an auditory tone at the frequency around β band is likely to boost driver's alertness. To conduct this pilot study, a smartphone was placed behind the steering wheel. A smartphone application, from Google play store, was used to play to β tone for 10 minutes (as shown in Fig. 7-34). However, the experimental results proved that this idea is also failed.

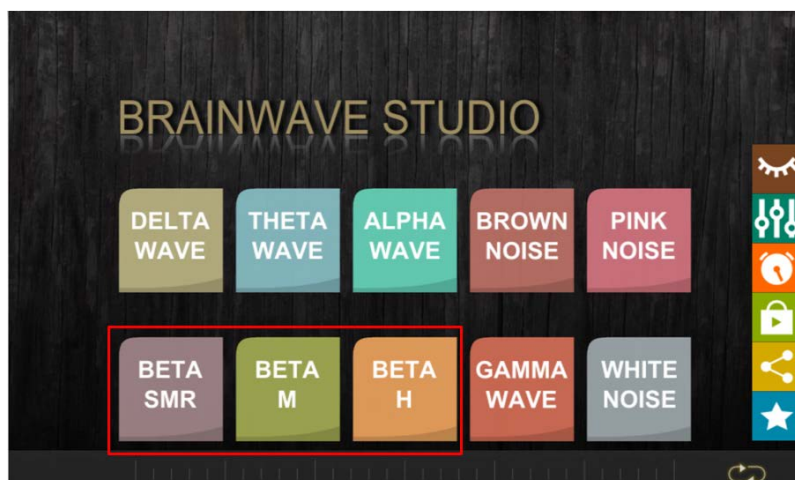


Fig. 7-34 The smartphone application used to play β tone. All β tones surrounded by red box were used in this pilot study.

7.5 Chapter Summary

The performance of the proposed context-aware and neuromodulation-enabled BMI system are investigated in three aspects. First, several basic functions are tested including the sampling rate, real-time FFT and SVM performance, as well as the pilot study on tDCS. Second, a driving simulation experiment is conducted to build SVM-based DDD prediction model and test its performance under real-life application environment. Third, another driving simulation experiment is conducted to test the performance of the proposed tDCS-based closed-loop algorithm. Experimental results show that the proposed BMI system could achieve a 93.67% 5-level overall detection accuracy and a 96.15% 2-level (alert vs slightly drowsy) binary detection accuracy. Also, the arousing effect of tDCS is confirmed by using bi-polar self-adhesive electrodes which were placed on the non-hairy forehead area. The maximum duration of after-effect of tDCS was 45min.

Chapter 8

8 Conclusions and Future Work

The design and implementation of a fully wearable and context-aware (CA) brain machine interface (BMI) system with integrated neuromodulation (NM) function is described in this paper. Also, its performance is evaluated through an everyday life situation - closed-loop driver drowsiness detection.

The system uses a Bluetooth Low Energy-enabled, EEG and gyroscope sensor-equipped headset and a machine learning model-enabled smartwatch with attempt to detect driver drowsiness at its early stage. This not only shifts DDD from reactive to preventive driver safety technology, but also achieves a simple and inexpensive on-line analysis platform. Also, this system combines a transcranial direct current stimulation (tDCS) based neuromodulation module together with attempt to boost drivers' alertness in real-time way. This shifts DDD from open-loop to closed-loop driver safety technology indicating the distinct contributions of the proposed system.

A comprehensive system evaluation, which involves a total of thirty-seven participants, was carried out including the verification of EEG signal quality, the evaluation of system computational load (e.g., real-time FFT calculation and SVM operation), the test of system power consumption and battery life, and the hours-long monotonous driving simulation experiments. Evaluation results indicate the feasibility of detecting and preventing driver drowsiness using wrist-worn and EEG-based wearable devices in an actual working environment. In addition, the comparison with other existing systems highly stood out the novelty of this study.

This dissertation has been primarily focused on the design and implementation of a CA-NS-enabled BMI system for tDCS-based closed-loop DDD application. The system evaluation was based on the long-distance monotonous highway driving environment where fatal drowsy driving events often happen. The evaluation results show that this study might lead to a practical system for noninvasive monitoring and managing driver's drowsy status in real-life highway driving situation. However, some notifications and limitations must be highlighted here.

- ①. The best way to have a safety driving is to rest 15~20 minutes after 2-hour continuous driving, according to the worldwide driver's handbooks. The proposed system is just an assistive technology that might be the next best choice for some commercial drivers (e.g., logistics couriers and long-distance bus drivers)
- ②. We did not study city driving and rural driving environment; therefore the proposed system here is not yet readily applicable to all driving environments.

Further studies considering an Internet-enabled DDD solution (as mentioned in Section. 2.4.3) need to be performed, in order to shift DDD from a standalone and self-tracked system to a connected and fully-supervised driver safety technology. In addition, we are considering enhancing the wearability of the developed headset using more flexible 3D printer material. Also, an extensive field test needs to be established before applying proposed system to a practical environment.

Reference

- [1] U. S. National Highway Traffic Safety Administration: Research on drowsy driving. [Online]. Available: http://www.nhtsa.gov/people/injury/drowsy_driving1/Drowsy.html (accessed on 1 September 2015).
- [2] Korean Expressway Corporation. 24% decrease in death in highway traffic accidents last year. Yearly report. 2014. 1-1. Available online: http://www.ex.co.kr/portal/cus/public_relations/press_release/1197307_3960.jsp?clickParentNum=3&clickNum=40&pageRow=10&startRow=5&pageURL=/portal/cus/public_relations/press_release/bodo_list (accessed on 18 August 2014).
- [3] Korean Expressway Corporation. Significant decrease in death in highway traffic accidents. Yearly report. 2012. 1-1. Available online: http://www.ex.co.kr/portal/cus/public_relations/press_release/1194829_3960.jsp?clickParentNum=3&clickNum=40&pageRow=10&startRow=21&pageURL=/portal/cus/public_relations/press_release/bodo_list (accessed on 18 August 2014).
- [4] V. Swarnkar, U. Abeyratne and C. Hukins, "Objective measure of sleepiness and sleep latency via bispectrum analysis of EEG," *Med Biol Eng Comput.* vol. 48, no. 12, pp. 1203–1213, Nov. 2010.
- [5] C. T. Lin, Y. C. Chen, T. Y. Hung, T. T. Chiu, L. W. Ko, S. F. Liang, H. Y. Hsieh, S. H. Hsu and J. R. Duann, "Development of wireless brain computer interface with embedded multitask scheduling and its application on real-time driver's drowsiness detection and warning," *IEEE Trans. Biomedical Engineering.* vol. 55, no. 5, pp. 1582–1591, May. 2008.
- [6] C. T. Lin, C. J. Chang, B. S. Lin, S. H. Hung, C. F. Chao and I. J. Wang, "A real-time wireless brain-computer interface system for drowsiness detection," *IEEE Trans. Circuits and Systems.* vol. 4, no. 4, pp. 214–222, Aug. 2010.
- [7] L. D. Liao, I. J. Wang, C. J. Chang, B. S. Lin, C. T. Lin and K. C. Tseng, "Human Cognitive Application by Using Wearable Mobile Brain Computer Interface," *Proceedings of IEEE Region 10 Conference,* pp.346-351, Fukuoka, Japan, 21-24 Nov. 2010.

- [8] C. T. Lin, L. W. Ko, C. J. Chang, Y. T. Wang, C. H. Chung and F. S. Yang, "Wearable and Wireless Brain-Computer Interface and Its Applications," Proceedings of 5th International Conference on Foundations of Augmented Cognition, Neuroergonomics and Operational Neuroscience, pp. 741-748, San Diego, USA, 19-24 July, 2009.
- [9] C. T. Lin, C. H. Chuang, C. S. Huang, S, F. Tsai, S. W. Lu, Y. H. Chen and L. W. Ko, "Wireless and Wearable EEG System for Evaluating Driver Vigilance," IEEE Trans on Biomedical Circuits and Systems., vol. 8, no. 2, pp. 165-176, May. 2014.
- [10] Y. T. Wang, C. K. Cheng, K. C. Huang, C. T. Lin, Y. J. Wang and T. P. Jung. (2012, Nov.). Cell-phone based drowsiness monitoring and management system. Proceedings of Biomedical Circuits and Systems Conference (BioCAS). [Online]. pp. 200-203. Available: <http://sccn.ucsd.edu/~yijun/pdfs/BIOCAS12.pdf>
- [11] M. Ingre, T. Åkerstedt, B. Peters, A. Anund and G. Kecklund, "Subjective sleepiness, simulated driving performance and blink duration: Examining individual differences," J. Sleep Res., vol. 15, no. 1, pp. 47–53, Mar. 2006.
- [12] Lane Departure Warning Technology in BMW vehicles. [Online]. Available: http://www.bmw.com/com/en/insights/technology/technology_guide/articles/lane_departure_warning.html (accessed on 09 March 2015).
- [13] S. Otmani, T. Pebayle, J. Roge and A. Muzet, "Effect of driving duration and partial sleep deprivation on subsequent alertness and performance of car drivers," Physiology & Behavior., vol. 84,no. 5, pp. 715-724, Apr. 2005.
- [14] P. Boyraz and J. H. L. Hansen, "Active Accident Avoidance Case Study: Integrating Drowsiness Monitoring System with Lateral Control and Speed Regulation in Passenger Vehicles," in Proc. IEEE Int. Conf. Vehicular Electronics and Safety. Columbus, USA, Sep. 22-24, 2008, pp. 293-298.

- [15] P. Thiffault and J. Bergeron, "Monotony of road environment and driver fatigue: a simulator study," *Accident Analysis & Prevention.*, vol. 35, no. 3, pp. 381-391, May. 2003.
- [16] D. F. Dinges and R. Grace, "PERCLOS: a valid psychophysiological measure of alertness as assessed by psychomotor vigilance," Report from US Dept. Transportation, Federal Highway Admin. Washington. DC. USA. pp. 1-4, 1998. [Online]. Available: <http://ntl.bts.gov/lib/10000/10100/10114/tb98-006.pdf> (accessed on 09 March 2015).
- [17] D. F. Dinges and R. Grace, "Research on vehicle-based driver status/performance monitoring; development, validation, and refinement of algorithms for detection of driver drowsiness," Report from US Dept. Transportation, National Highway Traffic Safety Admin. Washington. DC. USA. pp. 7-7. 1996. [Online]. Available: <http://ntl.bts.gov/lib/5000/5900/5911/887.pdf> (accessed on 09 March 2015).
- [18] R. J. Hanowski, M. Blanco, A. Nakata, J. S. Hickman, W. A. Schaudt, M. C. Fumero, R. L. Olson, J. Jermeland, M. Greening, G. T. Holbrook, R. R. Knipling and P. Madison, "The drowsy driver warning system field operational test: data collection methods," Final Report from US Dept. Transportation, National Highway Traffic Safety Admin. Washington. DC. USA. pp. 37-37, 2008. [Online]. Available: http://www.nhtsa.gov/DOT/NHTSA/NRD/Multimedia/PDFs/Crash_Avoidance/2008/810035.pdf (accessed on 09 March 2015).
- [19] G. Li and W. Y. Chung, "Detection of driver drowsiness using wavelet analysis of heart rate variability and a support vector machine classifier," *Sensors.*, vol. 13, no. 12, pp. 16494-16511, Dec. 2013.
- [20] S. J. Jung, H. S. Shin and W. Y. Chung, "Driver Fatigue and drowsiness monitoring system with embedded electrocardiogram sensor on steering wheel," *Intelligent Transport Systems.*, vol. 8, no. 1, pp. 43-50, Feb. 2014.
- [21] C. Papadelis, C. Kourtidou-Papadeli, P. D. Bamidis and I. Chouvarda, "Indicators of Sleepiness in an ambulatory EEG study of night driving Christos," in Proc. IEEE Int. Conf. Engineering in Medicine

- and Biology Society. New York, USA, Aug. 30 – Sep. 3, 2006, pp. 1557-170X.
- [22] A. Williamson and T. Chamberlain, “Review of on-road driver fatigue monitoring devices,” New South Wales, Australia: NSW Injury Risk Management Research Center, University of New South Wales. 2005. [Online]. Available: http://www.lumeway.com/Products_files/Review_of_on-road_driver_fatigue_monitoring_devices.pdf (accessed on 09 March 2015).
- [23] M. Golz, D. Sommer, U. Trutschel, B. Sirois and D. Edwards, “Evaluation of fatigue monitoring technologies,” Somnologie-Schlafforschung uand Schlafmedizin., vol. 14, no. 3, pp. 187-199, Sep. 2010.
- [24] A. Sahayadhas, K. Sundaraj and M. Murugappan, “Detecting Driver Drowsiness Based on Sensors: A Review,” Sensors. vol. 12, no. 12, pp. 16937-16953, Dec. 2012.
- [25] T. Brown, J. Lee, C. Schwarz, D. Fiorentino, A. McDonald, “Assessing the Feasibility of Vehicle-based Sensors to Detect Drowsy Driving,” Report from US Dept. Transportation, National Highway Traffic Safety Admin. Washington. DC. USA. 2014. [Online]. Available: www.nhtsa.gov/DOT/NHTSA/NVS/Crash_Avoidance/Technical_Publications/2014/811886-Assess_veh-based_sensros_4_drowsy-driving_detection.pdf (accessed on 09 March 2015).
- [26] R. N. Khushaba, S. Kodagoda, S. Lal and G. Dissanayake, “Driver Drowsiness Classification Using Fuzzy Wavelet-Packet-Based Feature-Extraction Algorithm,” IEEE Trans Biomed Eng., vol. 58, no. 1, pp. 121-131, Sep. 2011.
- [27] C. Iber, A. I. Sonia, L. Andrew, J. Chesson and S. F. Quan, “The AASM manual for the scoring of sleep and associated events,” American academy of sleep medicine. Westchester, USA. 2007. [Online]. Available: http://www.nswo.nl/userfiles/files/AASM_Manual_for_the_Scoring_of_Sleep_and_Associated_Events_-05-2007_2.pdf (accessed on 09 March 2015).

- [28] M. Malik, “Heart rate variability: Standards of measurement, physiological interpretation, and clinical use. Task Force of the European Society of Cardiology and the North American Society of Pacing and Electrophysiology,” *Eur. Heart J.*, vol. 93, no. 5, pp. 1043–1065, Mar. 1996.
- [29] M. Akin, M. B. Kurt, N. Sezgin and M. Bayram, “Estimating vigilance level by using EEG and EMG signals,” *Neural Computing and Applications.*, vol. 17, no. 3, pp. 227-236, Jun. 2008.
- [30] Smart cap that stops workers taking a nap [Online]. Available: <http://www.thetimes.co.uk/tto/business/industries/technology/article4487670.ece>
- [31] Smartcap (Fatigue Monitoring System) [Online]. Available: <http://smartcaptech.com/>
- [32] S. H. Seo, Y. J. Gil and J. T. Lee, “The effect of an Auditory stressor, with respect to affective style, on frontal EEG asymmetry and ERP analysis,” pp. 662-667, Proceedings of 4th International Conference on networked computing and advanced information management, Gyeongju, Korea, 2-4 Sept. 2008.
- [33] C. R. Madan and A. Singhal, “Motor imagery and higher-level cognition: four hurdles before research can sprint forward,” pp. 211-229, *Cogn Process*, vol. 13, no. 3, Aug. 2012.
- [34] C. T. Lin, C. H. Chuang, Y. K. Wang, S. F. Tsai, T. C. Chiu, and L. W. Ko. (2012, Jun.). Neurocognitive characteristics of the driver: A review on drowsiness, distraction, navigation, and motion sickness. *J. Neurosci. Neuroengin.* [Online]. 1(1), pp. 61–81. Available: <http://www.ingentaconnect.com/content/asp/jnsne/2012/00000001/0000001/art00010>
- [35] A. Delorme and S. Makeig, “EEGLAB: An open source toolbox for analysis of single-trial EEG dynamics including Independent Component Analysis,” *J. Neurosci. Meth.*, vol. 134, no. 1, pp. 9–12, Mar. 2004.
- [36] K. Patel, C. P. Chua, S. Fau and C. J. Bleakley, “Low power real-time seizure detection for ambulatory EEG,” *Proceedings of 3rd*

International Conference on Pervasive Computing Technologies for Healthcare, pp. 1-7, 1-3 Apr, 2009.

- [37] S. C. Lee, Y. H. Shin, S. G. Woo, K. S. Kim and H. N. Lee, “Review of Wireless Brain-Computer Interface Systems” in Brain-computer interface systems – recent progress and future prospects, 1st ed.; Intech Croatia, 2013, pp. 215-238. Available online: <http://cdn.intechopen.com/pdfs-wm/44252.pdf> (accessed on 09 March 2015).
- [38] G. Gargiulo et al., “A new EEG recording system for passive dry electrodes,” *Clin. Neurophysiol.*, vol. 121, no. 5, pp. 686–693, May 2010.
- [39] T. O. Zander et al., “A dry EEG-system for scientific research and brain-computer interfaces,” *Front Neurosci.*, vol. 5, no. 53, pp. 1–10, 2011.
- [40] Brainwave EEG Signal, NeuroSky, Dec. 5, 2009 [Online]. Available: <http://www.neuroskey.com>
- [41] C. Grozea, C. D. Voinescu, and S. Fazli, “Bristle-sensors—low-cost flexible passive dry EEG electrodes for neurofeedback and BCI applications,” *J. Neural. Eng.*, vol. 8, no. 2, pp. 1–8, Apr. 2011.
- [42] C.-T. Lin, L.-D. Liao, Y.-H. Liu, I.-J. Wang, B.-S. Lin, and J.-Y. Chang, “Novel dry polymer foam electrodes for long-term EEG measurement,” *IEEE Trans. Biomed. Eng.*, vol. 58, no. 5, pp. 1200–1207, 2011.
- [43] L.-D. Liao, I.-J. Wang, S.-F. Chen, J.-Y. Chang, and C.-T. Lin, “Design, fabrication and experimental validation of a novel dry-contact sensor for measuring electroencephalography signals without skin preparation,” *Sensors*, vol. 11, no. 6, pp. 5819–5834, 2011.
- [44] L. D. Liao et al., “A novel 16-channel wireless system for electroencephalography measurements with dry spring-loaded sensors,” *IEEE Trans. Instrum. Meas.*, vol. 63, no. 6, pp. 1545–1555, Jun. 2014.
- [45] Dry electrode for hair. [Online]. Available: <http://www.cognionics.com/index.php/products/sensors/flex>

- [46] Conventional wet Ag/AgCl sensors. [Online]. Available: <http://laxtha-eshop.kr/goods/view.php?seq=4>
- [47] Cognionics Cognionics, Dec. 5, 2013 [Online]. Available: <http://cognionics.com>
- [48] Wireless Low-Power Active-Electrode EEG Headset, IMEC, Dec. 5, 2013 [Online]. Available: <http://www2.imec.be>
- [49] Y. M. Chi, C. Maier, and G. Cauwenberghs, “Ultra-high input impedance, low noise integrated amplifier for noncontact biopotential sensing,” *IEEE J. Emerg. Sel. Topics Circuits Syst.*, vol. 1, no. 4, pp. 526–535, 2011.
- [50] The ModularEEG design. [Online]. Available: http://openeeg.sourceforge.net/doc/modeeg/modeeg_design.html
- [51] B. Lo and G. Z. Yang, Wireless sensor development platforms, in: *Body Sensor Networks*, G. Z. Yang ed., Springer Press, London, 2006, pp. 407.
- [52] C. T. Lin, R. C. Wu, S. F. Liang and W. H. Chao, “EEG-Based Drowsiness Estimation for Safety Driving Using Independent Component Analysis,” *IEEE Trans on Circuits and Systems I: Regular Papers.*, vol. 52, no. 12, pp. 2726-2738, Dec. 2005.
- [53] L. M. King, H. T. Nguyen and S. K. L. Lal, “Early Driver Fatigue Detection from Electroencephalography Signals using Artificial Neural Networks,” in *Proc. IEEE Int. Conf. Engineering in Medicine and Biology Society.*, New York, USA, Aug. 30 – Sep. 03, 2006, pp. 2187-2190.
- [54] B. S. Reddy, O. A. Basir and S. J. Leat, “Estimation of driver attention using Visually Evoked Potentials,” in *Proc IEEE Int. Conf. Intelligent Vehicles Symposium.*, Istanbul, Turkey, Jun. 13-15, 2007, pp. 588-593.
- [55] H. Yoshida, H. Kuramoto, Y. Sunada and S. Kikkawa, “EEG Analysis in Wakefulness Maintenance State against Sleepiness by Instantaneous Equivalent Bandwidths,” in *Proc. IEEE Int. Conf.*

Engineering in Medicine and Biology Society. Lyon, France, Aug. 22-26, 2007, pp. 19-22.

- [56] C. T. Lin, Y. C. Chen, T. Y. Huang, T. T. Chiu, L. W. Ko, H. Y. Hsieh, S. H. Hsu and J. R. Duann, “Development of Wireless Brain Computer Interface With Embedded Multitask Scheduling and its Application on Real-Time Driver’s Drowsiness Detection and Warning,” *IEEE Trans Biomed Eng.*, vol. 55, no. 5, pp. 1582-1591, May. 2008.
- [57] E. Michail, A. Kokonozi, I. Chouvarda and N. Maglaveras, “EEG and HRV markers of sleepiness and loss of control during car driving,” in *Proc. IEEE Int. Conf. Engineering in Medicine and Biology Society*. Vancouver, Canada, Aug. 20-25, 2008, pp. 2566-2569.
- [58] M. Akin, M. B. Kurt, N. Sezgin and M. Bayram, “Estimating vigilance level by using EEG and EMG signals,” *Neural Computing and Applications.*, vol. 17, no. 3, pp. 227-236, Jun. 2008.
- [59] S. D. Ridwan, R. Thompson, B. T. Jap and S. Lal, “Single Channel Wireless EEG: Proposed Application in Train Drivers,” in *Proc. 3th Int. Conf. Broadband Communications, Information Technology & Biomedical Applications*. Gauteng, South Africa, Nov. 23-26, 2008, pp. 58-63.
- [60] P. Y. Tsai, W. Hu, T. B. Kuo and L. Y. Shyu, “A Portable Device for Real Time Drowsiness Detection Using Novel Active Dry Electrode System,” in *Proc. IEEE Int. Conf. Engineering in Medicine and Biology Society*. Minneapolis, USA, Sep. 03-06, 2009, pp. 3775-3778.
- [61] C. T. Lin, C. J. Chang, B. S. Lin, S. H. Hung, C. F. Chao and I. J. Wang, “A Real-Time Wireless Brain-Computer Interface System for Drowsiness Detection,” *IEEE Trans Biomedical Circuits and Systems.*, vol. 4, no. 4, pp. 214-222, Apr. 2010.
- [62] L. Cao, J. Li, Y. R. Sun, H. P. Zhu and C. G. Yan, “EEG-Based Vigilance Analysis by Using Fisher Score and PCA Algorithm,” in *Proc. IEEE Int. Conf. Process in Informatics and Computing*. Shanghai, China, Dec. 10-12, 2010, pp. 175-179.
- [63] S. Gupta, S. Kar and A. Routray, “Fatigue in Human Drivers: A Study Using Ocular, Psychometric, Physiological Signals,” in *Proc.*

IEEE Int. Conf. Students' Technology Symposium. Kharagpur, India, Apr. 03-04. 2010, pp. 234-240.

- [64] C. A. Garces and L. E. Laciari, "An automatic detector of drowsiness based on spectral analysis and wavelet decomposition of EEG records," in *Proc. IEEE Int. Conf. Engineering in Medicine and Biology Society*. Buenos Aires, Argentina, Aug. 31 August – Sep. 06, 2010, pp. 1405-1408.
- [65] S. Tantisatirapong, W. Senavongse and M. Phothisonothai, "Fractal Dimension Based Electroencephalogram Analysis of Drowsiness Patterns," in *Proc. Int. Conf. Electrical Engineering/Electronics Computer Telecommunications and Information Technology*. Chiang Mai, Thailand, May. 19-21, 2010, pp. 497-500.
- [66] M. A. Li, C. Zhang and J. F. Yang, "An EEG-based Method for Detecting Drowsy Driving State," in *Proc. 7th Int. Conf. Fuzzy Systems and Knowledge Discovery*. Yantai, China, Aug. 10-12, 2010, pp. 2164-2167.
- [67] J. Park, L. Xu, V. Sridhar, M. Chi and G. Cauwenberghs, "Wireless Dry EEG for Drowsiness Detection," in *Proc. IEEE Int. Conf. Engineering in Medicine and Biology Society*. Boston, USA, Aug. 30 – Sep. 03, 2011, pp. 3298-3301.
- [68] S. Pritchett, E. Zilberg, M. X. Zheng, M. Karrar, S. Lal and D. Burton, "Strengthening association between driver drowsiness and its physiological predictors by combining EEG with measures of body movement," in *Proc. 6th Int. Conf. Broadband and Biomedical Communications*. Melbourne, Australia, Nov. 21-24, 2011, pp. 103-107.
- [69] B. T. Jap, S. Lal and P. Fischer, "Comparing combinations of EEG activity in train drivers during monotonous driving," *Expert Systems with Applications.*, vol. 38, no. 1, pp. 996-1003, Jan. 2011.
- [70] Y. Punyawad, S. Aempedchr, Y. Wongsawat and M. Panichkun, "Weighted-frequency index for EEG-based mental fatigue alarm system," *International Journal of Applied Biomedical Engineering.*, vol. 4, no. 1, pp. 36-41, 2011. [Online]. Available: <http://www.ijabme.org/File/vol4no1/07weighted.pdf> (accessed on 09 March 2015).

- [71] M. Simon, E. A. Schmidt, W. E. Kincses, M. Fritzsche, A. Bruns, C. Aufmuth, M. Bogdan, W. Rosenstiel and M. Schrauf, "EEG alpha spindle measures as indicators of driver fatigue under real traffic conditions," *Clin Neurophysiol.* , vol. 122, no. 6, pp. 1168-1178, Jun. 2011.
- [72] S. Pritchett, E. Zilberg, M. X. Zheng, M. Karrar, D. Burton and S. Lal, "Comparing accuracy of two algorithms for detecting driver drowsiness - single source (EEG) and hybrid (EEG and body movement)," in *Proc. 6th Int. Conf. Broadband and Biomedical Communications*. Melbourne, Australia, Nov. 21-24, 2011, pp. 179-184.
- [73] S. N. M. Ashtiani, Z. Mardim and M. Mikaili, "Spectral Characteristics Assessment in Recognition of Drivers' Drowsiness Using Statistical Tests," in *Proc. 18th Iranian. Conf. Biomedical Engineering*. Tehran, Iran, Dec. 14-16, 2011, pp. 72-76.
- [74] A. Murata, Y. Ohkubo, M. Moriwaka and T. Hayami, "Prediction of Drowsiness using Multivariate Analysis of Biological Information and Driving Performance," In *Proc. SICE Annual Conf.* Tokyo, Japan, Sep. 13-18, 2011, pp. 52-57.
- [75] A. Murata, Y. Matsuda, M. Moriwaka and T. Hayami, "An Attempt to Predict Drowsiness by Bayesian Estimation," in *Proc. SICE Annual Conf.* Tokyo, Japan, Sep. 13-18, 2011. pp. 58-63.
- [76] M. S. Chae, "Portable, Wireless Drowsiness-Detection System," in *Proc. 55th Int. Midwest Symposium on Circuits and Systems*. Boise, USA, Aug. 5-8, 2012, pp. 1548-3746.
- [77] D. J. Kim, H. S. Han, S. J. Cho and U. P. Chong, "Detection of Drowsiness with eyes open using EEG-Based Power Spectrum Analysis," in *Proc. 7th Int. Forum on Strategic Technology*. Tomsk, Russia, Sep. 18-21, 2012, pp. 1-4.
- [78] H. Yoshida, Y. Tanaka and S. Kikkawa, "EEG Analysis of Frontal Lobe Area in Arousal Maintenance State against Sleepiness," in *Proc. IEEE Int. Conf. Engineering in Medicine and Biology Society*. San Diego, USA, Aug. 28 – Sep. 01, 2012, pp. 2933-2936.

- [79] A. Picot, S. Charbonnier and A. Caplier, “On-Line Detection of Drowsiness Using Brain and Visual Information,” *IEEE Trans on Systems, Man and Cybernetics, Part A: Systems and Humans.*, vol. 42, no. 3, pp. 764-775, Sep. 2011.
- [80] F. C. Lin, L. W. Ko, C. H. Chuang, T. P. Su and C. T. Lin, “Generalized EEG-Based Drowsiness Prediction System by Using a Self-Organizing Neural Fuzzy System,” *IEEE Trans on Circuits and Systems I: Regular Papers.*, vol. 59, no. 9, pp. 2044-2055, Feb.2012.
- [81] A. Kalauzi, A. Vuckovic and T. Bojic, “EEG alpha phase shifts during transition from wakefulness to drowsiness,” *International Journal of Psychophysiology.*, vol. 86, no. 3, pp. 195-205, Dec. 2012.
- [82] R. R. Daphne and A. A. Raj, “A drowsiness detection architecture using feature extraction methodology,” *Procedia Engineering.*, vol. 38, pp. 959-963, 2012.
- [83] T. Sugi, T. Nagamine, M. Nakamura and A. Lkeda, “Development of Real-Time Evaluation System for Qualitative Improvement of Awake EEG Records,” in *Proc. ICME Int. Conf. Complex Medical Engineering*. Kobe, Japan, Jul. 1-4, 2012, pp. 545-550.
- [84] A. H. Zhang and Y. F. Chen, “EEG Feature Extraction and Analysis under Drowsy State Based on Energy and Sample Entropy,” in *Proc. 5th Int. Conf. Biomedical Engineering and Informatics*. Chongqing, China, Oct. 16-18, 2012, pp. 501-505.
- [85] Y. T. Wang, C. K. Cheng, K. C. Huang and C. T. Lin, “Cell-phone Based Drowsiness Monitoring and Management System,” in *Proc. IEEE Int. Conf. Biomedical Circuits and Systems*. Hsinchu, Taiwan, Nov. 28-30, 2012, pp. 200-203.
- [86] J. Arnin, D. Anopas, M. Horapong, P. Triponyuwasi, T. Yamsa-ard, S. Lampetch and Y. Wongswat, “Wireless-based Portable EEG-EOG Monitoring for Real Time Drowsiness Detection,” in *Proc. IEEE Int. Conf. Engineering in Medicine and Biology Society*. Osaka, Japan, Jul. 3-7, 2013, pp. 4977-4980.
- [87] Hu, S. Y.; Zheng, G. T.; Peter, B. Driver fatigue detection from electroencephalogram spectrum after electrooculography artefact removal. *Intelligent Transport Systems*. **2013**, 7, 105-113.

- [88] R. N. Khushaba, S. Kodagoda, S. Lal and G. Dissanayake, “Uncorrelated fuzzy neighborhood preserving analysis based feature projection for driver drowsiness recognition,” *Fuzzy Sets and Systems.*, vol. 221, pp. 90-111, Jun. 2011.
- [89] A. A. Putilov and O. G. Donskaya, “Construction and validation of the EEG analogues of the Karolinska sleepiness scale based on the Karolinska drowsiness test,” *Clinical Neurophysiology.*, vol. 124, no. 7, pp. 1346-1352, Jul. 2013.
- [90] S. D. Yu, P. Li, H. H. Lin and E. Rohani, “Support Vector Machine Based Detection of Drowsiness Using Minimum EEG Features,” in *Proc. Int. Conf. Social Computing*. Alexandria, USA, Sep. 8-14, 2013, pp. 827-835.
- [91] M. Murugappan, M. K. Wali, R. B. Ahmmad and S. Murugappan, “Subtractive Fuzzy Classifier based Driver Drowsiness Levels Classification using EEG,” in *Proc. Int. Conf. Communications and Signal Processing*. Melmaruvathur, India, Apr. 3-5, 2013, pp. 159-164.
- [92] S. Kulkami, S. Bs, K. Malthish and M. Meenakshi, “Development of Microcontroller Based Ambulatory Instrument to Detect Drowsiness,” in *Proc. Int. Conf. Biosignals and Biorobotics*. Rio de Janerio, Portuguesa, Feb. 18-20, 2013, pp. 1-4.
- [93] K. A. I. Aboalayon, H. T. Ocbagabir and M. Faezipour, “Efficient Sleep Stage Classification Based on EEG Signals,” in *Proc. IEEE Int. Conf. Long Island Systems, Applications and Technology Conference*. Farmingdale, USA, May. 02-02, 2014, pp. 1-6.
- [94] G. Li and W. Y. Chung, “A Low-Cost Driver Drowsiness Detection System Based on EEG Sensor and Smartphone,” in *Proc. the Korea Institute of Signal Processing and Systems Summer Conference*. Daegu, South Korea, Jun. 20-21, 2014, pp. 61-63.
- [95] C. T. Lin, C. H. Chuang, C. S. Huang, S, F. Tsai, S. W. Lu, Y. H. Chen and L. W. Ko, “Wireless and Wearable EEG System for Evaluating Driver Vigilance,” *IEEE Trans on Biomedical Circuits and Systems.*, vol. 8, no. 2, pp. 165-176, May. 2014.

- [96] A. Maglione, G. Borghini, P. Arico, F. Borgia, I. Graziani, A. Colosimo, W. Kong, Vecchiato and F. Babiloni, "Evaluation of the workload and drowsiness during car driving by using high resolution EEG activity and neurophysiologic indices," in *Proc. IEEE Int. Conf. Engineering in Medicine and Biology Society*. Chicago, USA, Aug. 26-30, 2014, pp. 6238-6241.
- [97] Y. Sun and X. B. Yu, "An Innovative Nonintrusive Driver Assistance System for Vital Signal Monitoring," *IEEE J Biomed Health Inform.*, vol. 18, no. 6, pp. 1932-1939, Nov. 2014.
- [98] C. A. Garces, L. Orosco and E. Laciari, "Automatic detection of drowsiness in EEG records based on multimodal analysis," *Med Eng Phys.*, vol. 36, no. 2, pp. 244-249, Feb. 2014.
- [99] N. Gurudath and H. B. Riley, "Drowsy Driving Detection by EEG Analysis Using Wavelet Transform and K-Means Clustering," *Procedia Computer Science.*, vol. 34, pp. 400-409, 2014.
- [100] M. Awais, N. Badruddin and M. Drieberg, "A Simulator Based Study to Evaluate Driver Drowsiness Using Electroencephalogram," in *Proc. 5th Int. Conf. Intelligent and Advanced System*. Kuala Lumpur, Malaysia, Jun. 3-5, 2014, pp. 1-5.
- [101] H. B. Van, S. Rhodes, B. Dunne and R. Bossemeyer, "Low-Cost EEG-based Sleep Detection," in *Proc. IEEE Int. Conf. Engineering in Medicine and Biology Society*. Chicago, USA, Aug. 26-30, 2014, pp. 4571-4574.
- [102] A. Murata, Y. Urakami and M. Moriwaka, "An attempt to prevent traffic accidents due to drowsy driving - Prediction of drowsiness by Bayesian estimation," in *Proc. the SICE Annual Conference*. Sapporo, Japan, Sep. 9-12, 2014, pp. 1708-1715.
- [103] Y. Peng, F. Wang, Y. D. Yang and P. Zhang, "Design and Implementation of Virtual Driving System Fusing Driver's Cognitive and Operating Characteristics," in *Proc. 9th IEEE Int. Conf. Industrial Electronics and Applications*. Hangzhou, China, Jun. 9-11, 2014, pp. 1826-1829.

- [104] W. W. Wierwille and L. A. Ellsworth, “Evaluation of driver drowsiness by trained raters,” *Accident Analysis & Prevention.*, vol. 26, no. 5, pp. 571–581, Oct.1994.
- [105] G. Li and W. Y. Chung, “Estimation of eye closure degree using EEG sensors and its application in driver drowsiness detection,” *Sensors.*, vol. 14, no. 9, pp. 17491–17515, Sep. 2014.
- [106] E. M. Dewan, “Occipital alpha rhythm eye position and lens accommodation,” *Nature*, vol. 214, pp. 975-977, June 1967.
- [107] D. O. Bos, “EEG-based emotion recognition,” in *Proce. Conf. Capita Selecta (MSc course)*. Enschede, Netherlands, 2006, pp. 1-17. [Online]. Available: http://hmi.ewi.utwente.nl/verslagen/capita-selecta/CS-Oude_Bos-Danny.pdf
- [108] G. S. Yang, Y. Z. Lin and P. Bhattacharya, “A driver fatigue recognition model based on information fusion and dynamic Bayesian network,” *Information Sciences.*, vol. 180, no. 10, pp.1942-1954, May. 2010.
- [109] Y. T. Liu, Y. Y. Lin, S. L. Wu and C. H. Chuang, “EEG-based Driving Fatigue Prediction System Using Functional-link-based Fuzzy Neural Network,” in *Proc. Int. Conf. Neural Networks*. Beijing, China, Jul. 6 – 11, 2014, pp. 4109-4113.
- [110] H. De Rosario, J. S. Solaz, N. Rodriguez and L. M. Bergasa, “Controlled inducement and measurement of drowsiness in a driving simulator,” *Intelligent Transport Systems.*, vol. 4, no. 4, pp. 280-288, Dec. 2010.
- [111] B. G. Lee, B. L. Lee and W. Y. Chung, “Mobile Healthcare for Automatic Driving Sleep-Onset Detection Using Wavelet-Based EEG and Respiration Signals,” *Sensors*, vol. 14, no. 10, pp.17915-17936, Sep. 2014.
- [112] N. S. Dias, J. F. Ferreira, C. P. Figueiredo and J. H. Correia, “A Wireless System for Biopotential Acquisition: an Approach for non-Invasive Brain-Computer Interface,” in *Proc. IEEE Int. Symposium on Industrial Electronics*. Vigo, Spain, Jun. 4 – 7, 2007, pp. 2709-2712.

- [113] N. S. Dias, J. P. Carmo, P. M. Mendes and J. H. Correia, “Wireless instrumentation system based on dry electrodes for acquiring EEG signals,” *Med Eng Phys.*, vol. 34, no. 7, pp. 972-981, Sep. 2012.
- [114] Zigbee Micaz module datasheet. [Online]. Available: http://www.openautomation.net/uploadsproductos/micaz_datasheet.pdf (accessed on 09 March 2015).
- [115] CC2540 datasheet. [Online]. Available: <http://www.ti.com/lit/ds/symlink/cc2540.pdf> (accessed on 09 March 2015).
- [116] X. Chen and J. Wang, “Design and Implementation of A Wearable, Wireless EEG Recording System,” in *Proc. 5th Int. Conf. Bioinformatics and Biomedical Engineering*. Wuhan, China, May. 10 – 12, 2011, pp. 1-4.
- [117] Zigbee Telosb module datasheet. [Online]. Available: http://www.cse.iitb.ac.in/synerg/lib/exe/fetch.php?media=public:proj:sujesha:telosb_datasheet.pdf (accessed on 09 March 2015).
- [118] D. W. Chang, S. F. Liang, C. P. Young, F. Z. Shaw, A. W. Y. Su,; Y. D. Liu, Y. L. Wang, Y. C. Liu, J. J. Chen and C. Y. Chen, “A Versatile Wireless Portable Monitoring System for Brain–Behavior Approaches,” *IEEE Journal on Emerging and Selected Topics in Circuits and Systems.*, vol. 1, no. 4, pp. 440-450, Jan. 2012.
- [119] CC2430 datasheet. [Online]. Available: <http://www.ti.com/lit/ds/symlink/cc2430.pdf> (accessed on 09 March 2015).
- [120] C. T. Lin, B. S. Lin, F. C. Lin and C. J. Chang, “Brain Computer Interface-Based Smart Living Environmental Auto-Adjustment Control System in UPnP Home Networking,” *IEEE Systems Journal.*, vol. 8, no. 2 pp. 363-370, Apr. 2014.
- [121] T. Torfs, V. Leonov, R. F. Yazicioglu and P. Merken, “Wearable Autonomous Wireless Electro-encephalography System Fully Powered by Human Body Heat,” in *Proc. IEEE Sensors Conf.* Lecce, Italy, Oct. 26 – 29, 2008, pp. 1269-1272.

- [122] nRF2401A datasheet. [Online]. Available: <https://www.sparkfun.com/datasheets/IC/nRF2401A.pdf> (accessed on 09 March 2015).
- [123] L. Brown, J. Van de Molengraft, R. F. Yazicioglu and T. Torfs, “Low-power, wireless, 8-channel EEG monitoring headset,” in *Proce. IEEE Int. Conf. Engineering in Medicine and Biology Society*. Buenos Aires, Argentina, Aug. 31 – Sep. 4, 2010, pp. 4197-4200.
- [124] nRF24L01 datasheet. [Online]. Available: <http://www.nordicsemi.com/eng/Products/2.4GHz-RF/nRF24L01> (accessed on 09 March 2015).
- [125] N. Verma, A. Shoeb, J. Bohorquez and J. Dawson, “A Micro-Power EEG Acquisition SoC With Integrated Feature Extraction Processor for a Chronic Seizure Detection System,” *IEEE Journal of Solid-State Circuits.*, vol. 45, no. 4, pp.804-816, Apr. 2010
- [126] CC2550 datasheet. [Online]. Available: <http://www.ti.com/general/docs/lit/getliterature.tsp?literatureNumber=swrs039b&fileType=pdf> (accessed on 09 March 2015).
- [127] S. Filipe, G. Charvet, M. Foerster, J. Porcherot, J. F. Bêche, S. Bonnet, P. Audebert, G. Régis, B. Zongo, S. Robinet, C. Condemine, C. Mestais and R. Guillemaud, “A wireless multichannel EEG recording platform,” in *Proc. IEEE Int. Conf. Engineering in Medicine and Biology Society*. Boston, USA, Aug. 30 – Sep. 3, 2011, pp. 1557-170X.
- [128] ZL70100 datasheet. [Online]. Available: <http://pdf1.alldatasheet.com/datasheet-pdf/view/134441/ZARLINK/ZL70100.html> (accessed on 09 March 2015).
- [129] TX2RX2 datasheet. [Online]. Available: <http://www.radiometrix.com/files/additional/TX2RX2.pdf> (accessed on 09 March 2015).
- [130] BRF6150 datasheet. [Online]. Available: <http://focus.ti.com/pdfs/vf/wireless/brf6150bulletin.pdf> (accessed on 09 March 2015).

- [131] CC2560 datasheet. [Online]. Available: <http://www.ti.com/lit/ds/symlink/cc2560.pdf> (accessed on 09 March 2015).
- [132] CC2560 datasheet. [Online]. Available: <http://www.ti.com/lit/ds/symlink/cc2420.pdf> (accessed on 09 March 2015).
- [133] Australia driver's handbook. [Online]. Available: <http://mylicence.sa.gov.au/road-rules/the-drivers-handbook/fatigue> (accessed on 09 March 2015).
- [134] Ireland driver's handbook. [Online]. Available: http://www.hsa.ie/eng/Publications_and_Forms/Publications/Work_Related_Vehicles/Safe_Driving_for_Work_Handbook_.pdf (accessed on 09 March 2015).
- [135] New York driver's handbook. [Online]. Available: <http://dmv.ny.gov/about-dmv/chapter-8-defensive-driving#drw-drv> (accessed on 09 March 2015).
- [136] B. G. Lee, B. L. Lee and W.Y. Chung, "Wristband-Type driver vigilance monitoring system using smartwatch," *IEEE Sensors Journal.*, pp. 5624 – 5633, vol. 15, no. 10, Oct. 2015.
- [137] S. M. Belz, G. S. Robinson, and J. G. Casali, "A new class of auditory warning signals for complex systems: Auditory icons," *Human Factors*, vol. 41, no. 4, pp. 608-618, Dec. 1999.
- [138] K. C. Huang, T. P. Jung, C. H. Chuang, L. W. Ko and C. T. Lin, "Preventing lapse in performance using a drowsiness monitoring and management system," in Proc. IEEE Int. Conf. Engineering in Medicine and Biology Society. Chicago, USA, August 28 – September 1, 2012, pp. 3336-3339.
- [139] S. Southworth, "A study of the effects of cranial electrical stimulation on attention and concentration," *Integr Physiol Behav Sci.*, vol. 34, no. 1, pp. 43-53, Jan-Mar. 1999.
- [140] L. K. Mcintire, R. A. Mckinley, C. Goodyear and J. Nelson, "A comparison of the effects of transcranial direct current stimulation and caffeine on vigilance and cognitive performance during extended

wakefulness,” *Brain Stimulation.*, vlo. 7, no. 4, pp. 499-507, July-August. 2014.

- [141] J. T. Nelson, R. A. Mckinley, E. J. Golob, J. S. Warm and R. Parasuraman, “Enhancing vigilance in operators with prefrontal cortex transcranial direct current stimulation (tDCS),” *NeuroImage.*, vol. 85 (part 3), pp. 909-917, January 2014.
- [142] H. Sakai, Y. Uchiyama, S. Tanaka, S. K. Sugawara and N. Sadato, “Prefrontal transcranial direct current stimulation improves fundamental vehicle control abilities,” *Behavioural Brain Research.*, vol. 273, pp. 57-62, October 2014.
- [143] E. Vural, M. Cetin, A. Ercil, G. Littlewort, M. Bartlett and J. Movellan, “Automated drowsiness detection for improved driving safety,” in Proc. Int. Conf. Automotive Technologies. Istanbul, Turkey, Nov. 13-14, 2008; pp. 1-15.
- [144] S. O. Regan, S. Faul and W. Marnane, “Automatic detection of EEG artefacts arising from head movements using EEG and gyroscope signals,” *Medical Engineering & Physics*, vol. 35, no. 7, pp. 867-874, July. 2013
- [145] S. O. Regan and W. Marnane, “Multimodal detection of head-movement artefacts in EEG,” *Journal of neuroscience methods*, vol. 218, no. 1, pp. 110-120, Aug. 2013.
- [146] Emotiv EPOC EEG Acquisition Device. [Online]. Available: <https://emotiv.com/epoc.php>
- [147] I. S. Kim. (2012, Jun.). The risk of accidents using DMB and smartphone when driving. *Traffic*. [Online]. 172, pp. 32-36. Available: <http://www.koti.re.kr/mail/news/2012-06.pdf>
- [148] State laws about distracted driving. [Online]. Available: <http://www.distraction.gov/content/get-the-facts/state-laws.html>.
- [149] Bluetooth 4.0 Low Energy Mini module. [Online]. Available: <http://redbearlab.com>

- [150] Ear-clip electrode. [Online]. Available: <http://www.laxtha.com/ProductView.asp?Model=LXEL-EAR-01&catgrpid=1&catidx=30>
- [151] Y. M. Chi, P. Ng, E. Kang, J. Kang, J. Fang and G. Cauwenberghs. (2010, Oct.). Wireless non-contact cardiac and Neural monitoring. Proceedings of the wireless health 2010. [Online]. pp. 15-23. Available: <http://www.isn.ucsd.edu/pubs/wh2010.pdf>
- [152] D. W. Chang, S. F. Liang, C. P. Young, F. Z. Shaw, A. W. Y. Su, Y. D. Liu and Y. L. Wang, Y. C. Liu, J. J. Chen and C. Y. Chen, "A versatile wireless portable monitoring system for brain-behavior approaches," IEEE journal on emerging and selected topics in circuits and systems, vol. 1, no. 4, pp. 440–450, Jan 2012.
- [153] M. A. Nitsche, P. S. Boggio, F. Fregni and A. Pascual-Leone, "Treatment of depression with transcranial direct current stimulation (tDCS): Review," Exp Neuro, vol. 219, no. 1, pp.14-19, Sep. 2009.
- [154] Moto 360 leads the first wave of Android Wear devices. [Online]. Available: <http://canalys.com/newsroom/moto-360-leads-first-wave-android-wear-devices>
- [155] S. W. Li, L. H. Wang, Z. F. Yang, B. K. Ji, F. Y. Qiao and Z. K. Yang. (2011, Aug.). An active driver fatigue identification technique using multiple physiological features. Proceedings of International conference on Mechatronic science, electric engineering and computer. [Online]. ,pp. 733-737. Available: <http://ieeexplore.ieee.org/stamp/stamp.jsp?tp=&arnumber=6025569>
- [156] S. Y. Hu, G. T. Zheng and B. Peters. (2012, Mar.). Driver fatigue detection from electroencephalogram spectrum after electrooculography artifact removal. Journal of IET Intelligent Transport Systems [Online]. 7(1), pp. 105-113. Available: <http://ieeexplore.ieee.org/stamp/stamp.jsp?tp=&arnumber=6518060>
- [157] S. D. Yu, P. Li, H. H. Lin, E. Rohani, G. Choi, B. T. Shao and Q. Wang. (2013, Sep.). Support vector machine based detection of drowsiness using minimum EEG features. Proceedings of International conference on social computing. [Online]. ,pp. 827-835. Available: <http://ieeexplore.ieee.org/stamp/stamp.jsp?tp=&arnumber=6693421>

- [158] S. Gunn. (1998, May.). Support vector machines for classification and regression. Univ. Southampton, Southampton, U. K., ISIS Tech. Rep, 1998. [Online]. pp. 6. Available: <http://www.svms.org/tutorials/Gunn1998.pdf>
- [159] C. C. Chang and C. J. Lin. (2011, May.). LIBSVM: A library for support vector machines. ACM Trans Intell Syst Technol. [Online]. 2(3), pp. 27:1-27:27. Available: <http://www.csie.ntu.edu.tw/~cjlin/papers/libsvm.pdf>
- [160] S. Alexander, F. A. Constantin, P. H. Douglas and G. Isabelle, SVMs for Multi-Category Classification in a Gental Introduction to Support Vector Machines in Biomedicine, 1st ed.; World Scientific Press: Singapore, 2011; pp. 91–96.
- [161] W. Z. Kong, Z. P. Zhou, S. Q. Hu, J. H. Zhang, F. Babiloni and G. J. Dai. (2013, Aug.). Automatic and direct identification of blink components from scalp EEG. Sensors. [Online]. 13(8), pp. 10783-10801. Available: <http://www.mdpi.com/1424-8220/13/8/10783/pdf>
- [162] S. Theodoridis, A. Pikrakis, K. Koutroumbas and D. Cavouras, “The receiver operating characteristic curve,” in *Introduction to pattern recognition: A Matlab approach*, Elsevier Press, 2010.
- [163] Y. M. Chi, T. P. Jung and G. Cauwenberghs, “Dry-contact and Noncontact bio-potential electrodes: Methodological review,” IEEE Reviews in Biomedical Engineering., vol. 3, pp. 106-119, Oct. 2010.
- [164] J. C. Platt, “Probabilistic outputs for support vector machines and comparison to regularized likelihood methods,” in *Advances in Large Margin Classifiers*, A. Smola, P. Bartlett, B. Scholkopf, and D. Schuurmans, Eds. Cambridge, MA: MIT Press, 2001.
- [165] H. T. Lin, C. J. Lin and R. C. Weng. (2007, Oct.). A note on Platt’s probabilistic outputs for support vector machines. *Machine Learning*. [Online]. 68(3), pp. 267-276. Available: <http://www.csie.ntu.edu.tw/~cjlin/papers/platprob.pdf>.
- [166] Final report. (2008, Sep.). The drowsy driver warning system field operational test: data collection methods. US Dept. Transportation, National Highway Traffic Safety Admin. Washington, DC. USA.

- [Online]. Available: <http://www.nhtsa.gov/DOT/NHTSA/NRD/Multimedia/PDFs/Crash%20Avoidabce/2008./810035.pdf>
- [167] B. L. Lee, B. G. Lee, G. Li and W. Y. Chung, “Wearable driver drowsiness detection system based on smarwatch,” in Proc. the Korea Institute of Signal Processing and Systems Autumn Conference. Busan, South Korea, Nov. 21-22, 2014, pp. 134-136.
- [168] J. M. Bland and D. G. Altman, “Statistical methods for assessing agreement between two methods of clinical measurement,” Lancet. vol. 1, no. 8476, pp. 307–310, Feb. 1986.
- [169] G. Geetha, “Scrutinizing different techniques for artifact removal from EEG signals,” International Journal of Engineering Science and Technology., vol. 3, no. 2, pp. 1167-1172, Feb. 2011.
- [170] When you are drowsy, please go to drowsiness shelter to have a rest. [Online]. Available: <http://korealand.tistory.com/987>
- [171] G. Li and W. Y. Chung, “EEG-based Driver Drowsiness Detection: A Review,” *IEEE Transactions on Human-Machine Systems* (under review).
- [172] https://en.wikipedia.org/wiki/Android_Wear
- [173] <https://en.wikipedia.org/wiki/WatchOS>
- [174] https://en.wikipedia.org/wiki/Android_Studio

List of Publications (SCI (E) Journal Only)

1. Gang Li, Boon-Leng Lee and Wan-Young Chung, “Smartwatch-based Wearable EEG System for Driver Drowsiness Detection,” *IEEE Sensors Journal* (SCIE, IF: 1.762, ISSN: 1530-437X), Vol. 15, No. 2, pp. 7169-7180, 2015.
2. Gang Li and Wan-Young Chung, “A Context-aware EEG Headset System for Early Detection of Driver Drowsiness,” *Sensors* (SCIE, IF: 2.245, ISSN: 1424-8220), Vol. 15, No. 8, pp. 20873-20893, August 2015.
3. Gang Li and Wan-Young Chung, “Estimation of Eye Closure Degree Using EEG Sensors and Its Application in Driver Drowsiness Detection,” *Sensors* (SCIE, IF: 2.048, ISSN: 1424-8220), Vol. 14, No. 9, pp. 17491-17515, September 2014.
4. Gang Li and Wan-Young Chung, “Detection of Driver Drowsiness using Wavelet Analysis of Heart Rate Variability and a Support Vector Machine Classifier,” *Sensors* (SCIE, IF: 1.953, ISSN: 1424-8220), Vol. 13, No. 12, pp. 16494-16511, December 2013.
5. Vega Pradana Rachim, Gang Li and Wan-Young Chung, “Sleep apnea classification using ECG-signal wavelet-PCA features,” *Bio-medical Materials and Engineering* (SCIE, IF: 1.087, ISSN: 2875–2882), Vol. 24, No. 6, pp. 465-474, September 2014

List of Publications (International Conference)

1. Gang Li, Boon Leng Lee and Wan-Young Chung, “A Wearable Brain-Machine Interface System for Real-time Driver Drowsiness Detection,” *Proceedings of the 18th International Conference on Electronics, Information and Communication (ICEIC’15)*, pp. 590-591, 28-31 January, 2015, Grand Hyatt Hotel, Singapore.
2. Gang Li and Wan-Young Chung, “Early Warning of Driver Drowsiness using EEG Signals and Support Vector Machine”, *Proceedings of the 1st International Biomedical Engineering Conference (IBEC’14)*, p. 350, 20 November – 22 November, 2014, Gwangju, Korea.
3. Gang Li and Wan-Young Chung, “A pilot study on the use of EEG sensors for measuring the eyelid closure degree”, *Proceedings of the FTRA 2013 International conference on ubiquitous computing and embedded systems (UCES’13)*, pp. 1-5, 18-20 December, 2013, Da Nang, Vietnam
4. Gang Li and Wan-Young Chung, “A Real-time Driver Fatigue Detection System Based on Non-stationary Analysis of Heart Rate Variability”, *Proceedings of the 10th International Conference on Ubiquitous Healthcare (u-healthcare’13)*, pp. 68-70, 12-14 September, 2013, Yokohama, Japan.

Awards

1. Best Paper Award – Gang Li and Wan-Young Chung, “A pilot study on the use of EEG sensors for measuring the eyelid closure degree”, Proceedings of the International conference on ubiquitous computing and embedded systems (UCES 2013), 18-20 December, 2013, Da Nang, Vietnam.
2. Excellent Paper Award – Gang Li and Wan-Young Chung, “A Low-Cost Driver Drowsiness Detection System Based on EEG Sensor and Smartphone”, Proceedings of the Korea Institute of Signal Processing and Systems Summer Conference, Vol. 15, No. 1, pp. 61– 63, 20-21 June, Catholic University of Daegu, 2014.
3. Excellent Paper Award – Gang Li, Sang-Joong Jung, and Wan-Young Chung, “Detection of Driver Fatigue Using Photoplethysmogram Signal and Wavelet Transform Analysis”, Proceedings of the Korea Institute of Signal Processing and Systems Summer Conference, 12-13 July, 2013, University of Ulsan, Korea.

Media Report

Yeohap News Agency :

<http://www.yonhapnews.co.kr/it/2014/01/02/2403000000AKR20140102074700051.HTML>

Appendix

Table 1 Fifty-four Studies on EEG-based DDD listed with montages, as well as time windows for feature extraction, if applied

Ref No.	Year	Number of channels	Channel Position*	Time window
[52]	2005	33	-	1 min
[53]	2006	19	F1, F2, F7, F8, F3, F4, T3, T4, C3, C4, T5, T6, P3,	1 s
[54]	2007	1	O1 or O2	1 s
[55]	2007	1	Fp1	10 s
[56]	2008	4	-	-
[57]	2008	2	C3,P3	10 s
[58]	2008	1	C3	5 s
[59]	2008	1	Fp1 & Fp2	-
[60]	2009	6	Fp1, Fp2, T5,T6, O1,O2	4 s
[61]	2010	1	Oz	8 s
[62]	2010	26	-	5 s
[63]	2010	1	-	2 min
[4]	2010	1	C3 or C4	30 s
[64]	2010	1	C3 & O1	30 s
[65]	2010	2	F7&T3 ; F4&C4	-
[66]	2010	16	-	1 min
[67]	2011	1	O1	1 min
[68]	2011	2	C4,O2	10 s
[69]	2011	2	Fp1 & Fp2 ; T3 & T4	-
[70]	2011	1	Fp1 & Fp2	2 s
[71]	2011	29	Frontal (F: 3, 1, z, 2, 4; Fc: 3, 1, z, 4), Central (C: 3, 1, 2, 4; Cp: 3, 1, z, 2, 4) and Parieto-occipital (P: 3, 1, z, 2, 4; Po: 3, z, 4; O: 1, z, 2)	20 min
[26]	2011	3	Fz,T8,Oz	1 min
[72]	2011	2	C4,O2	1 min
[73]	2011	19	-	2 s
[74]	2011	1	O1 & O2	1 min
[75]	2011	1	O1 & O2	30 s
[76]	2012	4	Forehand	10 min
[77]	2012	8	Fp1, Fp2, F3, F4, P3, P4, O1, O2	10 s
[78]	2012	1	Fp1	10 s
[79]	2012	1	P3	20 s
[80]	2012	6	Occipital	1 s
[81]	2012	14	F7, F8, T3, T4, T5, T6, F3, F4, C3, C4, P3, P4, O1 and O2	1 s
[82]	2012	2	Fz & Cz ; Pz & Oz	-
[83]	2012	21	-	30
[84]	2012	1	C4 & P4	1 min
[85]	2012	4	Occipital	-
[86]	2013	1	Fp1 & Fp2	2 s
[87]	2013	3	Fz, Cz, Oz	2 s
[88]	2013	3	Fz, T8, Oz	10 s
[89]	2013	2	Fz, Oz	1 min

[90]	2013	3	(Fp1, C3,O1) or (Fp2, C4,O2)	30 s
[91]	2013	14	-	1 s
[92]	2013	1	O1 & O2	<1 s
[93]	2014	2	Fz & Cz ; Pz & Oz	1 min
[94]	2014	1	O1 & O2	1 min
[95]	2014	4	Occipital	2 s
[96]	2014	2	Fz, Pz	-
[97]	2014	2	Fz, Oz	1 min
[98]	2014	1	-	5 s
[99]	2014	2	Fz & Cz ; Pz & Oz	30 s
[100]	2014	19	-	2 s
[101]	2014	1	Fp1	1 s
[102]	2014	1	O1 & O2	30 s
[103]	2014	14	-	-

* Symbol “&”, “,” and “;” represent bipolar channel (e.g., bipolar single channel: O1&O2), unipolar channel (e.g., unipolar two channels: Fp1, Fp2) and hybrid channel (e.g., hybrid two channels: Fz & Cz ; Pz & Oz) respectively.